Development of functional interfaces for sensing applications

by

Xiaoyun Yang

A dissertation submitted to the Graduate Faculty of
Auburn University
in partial fulfillment of the
requirements for the Degree of
Doctor of Philosophy

Auburn, Alabama
May 4, 2013

Keywords: Tricresyl phosphate, electrochemical analysis, PEDOT:PSS composites, electrode fouling, surface characterization, current-potential relationship

Approved by

Aleksandr Simonian, Chair, Professor, Materials Engineering
Jeffrey Fergus, Co-chair, Professor, Materials Engineering
Dong-Joo Kim, Associate Professor, Materials Engineering
Curtis Shannon, Professor, Chemistry

Abstract

An electrochemical device has been developed for the detection of gaseous tricresyl phosphate (TCP). Monitoring of neurotoxic TCP is important since it has been widely used as an additive in commercial jet engine oils, acting as a flame retardant and plasticizer. The process of air recirculation in most aircrafts could allow TCP to enter the cabin, if oil leakage occurs, and potentially harm the health and safety of the crew and passengers. Although a few of the new airplanes have begun to use a different air recirculation system which can reduce the possibility of TCP contamination, it is still a big issue for most airplanes that are currently in service throughout the world.

Since TCP has low saturated vapor pressure, a gaseous sample is not readily available and a special procedure was developed in our laboratory for conducting experiments. A TCP methanol solution was heated while N_2 was bubbled though a flow system to vaporize the TCP. Since TCP is not electro-active and cannot be detected with electrochemical approaches, it was hydrolyzed to cresol using a special hydrolysis column in the flow system. Both of these operations were also performed with an automatic sampling device that was built in our lab. The presence of TCP in the hydrolysate samples of TCP, as well as real TCP-contained engine oils, was successfully detected by the electrochemical device within the linear range of 30-300 ppb of TCP in gas phase.

However, the electrochemical detection procedure results in oxidative polymerization of cresol on the electrode surface and this significantly distorts the results of measurements. A functional interface of poly(3,4-ethylenedioxythiophene) poly(styrenesulfonate) (PEDOT:PSS) composites has been introduced on the electrode surface to prevent electrode fouling. With this modified electrode, a similar linear range was obtained. More importantly, the modified electrochemical device

was able to continuously detect gaseous TCP and has reliable responses over a longer period of time than with unmodified electrodes.

Electrode fouling is a common problem during the electrochemical analysis of phenolic compounds. A potential-drop-based model has been created in order to better understand the mechanism of electrode fouling, and it was able to quantitatively predict the electrode fouling in terms of time, applied potential, and the concentration of cresol. In order to obtain this model, the current-potential relationship was studied, and the amount of potential drop across the fouling layer was measured with a copper deposition method. This scientific model was comparable with experimental results, and would be helpful for the development of anti-fouling strategies.

Acknowledgments

In the first place, I would like to express my deepest and sincere appreciation to my advisor Prof. Aleksandr L. Simonian for his continuous support. Without his prudence and support, I couldn't realize the achievements in this project, and meanwhile take the opportunity of internship in this spring. I will cherish the advices he gave, not only in my research, but also in my life. I also want to express my earnest gratitude to Prof. Jeffrey Fergus. His patience and erudition always encouraged me to go deeper in my research and finally realize some scientific contributions in my PhD study. I would like to appreciate my committee members, Prof. Dong-joo Kim and Prof. Curtis Shannon for the suggestions provided on my research with their profundity of knowledge in Chemistry and Materials science. My sincere gratitude to Prof. Xinyu Zhang for being an external reader.

I am also grateful to Prof. Overfelt, Prof. Prorok, and Dr. Valber Pedrosa who led my way to this project and gave me support. Thank Dr. Alice Zitova who worked hard and took the burden from me and helped me publish the first paper. Thank my labmates Tony Gnanaprakasa and Saroja Mantha for teaching me the philosophy of life and research. Thank Jeffrey Kirsch who worked together with me for two years and for his patient help on my writings. I really appreciate the help from Mr. L.C. Mathison, Dr. H. Clyde Wikle, and Keith Krome on the mechanical and electronic work and Mr. M. Montgomery on the glass work. Thank Dr. Ricky Lance Haney, John Andrew, and Amendar Neer for their collaboration. Thanks for the chances to use SEM and TEM provided by Dr. Michael Miller, AFM by Prof. Maria Auad, profilometer by Prof. Robert Jackson, Ellipsometer helped by Prof. Bob Ashurst and Jie Zhong, GC by Dr. Wang, Raman by Prof. Shannon and Axline Sanghapi, and microfibers by Prof. Bruce Tatarchuk. Thank my former group members, Prof. JW Hong, Dr. Woon Seob Lee, Dr. Sachin Jambovane, and Hoon Suk Rho. Thank the

staffs, Mr. Roy Howard, Mr. Steven Moore, Ms. Alison Mitchell, and Ms. Amandar Y. Davids who made my work in the lab easier.

My friends made my life in Auburn enjoyable. Thank my family friends, Mr. Clay Humpries, Mrs. Pat Humpries, Clayton, and Kathryn for warming my heart in holidays and accidents, and letting me know a real American family. I really appreciate Wei Huang who let me settled down when I just came to Auburn and made my starting life in Auburn much easier. Thank all of my friends, Dan Liu, Lin Zhang, Jing Dai, Yating Chai, Yingjia Liu, Honglong Wang, Zhizhi Sheng, Hyejin, Victor, Naveed, Nitil, Shin, Wei Wang, Jing Zou, Yu Zhao, Peixuan Wu, Kewei Zhang, Dong Liu, Wen Shen, Hong Xie, Min Sheng, Zhongliang Lv, Zijie Cai, Chang Lin, Qing Dai, Cheng Guo, Haijun Duan, Song Chen, Jia Yao, Zhenfei Tang, Xue Wang, Wenchan Jiang, Jingyuan Xiong, Qiao Zhang, Hao Song, Yu Wang, Yajiao Yu, Shaomao Li, Ruoliang Tang, Jie Zhong, Hao Pan, AHM Shahadat Hussain, Mohiuddin Ovee, Austin Adamson, Sara Standifer, and Katie Andress. Finally, I would like to dedicate this work to my parents and my dear fiancé, Han Xu, who valued me always. I love all of you.

Table of Contents

Abstract ii
Acknowledgments ..... **Error! Bookmark not defined.**
List of Tables ix
List of Figures x
1. Introduction and Literature review 1
1.1. Introduction to sensors 1
1.2. Sensor transducers 2
1.2.1. Electrochemical sensors 2
1.2.2. Optical biosensors 6
1.2.3. SPR optical biosensors 9
1.3. Sensor recognition elements 11
1.3.1. Functional interfaces and recognition elements 12
1.4. Electrochemical sensor for detection of TCP 14
1.4.1. Introduction of TCP. 14
1.4.2. Current trends in TCP detection. 16
1.5. Electrode fouling during electrochemical analysis of phenolic compounds. 17
1.5.1. Introduction to phenolic compounds 17
1.5.2. Chemical reactions during anodic oxidation of phenol 19
1.5.3. Properties of the polymeric film and its effect on electrochemical analysis 21
1.5.4. Application of functional interfaces on anti-fouling modifications. 25
2. Research Objectives 35
2.1. Dissertation organization 35
3. Electrochemical analysis of TCP 37
3.1. Introduction 37
3.2. Experimental setup 38
3.2.1. Reagents and solutions 38
3.2.2. Electrodes and portable sensor 38
3.2.3. Alkaline catalyst for TCP hydrolysis 39

3.2.4. Automatic sampling system for hydrolysis of TCP and engine oils 39
3.3. Results and Discussions 41
3.3.1. Diffusion controlled anodic oxidation of cresol 41
3.3.2. Performance of the electrochemical sensor 44
3.3.3. Detection of hydrolysates from TCP samples 45
3.3.4. Detection of hydrolysates from engine oils 47
3.4. Conclusions 53
4. Anti-fouling PEDOT:PSS modification for continuous monitoring of TCP 54
4.1. Introduction 54
4.2. Experimental setup 55
4.2.1. Reagents and solutions 55
4.2.2. Electropolymerization of PEDOT:PSS on glassy carbon electrode 56
4.3. Results and Discussions 56
4.3.1. Microscopy images of electrode fouling 56
4.3.2. Controlled PEDOT:PSS modification on glassy carbon electrode 58
4.3.3. Detection of cresol with modified electrodes 59
4.3.4. Detection of TCP with modified electrodes 62
4.4. Conclusions 64
5. Study of Current-Potential Curves 65
5.1 A simplified approach to steady-state mass transfer limited reversible reactions 65
5.2 A rigorous approach to electrode reactions 71
6. A study of electrode fouling during electrochemical analysis of phenolic compounds 78
6.1. Introduction 78
6.2. Materials and Methods 80
6.2.1. Reagents and solutions 80
6.2.2. Flow system and electrochemical devices 80
6.2.3. Air bubbled fouled electrodes 81
6.2.4. Cu deposition on electrodes 82
6.2.5. Characterizations of fouling layer and Cu deposition 82
6.3. Results and Discussions 83
6.3.1. Characterizations of potential drop 83
6.3.2. Quantitative determination of potential drop 88
6.3.3. The potential drop based model to electrode fouling 90
6.3.4. Characterizations of the fouling layer 93

6.3.5. Electrode fouling during repetitive injections of cresol 95
6.4. Conclusions 98
7. Overall conclusions 99
References 101
8. Future work 118
8.1. Filters and absorbents to TCP 118
8.2. Optimization of alkaline catalyst to TCP analysis 120
8.3. Strategies to anti-fouling 121

List of Tables

Table 1-1 Partial publications about electrode surface modification. 34

Table 3-1 Amperometric results of oil hydrolysate samples. The conversion from concentration in ppb to concentration in % is mentioned in text. 52

List of Figures

Fig. 1-1 Schematic representative of a sensor. In general, a sensor includes a recognition element responding to specific analyte or a group of analytes, a transducer, and a signal processor [2]. 1

Fig. 1-2 Classification of sensors based on the type of transducer [2, 3]. 2

Fig. 1-3 Schematic representative of LSV, CV and amperometry methods. The applying of potential and *i*-*V* or *i*-*t* curves are depicted in LSV (Left), CV (2^{nd} Left), and amperometry methods (Right). The steps or peaks are resulted from the repetitive sample injections after the current reaches steady state (Right). 6

Fig. 1-4 Schematic representative of the phenomena of total reflectance, the evanescent wave, and surface plasmon polarity. (a, b) Light wave experiences reflection and refraction simultaneously at the n_2/n_1 interface; (c, d) Total reflection occurs when angle of incidence θ equals to or is greater than the critical angle θ_c. (e) The evanescent wave is created during the total reflection. (f) A surface plasmon (SP) is excited by an evanescent wave.....8

Fig. 1-5 Schematic representative of the working mechanism of SPR.....10

Fig. 1-6 Transformation of the curve of reflectivity *vs* θ into RU *vs* time in SPR device. An example of experimental results is presented in the right side, indicating the association, dissociation, and regeneration processes.....11

Fig. 1-7 Classification of sensors based on the type of recognition element [2, 3].....12

Fig. 1-8 Chemical structures of *o*- (left), *m*- (center), and *p*- (right) cresols. 14

Fig. 1-9 Chemical structures of tri-*o*-cresyl phosphate (left) and tri-*p*-cresyl phosphate (right). 14

Fig. 1-10 Schematic representation of air circulation in aircraft cabin. Air is 1) bled in through engine; 2) filtered; 3) combined with recirculated air; 4) flowed into cabin; 5) released for maintaining the pressure. TCP may enter cabin along with bleed in air during oil leakage in engine. Picture from http://informer.truth.travel/.....16

Fig. 1-11. Chemical structures of phenol, *p*-cresol, *o*-cresol, *o*- chlorinated phenol, and *p*- chlorinated phenol (from left to right).....18

Fig. 1-12 Schematic representative of the chemical reactions that occur during the oxidation of phenol. 21

Fig. 3-1 Schematic representative of the reaction pathway that happened during the alkaline hydrolysis of TCP. 37

Fig. 3-2 Sensor setup: (left) flow injection system and flow cell electrodes were used to detect aqueous samples containing cresol. A coin was used to show the size. (right) Besides desktop potentiostat and computers, handheld potentiostat and pocket PC were used to conduct amperometric detections. 39

Fig. 3-3 Schematic representative of TCP sampling system. TCP was heated to 230 ^{o}C in oil bath and gasified along with N_2 bubbling, and entered the alkaline catalyst column set inside an automatic TCP conversion box. In the electronically controlled TCP conversion box, as shown in the dotted square in above figure, TCP was hydrolyzed for later detection. The control of the automatic TCP conversion box was mentioned in ref. [160]. 40

Fig. 3-4 Schematic representation of automatic TCP sampling system. (top right) Arrangement of tubes, valves, and pumps. (top left) Electronic board consisting of electronic relays was used to control on/off of valves and pumps. (bottom) Running program in lab view software to control the electronic board. 41

Fig. 3-5 Cyclic voltammetry results of cresol oxidation on bare electrode. (a) First cycle of cyclic voltammetry of 100 μM cresol in 0.4M phosphate buffer solution at scan rates varying from 10 to 200 mV/s. scan rates increase along the arrow direction. Range of potential: 0 to 800 mV vs Ag/AgCl/3 M KCl. (b) Calibration of the relation between the peak current density and square root of the scan rate. The coefficient of determination R^2 indicates the variability from linear fit. Glassy carbon working electrode (3 mm ø) was used for all of detections and polished between uses. 43

Fig. 3-6 Calibration curve of cresol detection. The inserted figure shows the amperometry for cresol detection. Note that the baseline was subtracted. The decrease in response with subsequent injection is due to the fouling of electrode from cresol oxidation [28] (seen on the inset figure). R^2, coefficient of determination, representing the goodness of linear fit, in calibration curve is 0.992. Data points in calibration curve correspond to the average of the three injections. Error bars are the standard deviation of triple experimental results. Detection limit is 250 nM. 44

Fig. 3-7 Amperometric results from injections of TCP hydrolyzate samples. TCP samples were injected in random order. In some sets, some samples were measured again after all samples have been measured once. We consider the first 8 peaks as "1st cycle". Only data in 1st cycle were used for calibration, since fouling effect makes the response in the 2nd cycle weaker than the 1st one. 46

Fig. 3-8 Calibration curve of TCP hydrolysate samples. Linear concentration ranges from 5 ppb to 300 ppb in gas. The inset figure shows one set of raw amperometric results out of six times measurements. The linear fit for the inset figure is $y = 1.22x + 36.5$, and the R^2 is 0.99. The results show the ability of this sensing device to detect TCP in a wide concentration range. The conversion of concentration units between

ppb in gas and M is as below. As mentioned in section 3.2.4, TCP was dissolved in 0.5 mL of methanol, which would be vaporized and dispersed in 11 L of N_2. Approximately, 11 L of gas is 0.5 mol. Therefore, 1 M of TCP in methanol solution corresponds to 1 ppb in gas.....47

Fig. 3-9 Amperometric results from injections of TCP spiked BP274 hydrolyzate samples. For example, +50 means BP274 spiking with 50 ppb TCP. Injections were in random order. Only data in 1st cycle are used for calibration. The data +0, which represent BP274 sample, were also used in calibration of different oil samples.....49

Fig. 3-10 Amperometric results of injections of oil spiking TCP hydrolysate samples. The slope of linear fit is around 1 nA/ppb, which is close to Fig. 3.8. R^2 of 0.99 represents the goodness of linear fit. All samples were measured randomly for three times.....50

Fig. 3-11 Amperometric results from injection of oil hydrolyzate samples. The injections were in random order. Only data in 1st cycle are used for calibration.....51

Fig. 3-12 Amperometric results of injections of different oil hydrolysate samples inset with one example of raw data. They were prepared, gasified, and hydrolysed in the automatic sampling system before detection. Note that fouling contributes to the existence of error bar and the concentrations of TCP in these oil samples are much higher than what would be expected. The data in Fig. 3.9 were included for calibrating the BP274 injection current. 52

Fig. 4-1 Observations of fouling on glassy carbon electrode from SEM, EDS, and AFM. (a) SEM image of Au sputtering coated bare electrode, (b) SEM image of fouled electrode, (c) EDS results of the bare and fouled electrodes, (d) AFM image of bare electrode, (e) AFM image of 3 mm ø electrode fouled by 5 μC of charge in amperometry, and (f) AFM image of 3 mm ø electrode fouled by 20 μC of charge in amperometry. 57

Fig. 4-2 PEDOT:PSS modification of glassy carbon electrodes. (a) Amperometric results of 4 electrodes applied with 0.5 mC of charge in EDOT:PSS solution, (b-e) Optical images of these 4 electrodes after modification with 0.5 mC of charge, (f-i) Optical images of 4 electrodes after modification with 1, 1.3, 2, 4 mC of charge, (j-l) SEM images of electrode surface applied with 0.3, 0.5, and 2 mC of charge in EDOT/PSS solution. 59

Fig. 4-3 Amperometric results of 10 μM cresol on bare and modified electrodes. (a) Initial amperometric peaks obtained from successive injections of 10 μM cresol in 0.4 M phosphate buffer. Two experiments have been carried out on bare electrode and 5 on modified electrodes, two examples of which are shown here. (b) Calibration of peak current *vs* peaks. Note that the first peak in each case has been normalized to 100%. Unicell glassy carbon electrodes with 2 mm diameter were used. 60

Fig. 4-4 Amperometric results of injections of 0.2-10 μM cresol in 0.4 M phosphate buffer. (a) Two representative sets of continuously amperometric results. Different

concentrations of cresol samples were injected in random order to avoid potential system error and by this way electrode fouling could be seen more clearly. (b) Calibration curve of detection of cresol with different concentrations on modified electrode. The coefficient of determination R^2 indicates the variation of linear fit. Error bars are marked as bars above and below current symbols. Unicell glassy carbon electrodes with 2 mm diameter were used. 61

Fig. 4-5 Detection of TCP on bare/modified electrode. (a,left) Calibration of detection of TCP samples with concentrations of 10, 20, 30, 50, 100, 200, and 300 ppb on PEDOT:PSS modified electrode, (a,right) Calibration of detection of 30, 50, 100, and 300 ppb TCP on bare electrode. 10 and 20 ppb were not detected and compared with modified electrode, (b) Responses from modified electrode were normalized to 100% and the error bars and signals from bare electrode were relatively calibrated. Unicell glassy carbon electrodes with 2 mm diameter were used. Note that the bare electrode was polished after measurement of each set of 4 samples, while modified electrode was not polished through three sets of measurements. 63

Fig. 5-1 The *i-E* curve based on the naive approach. Additional potential equals to 0 when $E = E^{0'} + \frac{RT}{nF}\ln\frac{D_{Ox}}{D_{\mathrm{Re}}}$ ..... 70.

Fig. 5-2 The *i-E* curve of 10 μM $Fe(CN)_6^{4-}$ solution obtained in flow mode. The flow rates were 20 ml/h and 100 ml/h. 71

Fig. 6-1 Experimental setup for the flow mode analysis. A dual channel syringe pump (left side) was used to provide constant flow rate. A sample injector (right side) was used to swap the flow solution that ran through the unicell electrode set (center). 81

Fig. 6-2 Amperometric results and voltammograms of electrode fouling and Cu deposition. (a) Electrodes were fouled at 0.75 V vs. Ag/AgCl/10 μM NaCl with 10 μM cresol for 0, 100, 200, 300, 400, 500, and 600 s. (b,c) Electrodes were conducted with Cu deposition. One representative example set of potential sweep curves were shown. The scan rate was 10 mV/s. The forward potential sweep was negative, from 0.5 to -0.8 V, in which Cu deposition peaks presented. The peaks of Cu stripping were presented in the following positive sweep. All glassy carbon working electrodes had a diameter of 2 mm. 84

Fig. 6-3 Observation of Cu deposition on electrodes with optical microscope (a-d), SEM (e), and EDS (f). Cu deposition with potential sweep from 0.5 to -0.1 V on polished electrode (a) and 300 s fouled electrode (b); Cu deposition with potential sweep from 0.5 to -0.8 V and to 0.5 V on polished electrode (c) and 300 s fouled electrode (d); SEM images of Cu deposition on polished electrode (e); and corresponding EDS results (f). 85

Fig. 6-4 Characterization of with or without air bubbled fouled electrodes. (a) Current intensity curves of 10 μM cresol analysis in the amperometry mode. The applied

potential was 0.75 V. (b) Normalized current intensities. The highest current was normalized to unity. (c,d) Optical images of air bubbled 200 s and 500 s fouled electrodes. (e) Profilometry results of the line scan across the air bubbled area on 500 s fouled electrode. 86

Fig. 6-5 Cu deposition and optical images of air bubbled 500 s fouled electrodes. (a) Cu deposition on polished, fouled w/o air bubbled, air bubbled fouled electrodes. Only part of the forward potential sweep was shown. The order of the labels corresponded to the positions of the current intensity at ~-0.1 V. (b,c,d) Optical images of electrodes that were covered by an air bubble with different sizes. Values in percentage indicated the ratio of air bubble covered to the whole electrode surface. . 87

Fig. 6-6 Example of the 1st and 2nd differentiations of the current-potential curve of Cu deposition on polished electrode. 89

Fig. 6-7 Calibration of the potential drop measured with Cu deposition. The values of potential drop were obtained by subtracting the derivative minimum from the averaged value for polished electrodes. (a) Summary of all values of potential drop obtained with the 1st differentiation. (b) Summary from the 2nd differentiation. 89

Fig. 6-8 Schematic representative of the effect of the fouling layer on the potential profile and concentration profile close to electrode surface. (a) Cresol was oxidized at the interface of electrode-electrolyte. (b,c) The configurations of the working electrode, fouling layer, interface, diffusion layer, and bulk solution. (d,e) The potential profile close to the electrode surface w/ or w/o the fouling layer. The potential drop from the solution is ignored. (f,g) The simplified concentration profile of cresol close to the electrode surface. The concentration gradient was assumed to be linear. Some ideas were referred from literature [4, 175]. 90

Fig. 6-9 Model curve and experimental curves of cresol fouling. (a) One example of the theoretical current decay during amperometry analysis of cresol. (b) The comparison of theoretical and experimental current curves for analysis of 10 μM cresol at 0.75 V. The theoretical curve overlapped other curves. 92

Fig. 6-10 Impedance results with respect to the fouling time and cresol concentration. (a) The equivalent electric circuit used for the fouled electrode immersed in $Fe(CN)_6^{3-/4-}$ solution. (b) One example of impedance spectra of fouled electrodes. The curve overlap data points was the fit analysis based on the model of R(Q[RW]), which represented above electric circuit. (c) Calibration of all measured R_{CT} values with respect to the product of fouling time and the concentration of cresol used for electrode fouling. 93

Fig. 6-11 AFM images of polished and fouled electrodes. (a) The image of a polished electrode. The scan size is 500 nm. (b) The image of a 1 μM cresol 100 s fouled electrode with the scan size of 500 nm, (c) with the scan size of 200 nm. (d) The image of a 1 μM cresol 1hr fouled electrode with the scan size of 500 nm, (e) with the scan size of 200 nm. 95

Fig. 6-12 Amperometric results of repetitive injections of 10 μM cresol at different potentials. Potentials were kept at 0.75 V (left), 0.65 V (middle), and 0.55 V (right). Only one example for each case was shown representatively 96

Fig. 6-13 Data process for all amperometric results: (a) Every first peak was normalized to 1, (b) All scans were normalized corresponding to 0.75 V scan. Only examples of 0.55 V and 0.75 V scans were shown. 97

Fig. 6-14 Calibration curve for all amperometric results of electrode fouling. 97

Fig. 8-1 Amperometric results of TCP hydrolysate samples. The ten peaks correspond to 100, 200, 50, 500, and 50 ppb TCP collected by the 1st column (first 5 peaks in order) and the 2nd column (latter 5 peaks). The applied potential was 0.65 V, the flow rate was 20 mL/h, and the injection time was 10 s for all samples.....118

Fig. 8-2 CV results of the tail gas collection in 1M NaOH and cresol spiked medium. The mixture was spiked with cresol at the concentrations of 10 (blue), 20 (brown), and 50 μM (red). The potential range of 0.3-0.6 V was zoom in and shown in the inset figure. The scan rate was 100 mV/s, and the volume of sample was 3 mL. 119

1. Introduction and Literature review

1.1. Introduction to sensors

A sensor is a device giving a signal for the detection or measurement of a physical property to which it responds, as defined in the Oxford English Dictionary [1]. Sensors can be divided to three types, namely, physical sensors, chemical sensors, and biosensors. Physical sensors concern about physical properties, such as length, weight, pressure, and else. Chemical sensors, which respond to specific chemical or a group of chemicals, usually involve one or multiple chemical reactions and can be used to determine these chemicals qualitatively or/and quantitatively. Sometimes considered as a sub-set of chemical sensors, biosensors incorporate a biological sensing element and respond to specific analytes. They may target the same analyte as chemical sensors, but the key difference between biosensors and chemical sensors is the involvement of the biological sensing element, which is also the reason why biosensors are often treated as a separated topic [2].

In general, a sensor has three parts: the recognition element, the transducer, and the signal processor (**Fig. 1-1**). The recognition element responds specifically to either a single analyte or group of analytes, and then the observed changes are converted by the transducer into signals for processing. Sensors are classified based on the transducer and recognition element.

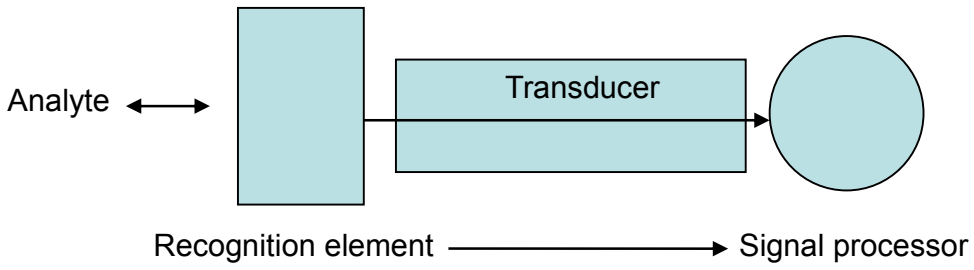

Fig. 1-1 Schematic representative of a sensor. In general, a sensor includes a recognition element responding to specific analyte or a group of analytes, a transducer, and a signal processor [2].

1.2. Sensor transducers

Sensors can be subdivided into four main types based on the type of transducer (**Fig. 1-2**) [2, 3]. The following discussion will be focused on the electrochemical transducer and surface plasmon resonance transducer.

1.2.1. Electrochemical sensors

Electrochemical transducers, which are often a set of electrodes, convert the interaction of recognition element with an analyte in solution to an electrical signal that can be processed. The interaction happens at the interface between electrode surface and analyte solution and produces a change in an electrical phenomenon such as potential, current, impedance, capacitance, etc. Electrochemical sensors can be subdivided into (1) potentiometry, (2) voltammetry, and (3) impedance. Potentiometry concerns the cell potential at zero current flow. Voltammetry, also called amperometry, monitors the current response to the applied potential in the analyte solution, in which reactions of species happen. In impedance spectroscopy, the analyte solution is perturbed by a small alternating signal and stays really close to steady state, and the information about kinetics and diffusion is obtained.

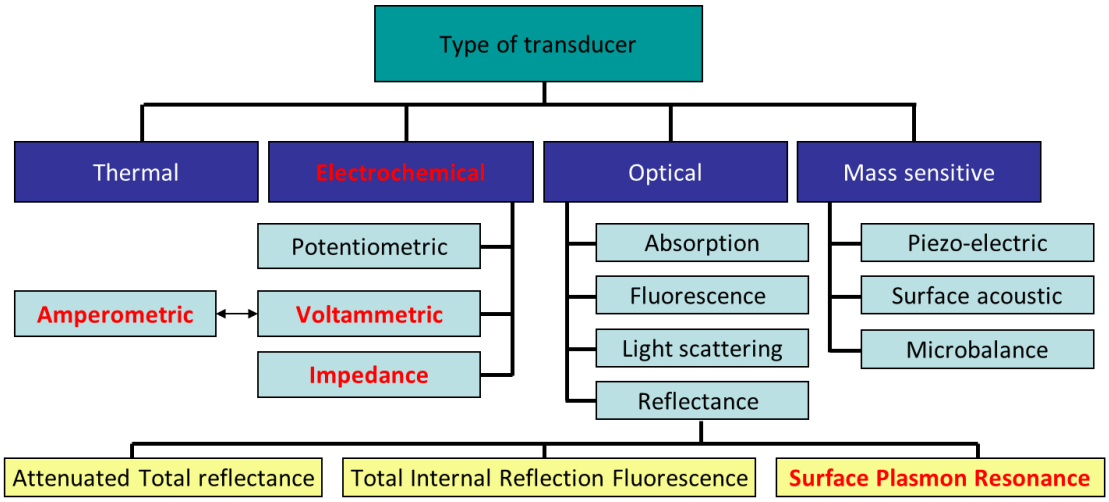

Fig. 1-2 Classification of sensors based on the type of transducer [2, 3].

1.2.1.1. Potentiometry

Once an electrode is immersed into an electrolyte solution, the charge distribution at the interface of electrode surface and solution yields an electron pressure, i.e., a potential. The potential can be measured via electrolytic coupling of electrodes in solution. An electrochemical cell consists of a set of electrodes and electrolyte, sometimes with the addition of a membrane that allows certain species to traverse it. The electrolyte is often an aqueous solution or sometimes organic solution, in which species of interest can be ionized. Usually, the potential is measured by a potentiometer (voltmeter) with high impedance and thus the current flow is almost zero. One electrode in the cell with known potential acts as a reference to other electrodes. The most commonly used reference electrodes are the silver-silver chloride electrode (Ag/AgCl) and the saturated-calomel electrode (Hg/Hg_2Cl_2). Most of the time, the combination of the metal/metal chloride is exposed to the solution including a specific concentration of chloride ions in a package to provide constant potential. In addition to the reference electrode, another electrode is used which interacts with the analyte solution and often of interest. The interaction is detected by the potentiometer and contains the information of (1) the nature of the electrode, and (2) the nature and concentration of the analyte.

1.2.1.2. Voltammetry (Amperometry)

In voltammetry / amperometry, two-electrode cell and three-electrode cell are used. The former cell includes one electrode of interest (called the “working electrode”), one reference electrode, and the solution containing target electroactive (oxidizable and reducible) species and the supporting electrolyte with no interference. The three-electrode cell is used quite often [4], which uses one additional electrode, called “counter” or “auxiliary” electrode. Potential is applied between the working electrode and counter electrode, and the current flowing through the solution between them is measured by an ammeter. A potentiometer with high impedance is used to monitor/regulate the potential between working electrode and reference electrode. The

advantage of three-electrode cell over the two-electrode one is that the reference electrode was placed parallel with the current-flowing solution, the current flows through the reference electrode is negligible, and thus its potential remains constant. In this way, a current-potential (*i-V)* curve has been obtained. Usually, the range of applied potential covers the standard redox potential of species. The *i-V* curve gives information of the nature and concentration of analyte and the current is governed by Faraday's law and the laws of mass transport [5].

Linear-Sweep Voltammetry (LSV) and Cyclic Voltammetry (CV) are two similar analysis modes which are often used. The potential is swept linearly and current response is monitored continuously in both modes. The difference is that the sweep is uni-directional in LSV, but there is an additional reverse and sometimes cycles of potential scan in CV. Correspondingly, A single curve will be obtained in LSV and double or multiple *i-V* curves will be obtained in CV.

Every electroactive substrate has a specific standard redox potential, E^0, at which the ratio of activity of oxidative to reductive substrates, Ox/Re (Oxidative/Reductive), is 1:1 in equilibrium. When the potential is higher than the standard value, the activity of oxidative product is higher than the reductive one, and vice versa. The values of activity is close to concentration at low values, but may be deviated at high ones. Since the ratio of redox couple changes with potentials comparatively faster in the vicinity of electrode surface, the concentration difference of the Ox or Re state of the analyte at the electrode surface from the bulk solution provides a gradient driving force for substrate diffusion and thus the current response. Under the combination of diffusion effect and kinetics of oxidation/reduction, one or multiple current peaks are always presented during the potential sweep. The peaks occur at specific potentials for one species, which is used for qualitative determination.

Usually, the cell is designed to avoid the convection by leaving the solution still, creating a laminar flow with constant low rates, or rotating the working electrode at constant rates. These states of electrolyte solution or electrode correspond to the batch mode, flow mode, and rotation disk electrode (RDE). Moreover, migration is always minimized by adding a comparatively high concentration of supporting electrolyte,

such as the $HPO_4^{2-}/H_2PO_4^-$ ion pair in the phosphate buffer. Therefore, only diffusion is responsible for the current peak in *i-V* curve, which enables the quantitative analysis of species concentration. The shape of the *i-V* curve can be used to obtain more information about the diffusion and kinetics of electron transfer.

Amperometry is a usual application of chronoamperometry technique which is closely related to the voltammetry. Instead of potential sweep, a constant potential or a step of constant potential is applied in this method. The potential, usually, is chosen just over the current peak obtained from CV, in order to make the state of analyte deviate from equilibrium. Instead of an *i-V* curve, an current-time (*i-t)* curve is obtained. In many cases, the curve has a characterized shape controlled by diffusion. A simple solution to the diffusion equation is the Cottrell equation as shown below [2],

$$i_d = \frac{nFADC_{Ox}}{\pi^{1/2} t^{1/2}} \qquad (1.1)$$

where

i_d = current, in the unit of A;

n = number of electrons;

F = Faraday constant, 96,485 C/mol;

A = area of the (planar) electrode, in cm^2;

D = diffusion coefficient, in cm^2/s;

C_{Ox} = bulk concentration of the oxidative analyte, in mol/cm^3;

t = time in s.

Based this equation, the decaying current is proportional to $1/(t)^{1/2}$. When this Faradic current decays to small, the non-Faradic current cannot be ignored. With certain cell configurations, the current reaches a steady state, following the equation 1.2 [2],

$$i = \frac{nFAD^{1/2}C_{Ox}}{\delta} \qquad (1.2)$$

where δ is the thickness of a “simplified” diffusion layer. Analysis in more

detail is available in Chapter 5.

By certain experimental setup, repetitive injections of analyte can be realized. The operation yields steps in signal in the batch mode and peaks in the flow mode. The peak height is proportional to the concentration of analyte, unless the electrode fouling occurs, which will be discussed in detail that follows. **Fig. 1-3** shows schematically how these modes work.

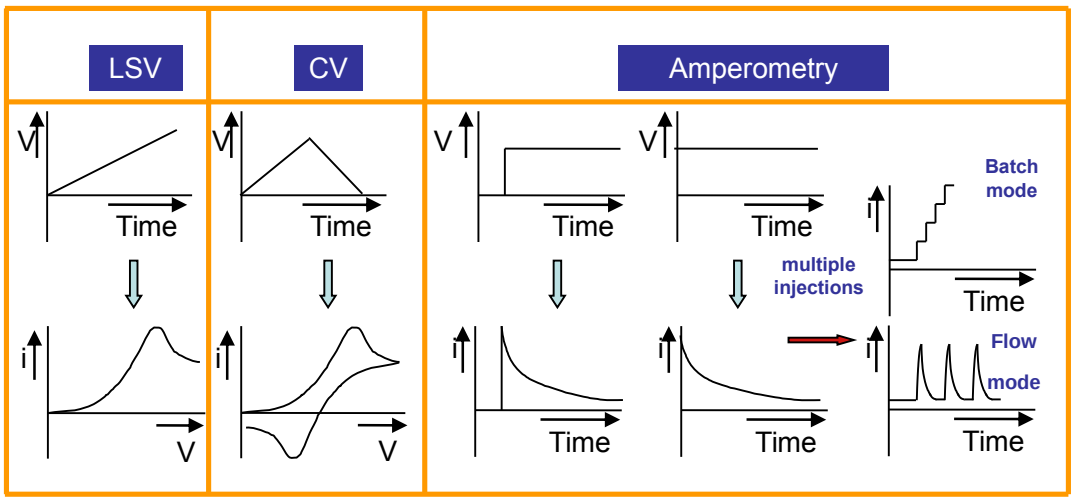

Fig. 1-3 Schematic representative of LSV, CV and amperometry methods. The applying of potential and *i-V* or *i-t* curves are depicted in LSV (Left), CV (2nd Left), and amperometry methods (Right). The steps or peaks are resulted from the repetitive sample injections after the current reaches steady state (Right).

1.2.2. Optical biosensors

Optical transducers have played an important role in biosensors over the last three decades [6]. They are advantageous due to their high sensitivity [7], real-time and non-destructive detection. For example, they are able to measure surface concentration of as low as 10^{12} molecules/cm^2, which is very low for the medium sized protein avidin [7]. Moreover, they are able to utilize special optical phenomena such as the evanescent wave which is sensitive to sensor-analyte interfaces. This evanescent wave enables surface analysis while excluding the bulk effects to a large extent. Finally, they offer real-time non-destructive analysis of the analyte.

Optical sensors can be subdivided to several types as described below.

1.2.2.1. Absorption

These sensors measure the intensity of absorbed light. The principle is based on the Lambert-Beer law, where the absorbance is proportional to the analyte concentration. Representatives are the UV/Visible spectroscopy and FTIR.

1.2.2.2. Fluorescence

Fluorescent reagents are perhaps the most developed area for biosensors [2]. This type of sensors involves the measurement of fluorescent response upon excitation.

1.2.2.3. Light scattering

There are many scattering modes, such as Rayleigh scattering, Rayleigh-Gans-Debye scattering, and Mie scattering. Many sensors involve light scattering and take advantage of the laser light. Normally, static and dynamic light scattering modes are used and the latter one is more useful in biosensors [2]. One representative is the Raman spectroscopy.

1.2.2.4. Reflectance methods

Reflectance sensors are based on the evanescent wave, which is created by total reflectance of incident light. Total reflectance occurs when a light wave travels from a medium with higher refractive index to lower one, e.g., from glass to air, with high incident angle.

Refraction is described by Snell's law,

$$\sin \theta_1 / \sin \theta_2 = n_2 / n_1 \qquad (1.3)$$

When a light wave travels from n_1 (the prism with higher refractive indices) to n_2

(air), the angle of refraction θ_2 is bigger than the angle of incidence θ_1 (**Fig. 1-4**a,b). A critical angle of incidence θ_c exists which makes θ_2 equal to 90 degrees. The light wave experiences only internal reflection when $\theta>\theta_c$, i.e., the light is completely reflected inside the prism (**Fig. 1-4**c,d).

Total internal reflection does not mean that there is no energy loss. In fact, it creates a decaying energy field in z direction across the n_2/n_1 interface (Fig.1.4.e). This finite electrical field decays exponentially to the depth of penetration d_p, called the "evanescent wave". By utilizing this evanescent wave, several techniques have been developed, such as Attenuated Total Reflectance (ATR), Total Internal Reflection Fluorescence (TIRF), and Surface Plasmon Resonance (SPR).

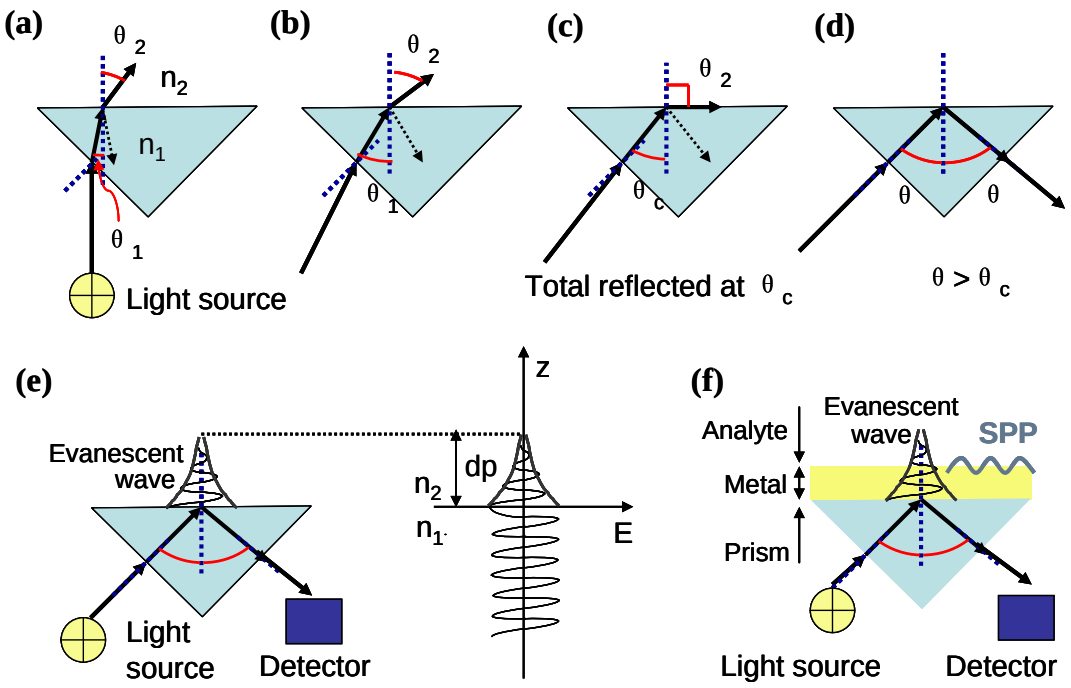

Fig. 1-4 Schematic representative of the phenomena of total reflectance, the evanescent wave, and surface plasmon polarity. (a, b) Light wave experiences reflection and refraction simultaneously at the n_2/n_1 interface; (c, d) Total reflection occurs when angle of incidence θ equals to or is greater than the critical angle θ_c. (e) The evanescent wave is created during the total reflection. (f) A surface plasmon (SP) is excited by an evanescent wave.

In ATR mode, the analyte is passed across and contacts the n_2-n_1 interface. The analyte attaches to the sensor interface, absorbs specific amount energy, and causes the attenuation of the totally reflected light, which is measured and provides signal for analysis. Differing from ATR, in TIRF mode, the signal for detecting is the emitted fluorescence.

Another important reflectance method is based on the surface plasmon resonance (SPR) (Fig.1.4.f), which will be discussed in more detail below.

1.2.3. SPR optical biosensors

SPR optical sensor is usually applied for detecting surface binding of biomaterials. The phenomenon of SPR was explained by Fano in 1941, the excitation of surface plasmons was observed by Powell and Swan in 1960, a famous configuration to realize the excitation was stated by Kretschmann in 1971, and in 1990, Biacore AB fabricated the first commercial SPR instruments [8, 9].

In the SPR method, a thin metal film, such as 50 nm Au, is deposited onto the prism surface (**Fig. 1-4**f). An incident light beam travels inside prism and is totally reflected at the metal-prism interface, which yields an evanescent wave that travels through the Au film. At the boundary of the metal film, electrons behave in a quasi-free manner [2]. They could be excited by the evanescent wave and experience charge oscillation, i.e., the surface plasmon (SP). The surface plasmon extends into space along with evanescent wave. The excitation of SPs occurs when the charge oscillation couples to the component of the wave vector of plane polarized incident light, which is called surface plasmon resonance (SPR). When surface plasmon resonance happens, part of the incident light energy is converted into an evanescent wave and thus decreases the intensity of reflected light. This decrease varies with different incident angles. In most commercial devices, a range of incidence angles are used and a curve of reflectivity *vs.* angle of incidence θ is obtained (**Fig. 1-5**). A resonance dip, where the reflectivity is minimum, occurs at the pseudo-Brewster angle [2], also called “SPR angle”.

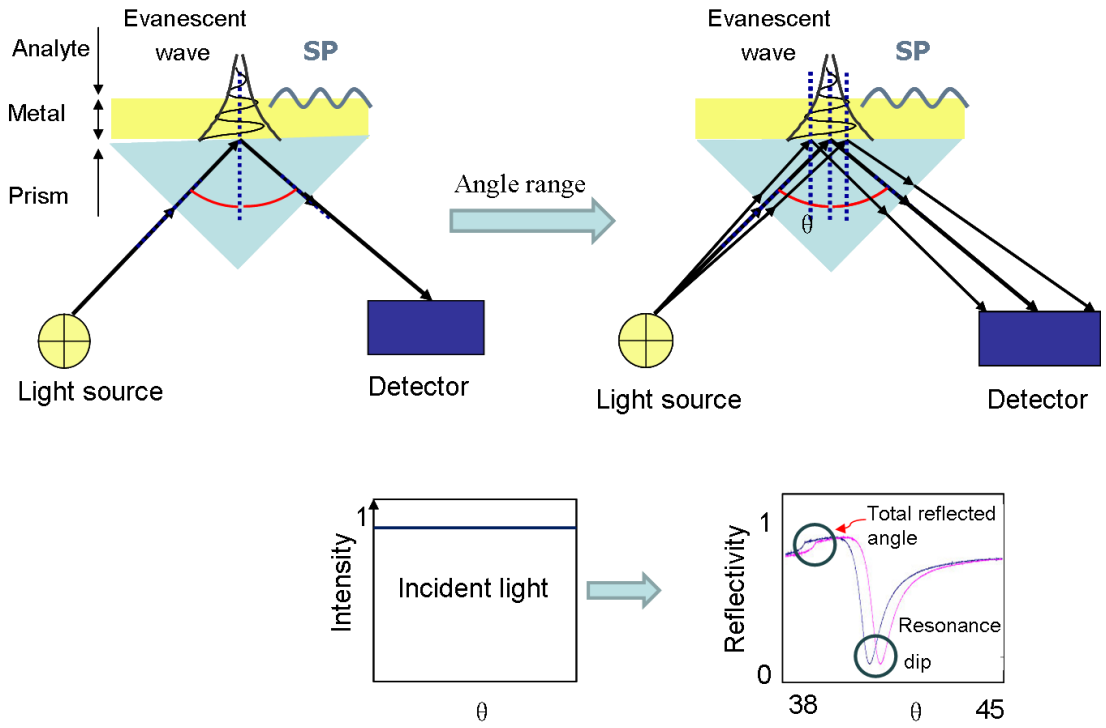

Fig. 1-5 Schematic representative of the working mechanism of SPR.

This resonance dip angle is sensitive to minute changes of the metal-analyte interface, which is determined by the change in refractive index (RI) of the bulk analyte solution, the surface adsorbed bio-materials, and their coverage density and thickness. Normally, 1 $\Delta\theta$ (the SPR angle change)≈ 0.01 RIU (Refractive Index Units) is applied in commercial devices, and 1 RIU≈ 1 μg/mm^2 attachment of protein [10]. RU (resonance unit) is most commonly used and equals 10^{-6} RIU, and thus 1 RU= 0.0001^o, and 1 RU ≈ 1 pg/mm^2 attachment of protein. Instead of reflectivity *vs.* θ curve, the curve of RU *vs.* time usually obtained in a SPR device (**Fig. 1-6**), which can be used to qualitatively and quantitatively analyze the binding of bio-materials in a real-time and label-free manner of detection.

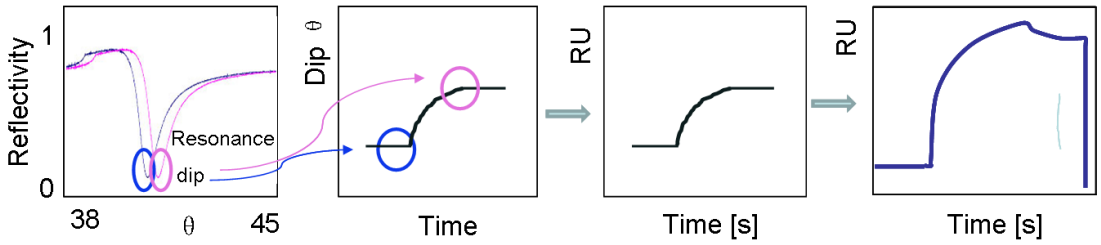

Fig. 1-6 Transformation of the curve of reflectivity *vs* θ into RU *vs* time in SPR device. An example of experimental results is presented in the right side, indicating the association, dissociation, and regeneration processes.

1.3. Sensor recognition elements

Recognition elements are very important for sensors. The functional interfaces on the recognition element make the sensor work specifically for one or group of analytes, or at least selectively respond to one analyte more than other species. An example is that the membrane in ion-selective electrode enables the specific response to certain ions. In the biosensor area, recognition elements could be enzymes, anti-bodies, bacteriophages, receptors, and nucleic acids. It is the bio-materials used as recognition elements that make biosensors differ from chemical sensors. Sensors can be divided based on different recognition elements (**Fig. 1-7**).

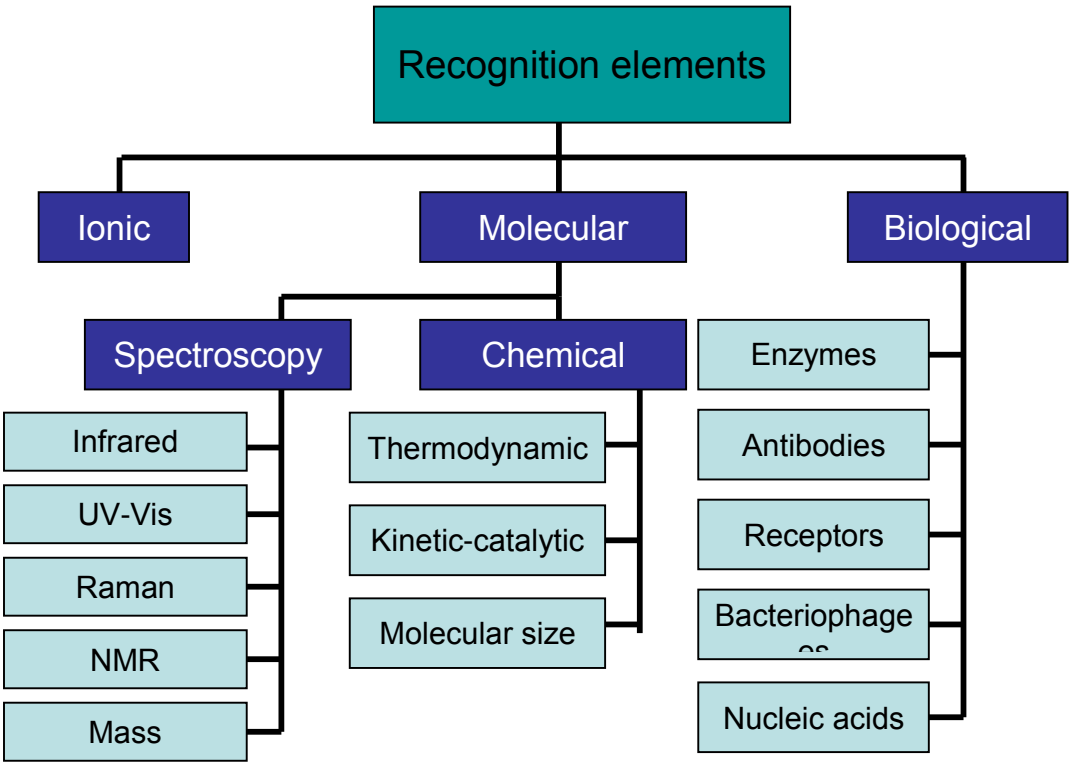

Fig. 1-7 Classification of sensors based on the type of recognition element [2, 3].

1.3.1. Functional interfaces and recognition elements

Since the recognition elements work based on the interaction of the sensor surface with the analyte, the initial or additional functional interfaces are key important. The ion-selective electrodes that were just mentioned is an example, where the functional interface involves a membrane with affinity to specific ionic species. The electrodes work based on the relationship between the electromotive force (*emf*) and the analyte concentration. The internal solution contains certain ions and electrodes which respond to a specific group of ions in the analyte solution. The membrane acts as a separator to those two solutions and affords the function of ion-selectivity.

For ionic recognition elements, surface modification is widely used. Although it is possible to discriminate species by detecting their redox potentials with bare electrodes, some strategies could enhance the selectivity much. One approach is to introduce the functional interfaces, usually via electrode surface modification with

polymers or composites. These modifiers mainly include conducting polymers, permselective polymers capable of size selectivity, metallic polymers, and polymer based composites. Moreover, polymer modification helps avoid problems that may occur at bare electrodes, such as electrode fouling during electrochemical analysis of phenolic compounds.

In molecular recognition elements, molecular size is a simple basis of selectivity, and molecular sieves work in this way. Sieves with different pore sizes allow molecules in specific size range to pass, while block others.

Spectroscopy is a molecular recognition technique with a wide range of applications. Provided with incident light beam, molecules may specifically absorb certain wavelengths of light by molecule vibration, rotation, or electron excitation to higher energy level, which is the mechanism of infrared, Raman, and UV-Visible spectroscopies. Nuclear Magnetic Resonance Spectroscopy (NMR) works via the interaction of nuclei with magnetic field. In its most basic application, NMR is used for discriminating Hydrogen atoms in different atmospheres such as the saturated group $-CH_2-$ from the less saturated =CH-. Carbon based NMR is also available. Mass Spectroscopy is a powerful technique which appears usually in the combination of GC-MS (gas chromatography- mass spectroscopy). It works by discriminating different mass/charge ratios of fragments created via electron beam ionization.

Compared to chemical sensors, biosensors are advanced mainly in terms of the specificity and selectivity with the help of bio-functional interfaces. Enzymes, the most used type of biomaterial, have much higher selectivity and velocity than chemical catalysis in terms of catalytic effect. Antibodies respond specifically to corresponding antigens. Bacteriophages affect specifically to one strain of bacteria. For optimal usage of biomaterials, immobilization on sensor surface is a key process and has been widely studied. Functional interfaces provide optimal platforms for immobilization of desired biomaterials and can be built via physical adsorption, including electrostatic and hydrophobic interactions, covalent binding, and specific interactions such as avidin-biotin, antigen-antibody and DNA hybridization [11, 12].

1.4. Electrochemical sensor for detection of TCP

1.4.1. Introduction of TCP.

Tricresyl phosphate (TCP) is an organophosphate that is an ester of phosphoric acid and cresol. Since cresol has 3 isomers (**Fig. 1-8**), specifically, *ortho*-, *meta*-, and *para*- types, there are 10 isomers of TCP from different combinations. They are divided into *o*- isomers and *m*-/*p*- isomers. *o*- isomers include tri-*o*-cresyl phosphate, di-*o*-cresyl-mono-*m*-cresyl phosphate, di-*o*-cresyl-mono-*p*-cresyl phosphate, mono-*o*-cresyl-di-*m*-cresyl phosphate, mono-*o*-cresyl-di-*p*-cresyl phosphate, and mono-*o*-mono-*m*-mono-*p*-cresyl phosphate. *m*-/*p*- isomers include tri-*m*-cresyl phosphate, di-*m*-cresyl-mono-*p*-cresyl phosphate, di-*p*-cresyl-mono-*m*-cresyl phosphate, and tri-*p*-cresyl phosphate. Two examples of TCPs are shown in **Fig. 1-9**.

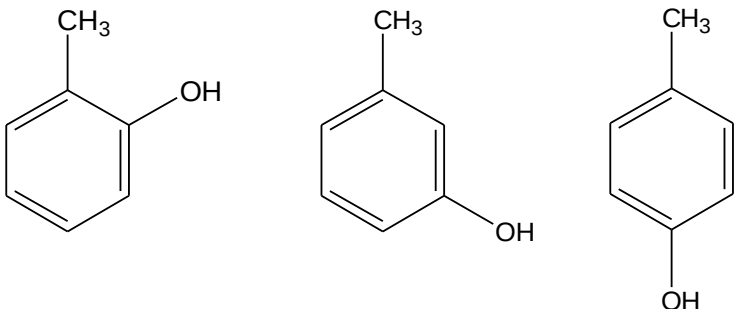

Fig. 1-8 Chemical structures of *o*- (left), *m*- (center), and *p*- (right) cresols.

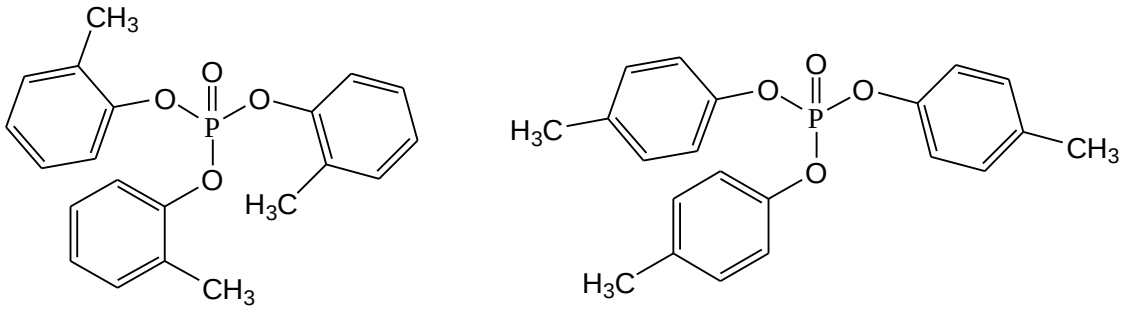

Fig. 1-9 Chemical structures of tri-*o*-cresyl phosphate (left) and tri-*p*-cresyl phosphate (right).

Organophosphates are well known as neurotoxins. Their acute toxic effects are due mainly to the inhibition of acetyl- and butyryl-cholinesterases. As one kind of organophosphate, TCP not only inhibits cholinesterases, but also can induce a delayed neurodegenerative condition known as organophosphorous-induced delayed neuropathy (OPIDN) [13-17]. Effects might not be expressed until a week or two after exposure. Acute exposure induces nausea, vomiting, diarrhea and abdominal pain followed by a long asymptomatic period of up to a month. Bilateral degeneration of sensory and motor functions follow acute toxic exposure, and the chance of recovering full motor coordination is poor. Because of its higher neurotoxicity, the *o*-isomers of TCP are intentionally excluded from commercial products [18]. That is the reason why tri-*p*-cresyl phosphate is chosen to be the object analyte in this dissertation.

Regardless of its acute toxicity, TCP is heavily used in many industrial applications, such as fluid additives, plasticizers, and flame retardants. The US Air Force has employed hydraulic fluids containing organophosphates since the 1970s in its high-performance aircraft [19]. Over the past 30 years, 3wt% tricresyl phosphate has been added into some commercial jet oils, such as Mobil Jet Oil [20]. Although some amount is decomposed during use [21], the remaining TCP could be released into the cabin air environment during oil leakage on aircraft hydraulic systems [22]. Exposure to passengers occurs mainly through ingestion, inhalation of aerosols, and dermal sorption. Recently, there are increasing concerns regarding some highly publicized incidents, in which illness of flight crew members and passengers have been attributed to possible exposure to jet engine oils containing tricresyl phosphate (TCP) entering the cabin air through the aircraft bleed air systems [23]. The possible pathway of TCP entering cabin is shown schematically in **Fig. 1-10**.

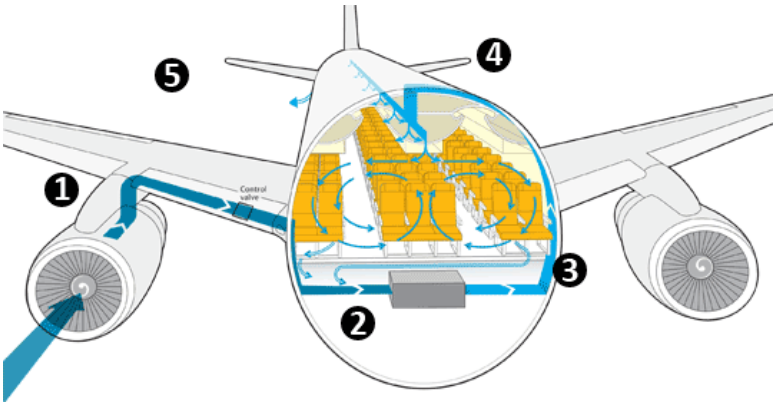

Fig. 1-10 Schematic representation of air circulation in aircraft cabin. Air is 1) bled in through engine; 2) filtered; 3) combined with recirculated air; 4) flowed into cabin; 5) released for maintaining the pressure. TCP may enter cabin along with bleed in air during oil leakage in engine. Picture from http://informer.truth.travel/

1.4.2. Current trends in TCP detection.

Determination of TCP can be divided into two different groups of methods, mostly distinguished by whether or not the TCP chemical structure is destroyed during analysis. The destruction of TCP by basic hydrolysis results in the appearance of cresols and phosphate ions. In general, the hydrolysis of TCP is demonstrated in Equation 1.4,

$$OP(OC_6H_4CH_3)_3 + 3NaOH \rightarrow Na_3PO_4 + 3HOC_6H_4CH_3 \qquad (1.4)$$

The hydrolysis yields three molecules of cresols and a phosphate ion from one molecule of TCP, and after the hydrolysis completes, either product can be determined. TCP can also be detected without any preliminary modification by chromatographic methods. The most commonly used methods for the detection of TCP include highly sensitive gas chromatography (GC) with a nitrogen-phosphorus sensitive detector (GC/NPD), a flame photometric detector (GC/FPD) [24] or mass spectrometric (MS) recognition [25], high-performance liquid chromatography (HPLC) [26] and thin-layer chromatography (TLC) [27]. Although they are able to

detect TCP below ppm level and with high selectivity, these devices have several drawbacks, such as large size, high cost, complexity, and a need for highly-trained operators, which make their use on aircraft impractical. Thus, a sensitive, easy to use, and rapid sensing system for TCP detection and monitoring might be useful in a large number of applications. Electrochemical detection can avoid the mentioned drawbacks for chemical analyses and offers considerable promise for micro-fabricated systems with features that include high sensitivity, ease of miniaturization, and low cost. Since TCP itself is electrochemically inactive, it is hydrolyzed to phosphate ions and cresol with the aid of an alkaline catalyst, as shown in equation 1.4 [28-32]. Cresol is detected electrochemically. However, this method brings the problem of electrode fouling, which will be discussed that follows.

1.5. Electrode fouling during electrochemical analysis of phenolic compounds.

1.5.1. Introduction to phenolic compounds

Phenolic compounds, such as phenol and cresol, have great importance in industry and are chemical pollutants widely presented in the atmosphere, water systems, and many food products [33-37]. Industries where phenolic compounds appear, in the wastewaters or else, include coal conversion, petroleum refining, pharmaceuticals, production of dyes, pesticides, surfactants, resins, and plastics [38-41]. Phenolic compounds are also found in smoke of cigarettes [41, 42]. They can be easily absorbed by animals and humans through the skin and mucous membranes, affect many organs, such as primarily lungs, liver, kidneys, and genitourinary system [43, 44], and are also toxic to plants [43]. Many of them are known for persistence in environment, reacting with chlorine during water treatment, and biomagnifications [38, 45-48].

Many phenolic compounds need to be discussed. Chlorinated phenols (CPs) (e.g., 2-chlorophenol, 2,4-dichlorophenol, 2,4,6-trichlorophenol, and pentachlorophenol), nitro-phenols (NPs) and amino-phenols (APs) present widely in the atmosphere wastewater, rivers, ground water, and pesticide treated soil [49-52]. They are highly

toxic and belong to priority pollutants classified by the Environmental Protection Agency (EPA) [53]. The limit of *p*-Nitrophenol set by European Commission is 0.1 ppb in drinking water [54, 55]. The accumulation in fish and other organisms increase their hazardous characteristics [49]. Bisphenol A (BPA) is commonly used as monomer in the production of polycarbonate plastics. Phenolic compounds also present in cells, such as dopamine (DA). It is one of important neurotransmitters in the function of central nervous, and usually coexists with many interfering compounds [56-58]. The chemical structures of some phenolic compounds are shown in **Fig. 1-11**.

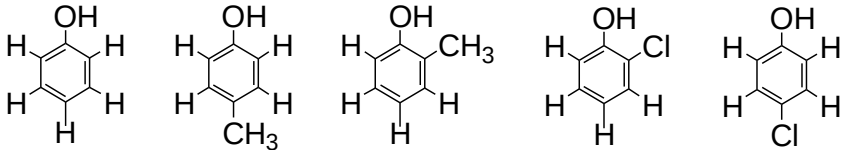

Fig. 1-11. Chemical structures of phenol, *p*-cresol, *o*-cresol, *o*- chlorinated phenol, and *p*- chlorinated phenol (from left to right).

Therefore, the reliable, effective, and quantitative determination of phenolic compounds is very important and has long been of interest [33, 34]. Many technologies have been used for determination of phenolic compounds, such as gas and liquid chromatography [59-62], spectroscopy [54, 63], and calorimetry [64]. However, they suffer from time consuming, low sensitivity, need of preconcentration, need of skilled operator, or high cost [41]. Electrochemical sensing provides an alternative technique. Most phenolic compounds can be easily electrochemically oxidized [34]. However, electrode fouling (electrode passivation) is one prime problem for electrochemical methods, as well as in battery area, when phenolic compounds are electrochemical oxidized [65-72], especially with high concentrations [34] and for the usage of solid electrodes, such as Pt, Au, Ag, Cu, Zn, Fe, Ni, Cr, and Ti [66, 67, 73, 74].

Electrode fouling means the occurrence of the current decay during repetitive scans, continuous flow, or injections of samples. It is often caused by the formation of

a passivating polymeric film on the electrode surface due to the electropolymerization of phenolic compounds [65, 66, 75, 76]. In some cases, this polymeric film can act as a protective coating, such as preventing metals from corroding [65, 66, 69, 77-81]. However, the fouling is always a problem in electrochemical measurements and delays important electrode processes [65, 66]. For example, it leads to a slow reaction rates during the treatment of wastewater [82, 83] or the synthesis of quinines [84]. Sometimes this problem can be lightened by applying higher over-potential, but it leads to lower efficiency on power usage and obstacles for commercial production [83].

1.5.2. Chemical reactions during anodic oxidation of phenol

To understand the electrode fouling, it is necessary to consider the chemical reactions that happen during anodic oxidation of phenolic compounds. Phenol will be discussed as a representative, which behaves similar as cresol. The oxidation of phenol is a complex process [65, 85-89]. When a positive potential is applied, one electron and one proton are deprived and phenol is oxidized to three types of phenoxy radical intermediates with a free electron on the oxygen atom, two identical *o*-sites, or *p*-site (**Fig. 1-12**, top series) [65, 77, 90]. The factors for each of three types of radicals are: 20% free electron on Oxygen atom, 34% free electron on *p*-site, and 23% free electron on each of two *o*-sites [85]. The chemical reaction continues on two pathways. One possible pathway is that individual radical loses one more electron and proton, and is oxidized to soluble products, such as hydroquinone or catechol, followed by losing two more electrons and protons, and is finally converted to benzoquinones (**Fig. 1-12**, left dashed box) [91, 92]. One alternative pathway, which occurs often, is the irreversible combination of two radicals and forming five different possible dimeric products (only two of them are shown representatively in **Fig. 1-12**, right dash box) [65, 77, 85]. The dimerization occurs due to the existence of high density of free electrodes, or unpaired electrodes [93]. This coupling can be realized by C-O-C binding, which results in the formation of ether, or C-C binding, which results in the formation of dimer. Dimeric ethers are produced in low yields in normal

conditions or acidic solutions, but are favored in alkaline solutions or for phenolic derivatives with high steric factors [93, 94]. In conclusion, the phenolate anion is oxidized to a free phenoxy radical, which is then oxidized to soluble products or coupled rapidly and irreversibly to dimeric products.

Compared to phenol, the dimeric substrates can be considered as a derivative from phenol with one additional branch group. The difference in molecular structure gives a lower oxidation potential for dimerics than phenol [77]. Apparently, the dimerics are readily oxidized to radicals, the same as what phenol has experienced. Both radicals from phenol and dimerics can undergo coupling to form new dimers or oligomers, adding one or multiple phenol units to existing oligomers, or the cross linking of polymer chains. A polymeric structure will be formed by further chain elongation and cross linking and contains the ether, hydroquinone, and benzoquinone type of structures [75, 79, 95]. While the polymeric film may experience further oxidation even leading the formation of CO_2 if high enough potential is applied [70], most of the time, the polymeric film along with dimers and oligomers will be attached onto electrode surface, and creates the electrode fouling.

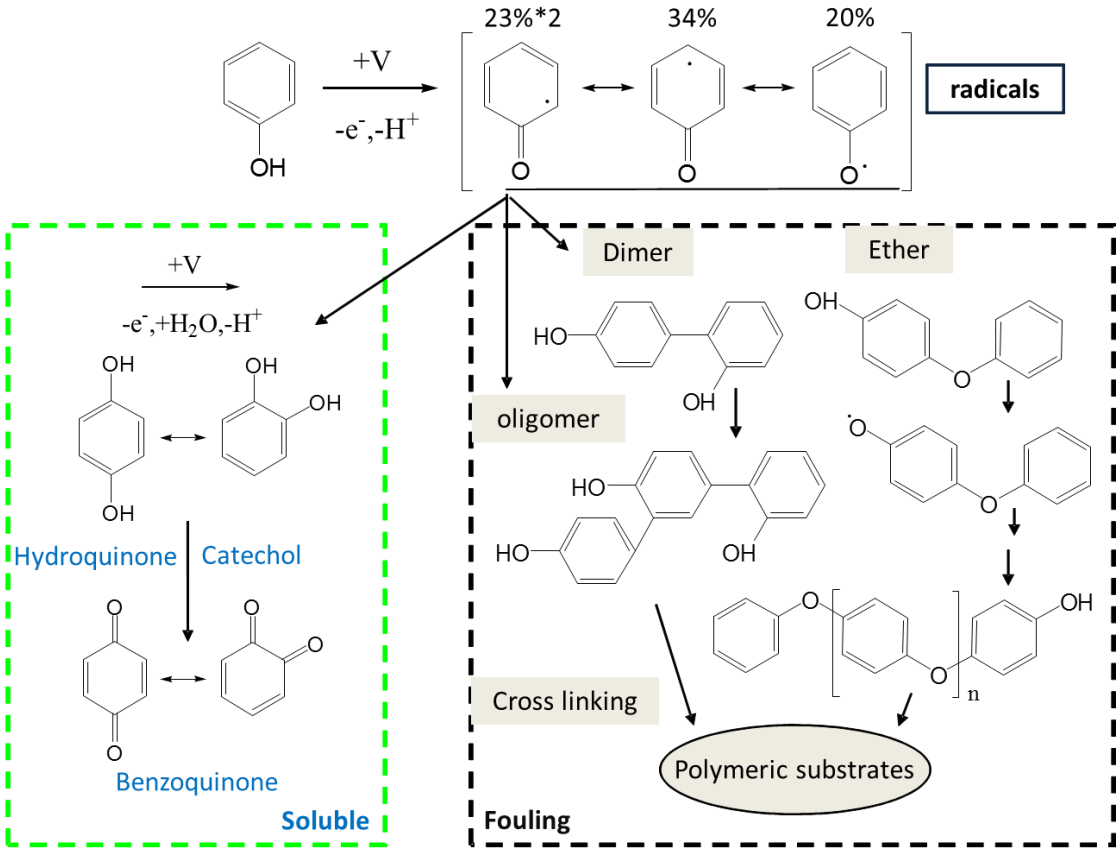

Fig. 1-12 Schematic representative of the chemical reactions that occur during the oxidation of phenol.

1.5.3. Properties of the polymeric film and its effect on electrochemical analysis

Many efforts have been made to study the chemical and physical properties of the polymeric film, sometimes called “tars” , that forms during the anodic oxidation of phenols and its effect on electrode performance [65, 68, 69]. Briefly, this film is tough, low permeability [96], thermally stable, and so chemically inert that little further oxidation or hydrolysis occurs in either acidic or basic media [69]. Consisted of high molecular weight species, this coherent film adheres tightly to the electrode, which results in the electrode fouling [68, 70-72, 94].

The technologies that have been used include gel permeation chromatography (GPC) [77], gas chromatography with mass spectrometry detection (GC-MS) [94], Fourier transformed infrared spectroscopy (FTIR) [71, 94], surface enhanced Raman spectroscopy (SERS) [68], X-ray photoelectron spectroscopy (XPS) [66, 77], cyclic

voltammetry (CV) [66, 70, 77, 97], chronoamperometry [66], electrochemical impedance spectroscopy (EIS), electrochemical quartz crystal microbalance (EQCM) [72], ellipsometry [98], and scanning tunneling microscopy (STM) [97],

Studied physically with GPC, Glarum found that the polymeric film produced from substituted phenols in alkaline medium consisted of materials with high molecular weight ~8000 g/mol after 5 min of fouling, and contained mainly the ether linkage [99]. Gatrell and Kirk invested the polymeric film created from phenol oxidation in acidic media and observed the average molecular weights around 1000 g/mol after less than 0.1 s of oxidation and it was not a simple linear structure [77].

With GC-MS, Ezerskis and Jusys stated that the polymeric film includes not only high molecular weight mixtures but also low molecular weight oligomers, such as dimers, trimers, and tetramers [94]. The mass spectra revealed the ether-linked structure existing in the polymeric film.

Based on FTIR results, the properties of the polymeric film were reported , such as the chemical structures. Mourcel stated that -OH groups and intramolecular hydrogen bonds ceased to exist after polymerization which indicated C-O-C bonds were formed [80]. Gatrell and Kirk investigated the electropolymerization of phenols in acidic medium and found that the connections between each of the two phenol rings were mainly C-C bonds along with some C-O-C bonds [77, 85]. Glarum et al. reported a head to tail coupled structure existing in the film produced from 2,6-dimethylphenol (DMP) in a NaOH medium [100]. Ezerskis and Jusys [72] confirmed the oxidative coupling of phenolic monomers by observing the aromatic structure in the high molecular weight polymeric film. The C-O-C bond coupling of phenol radicals in 1 M NaOH solution was suggested by the observation of ether bond vibration and no hydroxyl group vibration. Further oxidation to quinone and other saturated species from phenols is revealed by IR spectra [72]. Dubois et al. reported that the polymeric film adhered perfectly to the anode surface [80, 91].

The Raman spectroscopy gives the information about bonds and orientation, and the finger printing of the species by their vibration spectra. Using Surface enhanced Raman spectroscopy (SERS), Fleischmann studied the polymeric film on a silver

anode [68]. By comparing the spectra of absorbed species within solution, they stated that both phenol and phenoxide were adsorbed in a flat orientation, rather than a perpendicular one, on electrode and formed a highly insulated film.

Using XPS along with amperometry and CV, Gattrell and Kirk investigated phenol electrolysis and the resulting electrode passivation based on the comparison between platinum and platinum oxide electrodes [66]. Based on their analysis, phenol electrolysis led to the formation of successive films. Closer to the electrode surface, a blocking film of high molecular weight (MW) unreactive substrates were created. While in further distances, a low MW, more reactive bulk film was created. This blocking film closer to the electrode surface mainly contributed to the fouling. Initially, the phenol oxidation current was mainly contributed by outer Helmholtz layer (OHL) reactions which led to the formation of quinones and polymeric substrates. Following the formation of polymer that was hard to further oxidize, the outer Helmholtz region was partially blocked. The reaction in bulk solution continued as long as electrons could tunnel to the electrode surface, the distance of which could be 2 nm [101]. Thus, electron tunneling was the rate determining step during the electrode passivation. As the blockage in the outer Helmholtz region slowly increased, the initially slower inner Helmholtz reactions eventually dominated the current flow. The residual current at the passivating electrode came from reactions happening via electron tunneling through the blocking film or the slow reaction of the blocking film itself [77].

CV was carried out in many papers in order to study the mechanism of phenol electropolymerization and subsequent electrode passivation. Ezerskis and Jusys [70] investigated the oxidation of different phenols on Pt electrode in 1 M NaOH solutions containing 0.1 M phenol or its derivatives. They observed a decrease in oxidation current on the fouled Pt electrode. After electrode passivation, some residual currents exist which may come from the inner Helmholtz layer reactions.

EQCM was used by Ezerskis and Jusys in order to study the electropolymerization kinetics [72]. As a mass sensitive probe, it was used to distinguish among the formation of polymerization, deep oxidation to an open ring

structure, and the formation of soluble products during the oxidation of phenol. Since the polymeric film attached rigidly to electrode surface [73, 102], The attachment increased the electrode mass and decreased the resonant frequency. The relationship between the charge flow and total increase in electrode mass was monitored, and the number of electrons transferred was reported to be ~ $2e^-$ per monomer molecule in most cases. Among the different derivatives, the ones that had a higher degree of chlorination, such as 2,5-dichlorophenol, led to the formation of easier permeable films and higher electropolymerization rate.

Using ellipsometry, Babai and Gottesfeld studied the growth of the polymeric film [98]. The growth rate was found to be inversely proportional to the square root of time and varied with applied potential. The rate-limiting step was considered to be the charge diffusion.

Using STM incorporated with an electrochemical cell, Wang investigated the influence of several parameters on the growth pattern, surface microstructure, and degree of passivation of the polymeric film [97]. He found that the formation of this film was strongly dependent on the anodization conditions. After one CV scan at a lower scan rate such as 5 mV/s in the presence of 1 mM phenol, large scattered aggregates such as mountains and valleys were observed, while at higher scan rates, such as 50 mV/s, the structure was smoother or fibrous with lower but sharper hills. Amperometry process, using a mass transport limited potential, had different results from the CV scans. A wave-shape folded layer structure was formed by applying amperometry process on the electrode in the same phenol solution. Basically, potential scan yielded the nucleation-and-growth process and discrete aggregates, while amperometry yielded layer-by-layer growth and a more uniform film. Inevitably, the difference in film structure influenced the fouling effect and hence the electrochemical response. Other fouling factors such as phenol concentration, solution pH, phenolic compounds, and electrode materials also affected the formation of fouling layer.

One interesting point was the estimation of the thickness of polymeric film by measuring the electric charge flow [97]. In one experiment, the charge was measured

to be 225 μC which corresponded to ~13 layers (bond lengths were used to estimate the size of unit cell which was attached flat to 5 mm-diameter electrode surface). The thickness was estimated to be 13*0.4 nm ≈ 5 nm. The thickness was too high for pure electron tunneling which suggested the discontinuous nature of the film.

1.5.4. Application of functional interfaces on anti-fouling modifications.

Since the electrode fouling during the electrochemical analysis or disposal of phenolic compounds was a common problem, many efforts have been made in order to alleviate this problem. Introduction of functional interfaces for electrode surface modification was an important approach. These functional interfaces were expected to prevent polymeric substrates from adsorbing onto the surface of electrode, or form soluble complexes with polymeric substrates.

1.5.4.1. Polymer modifications

Electrodes modified with polymers, especially conducting polymers, have attracted considerable interest in recent years. Conducting polymers were used in many applications of energy-conversion devices [103], electro-oxidation [104], and sensors [105]. Conducting polymers, Such as polypyrrole, polyaniline, polythiophene, polyazulene, and their derivatives, had the advantages of high electronic conductivity and high porosity [45]. Modification of conductive polymer to prevent electrode fouling has been reported by many researchers [106-109].

Poly(3,4-ethylenedioxythiophene) (PEDOT) was one of widely used conductive polymers. Patra studied the oxidation of phenol on a stainless steel (SS) anode modified with PEDOT in acid solution [45]. A stainless steel foil with a thickness of 0.2 mm was used as the anode and was dipped in the electrolyte including 0.1 M H_2SO_4, 0.01 M Ethylenedioxythiophene (EDOT), and 0.01 M sodium dodecylsulphate (SDS). 0.7 C cm^{-2} charge was passed at constant potential of 0.9 V *vs.* SCE. The PEDOT modified stainless steel electrode had a slower fouling compared with the Pt electrode, and the current responses increased linearly for 0.005

to 0.5 M phenol.

Heras modified a Pt electrode with the composites containing PEDOT and different surfactants for the detection of phenol. The addition of a surfactant improved the reproducibility of responses. The electropolymerization was achieved by applying 3 mC charge in potentiostatic mode on a Pt disk working electrode which was immersed in $LiClO_4$ acetonitrile solution. Poly(sodium-4-styrenesulfonate) (NaPSS) behaved the best out of other surfactants including polyethylene glycol mono[4-(1,1,3,3-tetramethylbutyl)phenyl] ether (Triton X-100), dodecylbenzenesulphonic acid sodium salt (SDBS), and dodecyl trimethylammonium bromide (DTAB). The hydrophilic groups in the surfactant that was incorporated in the composite modifier dramatically reduced the electrode fouling. with square wave voltammetry (SWV) method, A linear calibration was obtained for 1-500 ppm phenol in aqueous solution [33].

The behavior of PEDOT/NaPSS modified Pt electrode to chlorinated phenols (CP) has been studied with techniques of EIS, EQCM, and AFM. It was shown that the film formed during the oxidation of CP on PEDOT/NaPSS modified Pt electrode had high (ionic) conductivity and permeability towards CP molecules, thus CP could enter the charged film and be oxidized inside. The formed cations could permeate through the film and realized the electroneutrality. The NaPSS played a crucial role in avoid ing fouling on PEDOT modified Pt electrode during CP oxidation [49].

Lupu modified a Pt electrode with the composites of PEDOT and PB. The organic component, PEDOT, acted as a permselective membrane or a stable matrix, while the inorganic transition metal hexacyanoferrate, PB, was a redox mediator [38]. This hybrid inorganic-organic modification was prepared in two steps. First, the electrode was immersed in 0.01 M 3,4-Ethylenedioxythiophene (EDOT) and 0.1 M $K_3[Fe(CN)_6]$ and applied by potential sweep from -0.6 to 1.0 V vs Ag/AgCl for five cycles, which resulted in the formation of a Pt/PEDOT-FeCN modified electrode. Then, this modified electrode was immersed in 0.01 M $FeCl_3$, 0.1 M KCl, and 0.01 M HCl and scanned from -0.2 to 0.6 V for 5 cycles at a scan rate of 0.05 V/s, resulting in the formation of PB inside the PEDOT matrix and finally the formation of a

Pt/PEDOT/PB modified electrode. This modified electrode had a linear current respond to 2-100 μM dopamine, a correlation coefficient R^2 of 0.996. The sensitivity was 0.12 μA/μM, and the detection limit was 25 μM.

A polypyrrole (PPy) plus *o*-amino-benzenesulfonic acid (*o*ASA) modified Pt electrode was prepared to avoid fouling from phenol oxidation [34]. *o*ASA was used because its hydrophilic groups made the polymeric products deposit harder. The electrode was immersed in a polymerization solution of 0.1 M oASA and 0.2 M pyrrole, and applied current of 2.0 mA/cm^2 in galvanostatic mode for 2 minutes. With this modified working electrode, no significant difference was observed in 20 successive cycles of CV scan of 1 mM phenol in 0.1 M HCl. In amperometry analysis, the linear concentration range of phenol was up to 0.1 mM (~10 ppm the mass ratio to water). The estimated detection limits were 50 ppb for direct current (DC) amperometry and 10 ppb for pulse amperometry, with the R^2 of 0.998 and 0.999, respectively. And the current response for phenol oxidation was reduced to ~0.4 times of bare electrode.

Another widely used polymer was Poly(N-vinylpyrrolidone) (PNVP) since it formed complexes with phenolic compounds. Wheeler coated a PNVP film on an electrode surface by gamma irradiation and characterized this modifying effect on detection of phenol derivatives with voltammetry [110, 111]. Less evident fouling on PNVP-coated electrodes was observed from the oxidation of phenolic compounds than bare graphite electrodes. The mechanism of anti-fouling was discussed by comparing the behavior for different phenolic compounds. Comparing with the bare electrodes, although the modification decreased the oxidation current for tyrosine, it didn't change or even increased the current for methoxyphenols such as eugenol and Homovanillic acid (HVA). One possible reason was the formation of multiple products due to the modification. Sufficient evidences showed that PNVP modification prevented the fouling under certain conditions [112], although the deeper understanding was still in need.

A poly(2-[(E)-2-azulene-1-ylvinyl]thiophene) (PAVT) modified Pt electrode was prepared to detect phenol. Pt electrode was immersed in acetonitrile containing 1 mM

AVT [prepared following literature], 0.1 M TBAT4S, and applied by 10 CV cycles from -0.6 to 1.2 V with the scan rate of 50 mV/s. The good electroactivity of PAVT film was due to the high effective conjugation length and high delocalization of π-electrons. This modified electrode was used to detect phenol with SWV. The peak current responded linearly to phenol with 30-100 nM, with a sensitivity of 55 nA/nM and a correlation coefficient R^2 of 0.99. The detection limit was estimated to be 9.8 nM [113].

A Prussian Blue and poly(azulene) modified Pt electrode(Pt/PB/PAZ) was prepared [41]. PB was a dark blue pigment with the formula of $Fe_4^{III}[Fe^{II}(CN)_6]_3$. This ferric ferrocyanide could be made from potassium ferrocyanide and iron(III). First, The platinum disk electrode was immersed in a solution of 1 mM $FeCl_3$, 1 mM $K_3Fe(CN)_6$, 0.1 M KCl, and 0.01 M HCl, and 8 cycles of CV from -0.2 to 1.0 V at the scan rate of 50 mV/s were applied to deposit a layer of PB. Then, Pt/PB was immersed in 1 mM azulene and 0.1 M tetrabutylammonium-toluene-4-sulfonate (TBAT4S) -CAN and applied by 3 cycles of CV from -0.6 to 1.2 V at 50 mV/s. In the determination of phenol, this modified electrode Pt/PB/PAZ had a sensitivity of 22 μA/nM and responded linearly in current to 10-100 nM phenol in 0.1 M PBS (pH=6), with the R^2 of 0.991 [41].

Some other metallic compounds have also been used. The transition metal Schiff bases, porphyrins, and phthalocyanines could be used as an electrocatalytic membrane in CV measurements due to their redox properties [114]. Metallophthalocyanines (MPc) were complexes of metals and Phthalocyanines, i.e. the macrocyclic compounds, and widely used in dyeing [115]. MPc modified electrodes showed good electrocatalytic activity towards a wide range of chemical substances [116-119]. In particular, Ni(II) macro complexes offered efficient electrocatalytic activation for phenols usually due to the structure of the ring substituent on the phthalocyanine macrocycle and the creation of coordinating O-Ni-O oxo bridges [114, 120-125].

A nickel tetraamino phthalocyanine (Ni(II)TAPc) modified gold electrode was developed to detect Bisphenol A [35]. The modification was done by electropolymerization of NiTAPc (prepared following literature [126]) in

dimethylformamide (DMF) with CV scans at a constant scan rate of 0.1 V/s. The thickness of the modifier was controlled by the number of scans and influenced the anti-fouling effect. It was found that the modification from 70 scans yielded the highest sensitivity for Bisphenol A analysis. One more step was done to the Ni(II)TAPc modified electrode. Immersed in 0.1 M NaOH medium, It was applied with CV cycles between -0.2 and 1.0 V to create an 'O-Ni-O oxo bridge' from poly-NiTAPc. Then this further modified electrode was represented as poly-70-Ni(OH)TAPc-Au, for example, where 70 represents the number of scans. This modified Au electrode was able to detect Bisphenol A in the concentration range of 0.7 to 30 mM, with the limit of detection of 3.7 nM and the sensitivity of 326 μA M^{-1} cm^{-2} [35].

Poly(nickel hydroxyl tetraphenoxypyrrolephthalocyanine) (poly-Ni(OH)TPhPyPc) modified vitreous carbon electrodes were developed to detect phenol. The electrode was immersed in dichloromethane containing 1.5 mM NiTPhPyPc (prepared following literature [127]) and 0.1 M tetrabutylammonium tetrafluoroborate (TBABF4), and was applied with 20 CV cycles from -0.6 to 1.2 V vs. Ag/AgCl. Then, $[poly\text{-}NiTPhPyPc]_{20}$ modified electrodes were immersed in 0.1 M NaOH solution and scanned 37 times in CV from -0.1 to 1.1 V to create the O-Ni-O bridge. In the analysis of 0.7 mM phenol, the oxidation peak in CV curve with the modified electrode shifted ~-0.06 V comparing with unmodified electrode due to the catalytic effect of the modifier. And the modified electrode showed a recovery of 92% in current response after 5 hr, while no recovery for unmodified electrode [114].

A poly(propyleneimine) (PPI) and gold nanoparticle (AuNP) modified glassy carbon electrode (GCE) was prepared to detect *o*-Nitrophenol (*o*-NP) [48]. GCE was immersed in PBS solution at pH 7 containing 5 mM Generation 2 PPI and 2.5 mM $HAuCl_4$, and applied 10 cycles of CV from -0.35 V to 1.1 V. The modified electrode GCE/PPI-AuNP was used to detect *o*-NP with CV, SWV, and differential pulse voltammetry (DPV). The linear current response was obtained to *o*-NP in the concentrations range of 0.61 to 625 μM and the detection limit was estimated to be 0.45 μM [48].

Permselective polymer films films have highly ordered array of pores inside with controllable pore sizes. The advantage of size-selectivity enabled the permeability toward anions, cations, and neutral species, which can be controlled by altering electrolyte concentration [128]. This kind of polymer can be the modifiers to prevent electrode fouling and are useful in the area of electroanalysis and catalysis [129-131].

Using topology hexagonal liquid crystalline phases (H_I) template, Elliott modified 1,2-diaminobenzene polymer film on both glassy carbon electrode and gold electrode. The film contained an ordered array of uniform pores extended over a hexagonal lattice. Electrodes were immersed in an $C_{16}EO_8/H_2O$ solution (1:1, w/w, to create the H_I phase) that contained 10 mM 1,2-diaminobenzene and 0.1 M KCl, and then placed in oven at ~45 ^oC. Eight CV scans from 0 to 1 V vs SCE at 50 mV/s were applied for electropolymerization. This polymer film suppressed the transport of negatively charged ions by charge repulsion, while didn't affect the permeation of cations with similar size. Moreover, the permselective behavior could be controlled by changing the electrolyte concentration. The mentioned type of modified electrode led less susceptibility to electrode fouling [132].

1.5.4.2. CNT and CNF modifications

Carbon nanotubes (CNT) are allotropes of carbon with a cylinder structure. Due to the unusually high length-to-diameter ratio, they have unique electronic, mechanical, and structural properties [133-136]. Defects exist frequently on the edge-plane of CNT surface, which break the carbon bonds and enhance the electron transfer [137-139]. As a good modifier, CNT can notably enhance the electroanalytical characteristics of the electrodes in terms of higher sensitivity, lower oxidation potential, and impeding fouling [28, 133]. One critical issue for the usage of CNT is its dispersion. Two main approaches are (1) functionalizing CNT wall or ends to increase its attraction with solvent and (2) choosing a specific solvent such as some types of polymer solution.

CNT were usually dispersed in Nafion [81, 140, 141] or polyethylenimine (PEI) [133]. PEI contains high density of amine groups which is capable of electron donating. Adsorbed irreversibly onto the side walls of CNT, PEI made CNTs become n-doping and brought good dispersion [133]. Nafion is a sulfonated tetrafluoroethylene based fluoropolymer-copolymer. It is characterized by unique ion-exchange and biocompatibility properties and has been used extensively for the electrode modifications [140]. The polar side chain in Nafion promotes the dispersion of CNT. CNT has also been mixed inside the composite which consists of the electrode substrate. Prasad fabricated a class of composite electrodes, which was made of sol-gel ceramic and CNT, to detect DA [142].

Multi-wall carbon nanotubes (MWCTs) in PEI modified glassy carbon electrodes (GCE) has been developed to detect phenolic compounds [133]. The modifier was 1 mg/mL MWCTs and 1 mg/mL PEI in ethanol/water (50:50, v/v) solution. 20 μL of such solution was dropped on polished GCE and left dry. The modified electrode GCE/(CNT/PEI) gave almost the same amperometric response after 30 successive injections of 10 μM phenol, i.e., there was almost no electrode fouling. When exposed continuously in 10 μM phenol for 30 min, the modified electrode had constant amperometric response as initial while the signal from the bare electrode decreased by 54% [133].

A slightly different GCE/(CNT/PEI) was prepared by dropping 1:1 ethanol/water solution containing 0.5 mg/mL CNT and 0.5 wt% PEI to detect 2,4-Dichlorophenol (2,4-DCP) [81]. Repetitive injections and continuous flow of 20 μM DCP at 0.7 V vs. Ag/AgCl/3M KCl were used to check the performance. In the repetitive injection mode, the amperometric signals had no significant difference in 40 peaks and the relative standard deviation (RSD) was 2.2%, comparing to 12.6% for bare electrode. In the continuous flow mode, the amperometric signal decreased by <4% in 30 min, comparing to 21% for bare electrode [81].

MWCTs dispersed in Nafion have been reported by Wang and used for biosensor modification. The optimal condition was dispersing 2 mg/mL CNT in 0.5 wt %

Nafion ethanol solution [140]. MWCTs/Nafion modified GCE was also used to detect paeonol [141].

Kumar prepared a good review about polymer/carbon nanotubes modification on electrodes to analyze nicotinamide adenine dinuceltoide (NADH), the oxidation of which also resulted in electrode fouling [143]. Salimi et.al studied the advantages of applying enzymes on MWCTs modified electrodes [144-146].

Carbon nanofibers (CNFs) have also been used in electrode modification. It has similar conductivity and stability as CNTs and more edge sites on the outer wall than the latter one, thus enhances more the electron transfer during electrolysis. Huang has done a good review about CNFs based electrochemical sensors [147].

1.5.4.3. Other modifications

Alizarin (AZ) modified carbon paste electrodes (CPEs) were used to detect dopamine [148]. The orange-red compound, alizarin, $C_{14}H_8O_4$, presented naturally as the glucoside in the madder plant. In the preparation process, AZ in the milligram level was added into the mixture of 70% graphite powder and 30% silicone oil and then packed into a carbon paste electrode. This AZ-CPE was used to detect dopamine in 0.1 M acetate buffer (pH=7.0) with CV. The anodic peak current increased linearly in the concentration range of 50 to 500 μM, and the detection limit was estimated to be 0.24 μM.

Several other modifications have been reported, such as Nafion modified GCE to detect phenol in the aid of surfactant [149], nickel macrocyclic composite modified vitreous carbon electrode for detecting phenolic compounds [150], electro-depositing tin on Pt electrode [151], Cellulosic film on GCE [152], clay modifications on enzyme based electrode [153], as well as the addition of EDTA into the analyte solution [154].

1.5.4.4. Summary

Functional interfaces have been widely applied by surface modification on electrodes to enhance the performance of the electrode for the analysis of phenolic compounds. In many cases, electrode fouling was reduced significantly or avoided, as shown in Table 1-1.

Table 1-1 Partial publications **about electrode surface modification.**

Modifiers, Electrodes	**Modification Processes**	**Detection methods**	**Modification effect /comparing with bare one**	**Ref.**
PNVP, N/A	Gamma irradiation	CV, FIA	Preventing fouling under certain conditions.	[112]
PB/PAZ Pt	CV; coating PB then PAZ	N/A	Linear range 10-100 nM phenol, R^2 = 0.991; Sensitivity 22 μA/nM.	[41]
PAVT, Pt	CV	SWV	Linear range 30-100 nM, R^2 = 0.99. Sensitivity 55 nA/nM; LOD= 9.8 nM phenol	[113]
PEDOT, SS	0.9 V vs. SCE, 0.7 C/cm^2	N/A	Slower fouling than bare Pt; Linear range 5-500 mM phenol	[45]
PEDOT:PSS, Pt	Potentiostatic 3 mC,	SWV	1-500 ppm phenol in water; Avoid fouling during CP oxidation.	[33, 49]
PEDOT/PB, Pt	CV	N/A	Linear range 2-100μM, R^2 = 0.996; Sensitivity 0.12 μA/μM; LOD= 25μM	[155]
PPy/*o*ASA, Pt	Galvanostatic 2.0 mA/cm^2	DC and pulse Amperometry	No significant fouling in 20 CV of 1 mM phenol; Linear range < 0.1 mM (10 ppm in water); Sensitivity 50 ppb (DC) and 10 ppb (pulse), Response ~0.4 times of bare electrode.	[34]
H_I phase 1,2-diamin-obenzene, GCE	CV	N/A	Less fouling.	[132]
poly-70-Ni(OH)TAPc, Au	CV	N/A	Linear range 0.7-30 mM; Sensitivity 326 μA M^{-1} cm^{-2}; LOD= 3.7 nM,	[35]
(poly-Ni(OH)TPhPyPc), VCE	CV	CV	Oxidation peak shifted -60 mV from bare one; 92% recovery after 5h exposing in 0.7 mM phenol, while no recovery for bare one.	[114]
PPI/AuNP, GCE	CV	CV, SWV, DPV	Linear range 0.61- 625 μM; LOD= 0.45 μM	[48]
MWCNT/PEI, GCE	Mixing and dropping	Amperometry	Same response for 30 injections of 10μM phenol; Same in 30 min flow, while half decayed for bare.	[133]
MWCNT/PEI, GCE	Mixing and dropping	Amperometry	2.2% RSD in 40 injections of 20 μM 2,4DCP (12.6% for bare); 4% decrease in 30 min exposing and (21% for bare).	[81]
MWCNT/Nafion, GCE	dispersing 2 mg/mL CNT in 0.5 wt % Nafion ethanol solution	N/A	Detecting paeonol	[141]
CNFs	N/A	N/A	N/A	[147]
AZ, CPE	Mixing and packing	CV	Linear range 50-500 μM; LOD= 240 nM DA	[148]

2. Research Objectives

The project involved in this dissertation was to develop a device for long-term monitoring of gaseous TCP at low concentrations in aircraft cabins. Conventionally, HPLC and GC are used for monitoring low concentrations of TCP in air. However, they are limited by their high cost, bulky size, and need of trained operators. Electrochemical sensing technology provided an alternative pathway, which had the advantages of high sensitivity and ease of use. In this technology, TCP was converted to cresol which enabled electrochemical analysis. However, electrode fouling commonly occurred during electrochemical analysis of phenolic compounds, such as cresol. Many efforts have been made to develop anti-fouling functional interfaces on electrodes, such as PEDOT:PSS composites modifications. This dissertation was trying:

(1) To develop an automatic TCP sampling system and an electrochemical device for the analysis of gaseous TCP;

(2) To perform the modification of PEDOT:PSS composites for preventing electrode fouling and to realize the long term monitoring of TCP.

The common problem of electrode fouling has been studied by many researchers, but a deeper understanding is still needed. This dissertation was devoted to understanding:

(1) The current-potential relationship in different electrochemical systems;

(2) The scientific model of electrode fouling that was able to predict the fouling current in terms of time, applied potential, and species concentration;

(3) The growth of the fouling layer on electrode surface.

2.1. Dissertation organization

Sensor development and performance enhancement were interdisciplinary issues and required performing experiments in different areas such as chemistry, surface analysis, characterization techniques, and model fitting. To be consistent, Chapter 3, 4,

and 6 were organized similarly, including introduction, experimental setup, results and discussion, and conclusions.

Chapter 3 presented the principles and experimental setup of TCP electrochemical analysis, from the results of which we noticed the problem of electrode fouling. In chapter 4, the PEDOT:PSS functional interface was introduced to the electrode which enabled the continuous monitoring of gaseous TCP. The performance of the modified sensor was studied experimentally. The functional interfaces were characterized by SEM and other techniques.

A deeper understanding to the scientific model of electrode fouling was realized in latter part of the dissertation. Chapter 5 discussed the current-potential relationship in different systems of reversible and irreversible reactions. Chapter 6 developed a model, based on the potential drop across the fouling layer, which was able to predict the fouling current decay in terms of time, applied potential, and the concentration of cresol. Chapter 7 gave an overall conclusion. All references were listed after Chapter 7. Chapter 8 recommended two future works that were considered as meaningful.

3. Electrochemical analysis of TCP

3.1. Introduction

A portable electrochemical sensor has been developed for determination of tricresyl phosphate (TCP) in gas phase [30]. An automatic TCP sampling system including an alkaline catalyst column was used to hydrolyse gasified TCP to cresol, making it electrochemically detectable, as shown in Fig.3.1. Hydrolysates were then detected in the flow injection analysis (FIA). Amperometric measurements were performed utilizing the unicell package, which consists of a glassy carbon working electrode unicell, a silver/silver chloride (Ag/AgCl) reference electrode and a stainless steel auxiliary electrode unicell, and in between a gasket to create a space with constant volume.

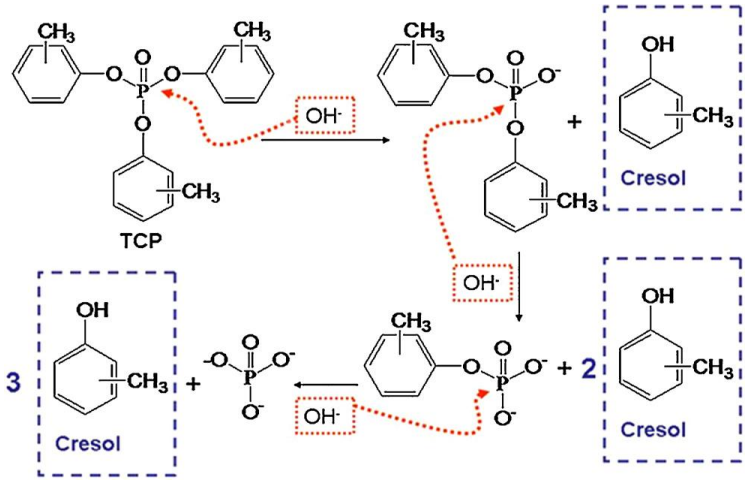

Fig. 3-1 Schematic representative of the **reaction** pathway that happened during the alkaline hydrolysis of TCP.

3.2. Experimental setup

3.2.1. Reagents and solutions

TCP samples were converted by alkaline hydrolysis to cresol which enables electrochemical detection. Alkaline powder was made from NaOH (Fisher, NJ) and neutral aluminum oxide (Al_2O_3) (Sigma–Aldrich, MO). Pipet filter tips (USA Scientific, Inc. 50 L beveled filter tips) were used to pack alkaline powder. p-Cresol (Acros Organics, NJ, 99+%) was dissolved in 0.2 M Na_2HPO_4/0.2 M KH_2PO_4 buffer (pH = 6.67, NaCl = 10 mM). Na_2HPO_4 and KH_2PO_4 were obtained from Fisher, NJ. D.I. water was from Millipore Direct-Q water purification system (resistivity= 18 ohms-cm). TCP methanol solution and engine oil samples (BP Turbo Oil 274, BP Turbo Oil 2380, and Mobile Jet Oil II) were gasified and hydrolysed in the automatic TCP sampling box.

3.2.2. Electrodes and portable sensor

All amperometric experiments were performed with CH Instruments (CH1910B) Bi-Potentiostat and duplicated with a handheld potentiostat (Palm-Sens). A desktop computer and pocket PC were used to collect the respective data. The handheld potentiostat communicates wirelessly with the Pocket PC via Bluetooth® (Fig. 3.2, right). Flow injection analysis (FIA) was carried out using cell electrodes, one of which includes glassy carbon working electrode (2 mm Ø), and another of which includes stainless steel auxiliary electrode and Ag/AgCl reference electrode (BASi, IN) (Fig. 3.2, left). A coating solution was applied for the Ag/AgCl reference electrode before detection as per instruction from the company. The working electrode was polished with alumina powder (1, 0.3, and 0.05 μm in order). 10 mM NaCl was used to maintain the potential of reference electrode. A switch injection unit (Valco Instruments Co. Inc) was used with a 50 μL sample loading loop. The flow rate was maintained at 200 μL/min by using a single syringe pump (KD Scientific, MA).

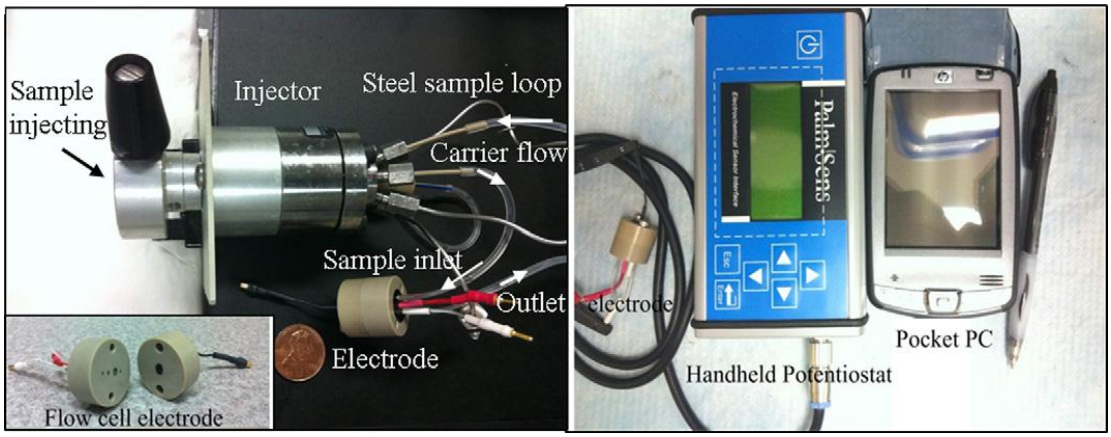

Fig. 3-2 Sensor setup: (left) flow injection system and flow cell electrodes were used to detect aqueous samples containing cresol. A coin was used to show the size. (right) Besides desktop potentiostat and computers, handheld potentiostat and pocket PC were used to conduct amperometric detections.

3.2.3. Alkaline catalyst for TCP hydrolysis

Alkaline powder catalyst was prepared by mixing NaOH and Al_2O_3 (1:10 wt) in ethanol on an automatic stirrer for 1 h to make all NaOH dissolved. The mixture was dried in a vacuum chamber. The dried powder was heated at 100^{o}C for 5 min in oven before use. 100 mg of powder was packed into a pipette tip with an filter at the end, which constituted the hydrolysing column. The conversion of TCP to cresol in alkaline medium is shown in Fig.3.1.

3.2.4. Automatic sampling system for hydrolysis of TCP and engine oils

Since *p*-TCP has a very low saturated vapor pressure at room temperature ($\approx 1*10^{-4}$ mmHg $\approx$0.01 Pa at 20^{o}C, $\approx$100 Pa at 220^{o}C, $\approx$1000 Pa at 260^{o}C, [156-158]), TCP samples in a gas phase are not readily available, so it was necessary to prepare such samples for the system calibration. The stock TCP solution (2 mmol*L^{-1}) was prepared in methanol and diluted to obtain TCP samples with concentrations of interest. Different concentrations of TCP (0, 5, 10, 20, 50, 100, 200, and 300 μM) in 0.5 mL of methanol were prepared and evaporated by 10 min N_2

bubbling (during latter 5 min an elevated temperature of 230^{o}C was used to make sure all TCP was evaporated) (Fig.3.3). N_2 flow rate was maintained at 1.1 L/min, which made the total air volume equal to 11 L (11 L/22.4 L ~ 0.5 mole). Therefore, the concentrations of 0, 5, 10, 20, 50, 100, 200 and 300 ppb of TCP in gas were realized. All gaseous TCP samples were blown through alkaline powder catalyst column, and then 3 mL of Na_2HPO_4/KH_2PO_4 (0.2 M/0.2 M final concentrations, added 10 mM NaCl) buffer was flushed through the column to collect the hydrolysed products. 10 mM NaCl was added into buffer to maintain the potential of reference electrode. All above steps from gas sample collection to buffer flushing were done with the automatic TCP sampling system built in our lab (Fig. 3.4). By these processes, TCP gas samples were converted to liquid samples containing corresponding concentrations of cresol, making it possible to detect TCP quantitatively by an electrochemical method.

Engine oil samples were prepared by dissolving the samples into methanol in 2 μL/0.5 mL ratio and with the same processes as TCP samples. Oil BP274 does not include TCP, Mobile Jet Oil II includes 1-3%, and BP2380 includes 1-5% TCP [159]. BP274 oil spiking with TCP with different concentrations were also prepared, sampled, and measured.

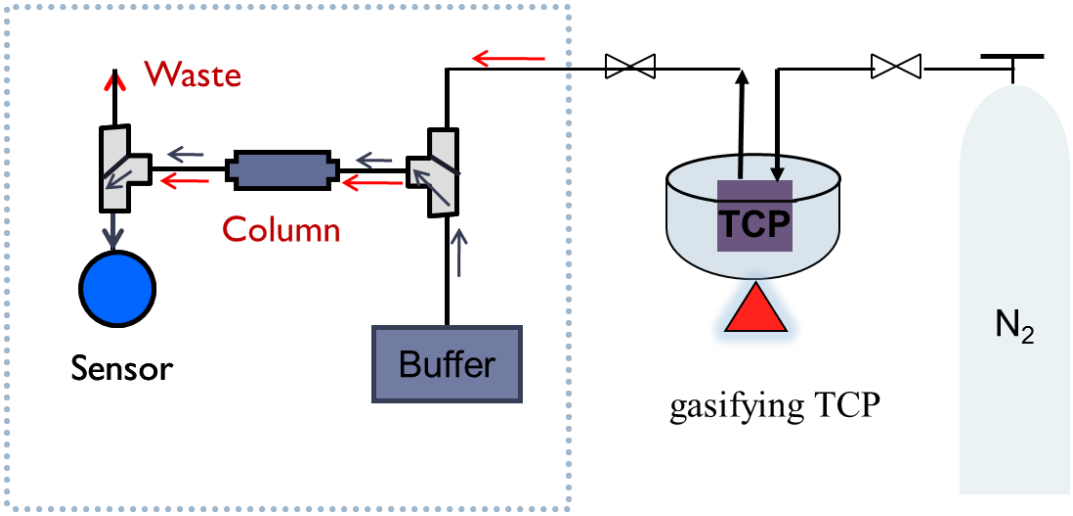

Fig. 3-3 Schematic representative of TCP sampling system. TCP was heated to 230 ^{o}C in oil bath and gasified along with N_2 bubbling, and entered the alkaline catalyst

column set inside an automatic TCP conversion box. In the electronically controlled TCP conversion box, as shown in the dotted square in above figure, TCP was hydrolyzed for later detection. The control of the automatic TCP conversion box was mentioned in ref. [160].

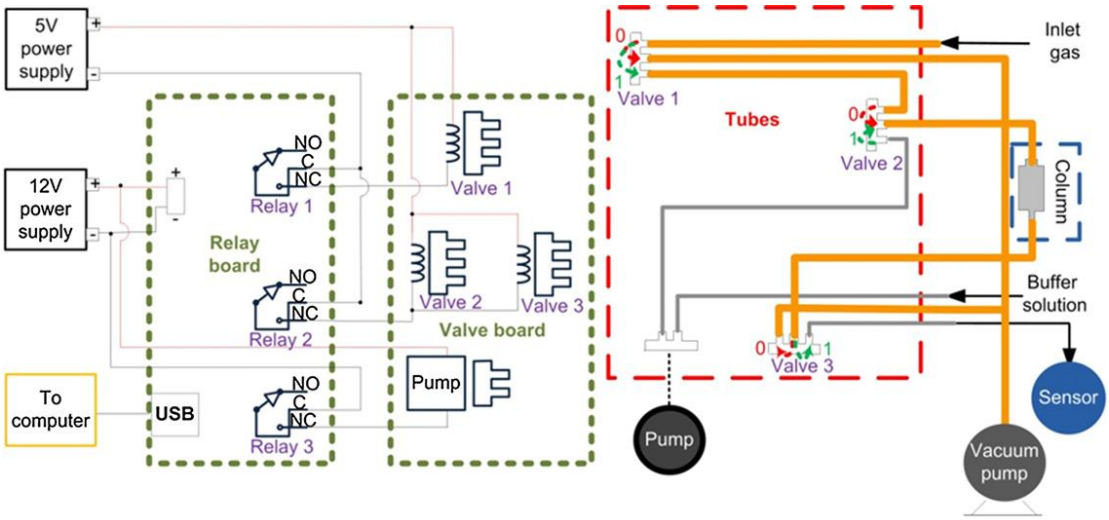

Steps	Actions	Valves			Relays	Duration
		1	2	3		
1	Vacuum pump on; Initial.	/	/	/	All off	
2	Set column; Start gas input.	on	/	/	Only 1 on,	10 min.
3	Finish gas input.	/	/	/	All off	
4	Start flushing. Pump on	/	on	on	2 and 3 on	5 min.
5	Finish flushing. Pump off. Column changed for next cycle.	/	/	/	All off	
summary	Relay 1 turned on for 10 min, then off. Then relays 2 and 3 turned on for 5 min, then off.					

Fig. 3-4 Schematic representation of automatic TCP sampling system. (top right) Arrangement of tubes, valves, and pumps. (top left) Electronic board consisting of electronic relays was used to control on/off of valves and pumps. (bottom) Running program in lab view software to control the electronic board.

3.3. Results and Discussions

3.3.1. Diffusion controlled anodic oxidation of cresol

Three-electrode system was used through all experiments. During the oxidation of cresol, electrons were released and transferred to the working electrode. The same

amount of electrons was compensated from the auxiliary electrode (or called counter electrode) [161]. The total number of electrons transferred at the electrode in a unit time must be proportional to the quantity of cresol reaching the electrode in that time period.

The oxidation process of cresol on a bare glassy carbon working electrode was studied with cyclic voltammetry (CV). In the CV curve (Fig.3.5), current increased quickly at the beginning in each potential scan due to the charging current, followed by a flat line. Starting from around 0.4 V, current increased again which indicates the onset of oxidation of cresol. The oxidation was restricted to the vicinity of electrode surface and reduced the concentration of oxidizable cresol in this area. Once the concentration gradient existed between the vicinity of electrode surface and the bulk solution, diffusion occurred which yielded a mass flow of cresol from bulk to electrode surface. In this batch mode, migration was reduced to negligible levels by addition of a high concentration of phosphate ions and convection was avoided by preventing stirring and vibrations, which made diffusion the only path for mass transfer. We define a diffusion layer where linear concentration gradient exists. The thickness of the diffusion layer increased with time which would flatten the concentration profile. In contrast, the potential continued to scan positively and decreased the concentration of oxidizable cresol in the vicinity of electrode surface, which steepen the concentration profile. The slope of concentration difference was intensified; when the effect of potential scan dominated first, so did the diffusion, and thus the current increased which yields the left shoulder of CV peak. Potential scan kept going positively and the concentration of oxidizable cresol in the vicinity decreased approaching zero. By the point when vincinity concentration dropped relatively slower, since it already approached zero, the diffusion layer thicken effect dominated and thus the slope of concentration difference reduced. The current started to decrease, meanwhile, an i-V peak was created [4].

The results of CV experiments demonstrating the change of the i-V at different scan rates are shown in Fig.3.5. 100 μM *p*-cresol in 0.4 M phosphate buffer was used as the analyte solution, and the potential was scanned in the range of 0-0.8 V *vs*

Ag/AgCl/3 M KCl with scan rates of 10, 20, 50, 80, 100, 120, 150, and 200 mV/s. Following the higher scan rate, the whole i-V cycle expanded due to the increased charging current. The peak current also increased (Fig.3.5a). Fig.3.5b shows the calibration of current density *vs.* square root of scan rate. The linear relation indicates the oxidation process of cresol is limited by the diffusion to electrode surface, while the electron transfer at electrode/solution interface is relatively quick [162, 163]. The diffusion controlled property of cresol oxidation ensures that current signal is proportional to the bulk concentration in CV as well as amperometry mode. Since the applied potential would be hold in certain amount higher than standard potential in amperometry mode, the concentration near electrode surface is relatively very small and can be negligible, ensuring the peak current being proportional to the concentration of injected cresol [161]. Analysis in more detail is available in Chapter 5 and 6.

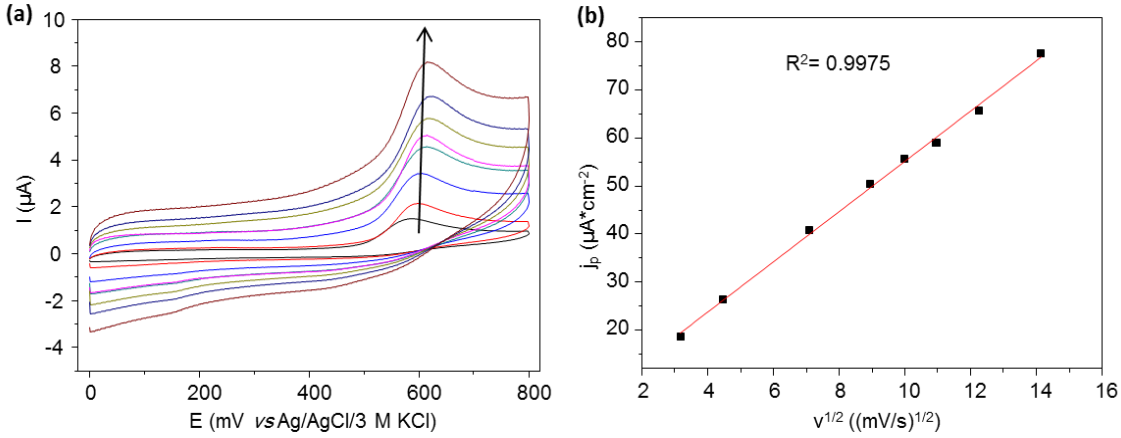

Fig. 3-5 Cyclic voltammetry results of cresol oxidation on bare electrode. (a) First cycle of cyclic voltammetry of 100 μM cresol in 0.4M phosphate buffer solution at scan rates varying from 10 to 200 mV/s. scan rates increase along the arrow direction. Range of potential: 0 to 800 mV vs Ag/AgCl/3 M KCl. (b) Calibration of the relation between the peak current density and square root of the scan rate. The coefficient of determination R^2 indicates the variability from linear fit. Glassy carbon working electrode (3 mm ø) was used for all of detections and polished between uses.

Looking at the reversal scan curve in Fig.3.5a, we note the absence of reduction peak which indicates the process was not reversible. Indeed, while this fouling layer could be removed by physical polishing, it is inert to chemicals and cannot be oxidized until a potential of up to 3 V is applied [164].

3.3.2. Performance of the electrochemical sensor

The performance of the three-electrode system was examined by flow-injection of cresols with differing concentrations. The calibration curve for cresol injections is shown in Fig. 3.6. Five different concentrations of cresols were injected into the measurement cell, as shown in the inset figure. The current peak increases linearly with the concentration of cresol (250-3000 nM). The sensitivity is 0.025 nA/nM. The R^2 coefficient of determination, 0.992, shows the goodness of linear fit in such a concentration range. The detection limit of 250 nM was estimated from the signal-to-noise ratio (S/N=3), while the previously reported detection limit in our lab was 600 nM [28]. The decay in current response with subsequent injections of high concentration of cresol is due to the fouling of electrode from cresol oxidation.

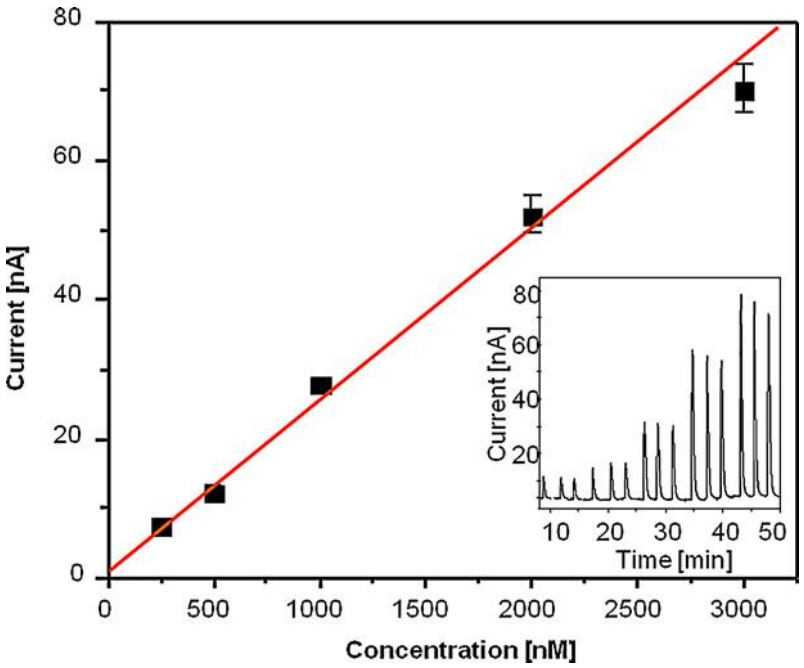

Fig. 3-6 Calibration curve of cresol detection. The inserted figure shows the

amperometry for cresol detection. Note that the baseline was subtracted. The decrease in response with subsequent injection is due to the fouling of electrode from cresol oxidation [28] (seen on the inset figure). R^2, coefficient of determination, representing the goodness of linear fit, in calibration curve is 0.992. Data points in calibration curve correspond to the average of the three injections. Error bars are the standard deviation of three experimental results. Detection limit is 250 nM.

3.3.3. Detection of hydrolysates from TCP samples

To show the ability of this system for detection of TCP in gas, TCP with concentrations of 0, 5, 10, 20, 50, 100, 200, 300 ppb were sampled and measured (the conversion from μM to ppb is shown in 3.2.4). The data obtained in the flow injection system are shown in Fig. 3.7 and Fig. 3.8 (calibration curve). For each set of amperometric measurement, several TCP concentrations were injection in random order, one example of which is also shown in the inset of Fig. 3.8. This procedure was repeated six times, as shown in Fig. 3.7. The equation of linear fit is y (nA) = 1.22 x (ppb) + 36.5. The R^2 coefficient of determination, 0.99, shows the goodness of linear fit in such a concentration range.

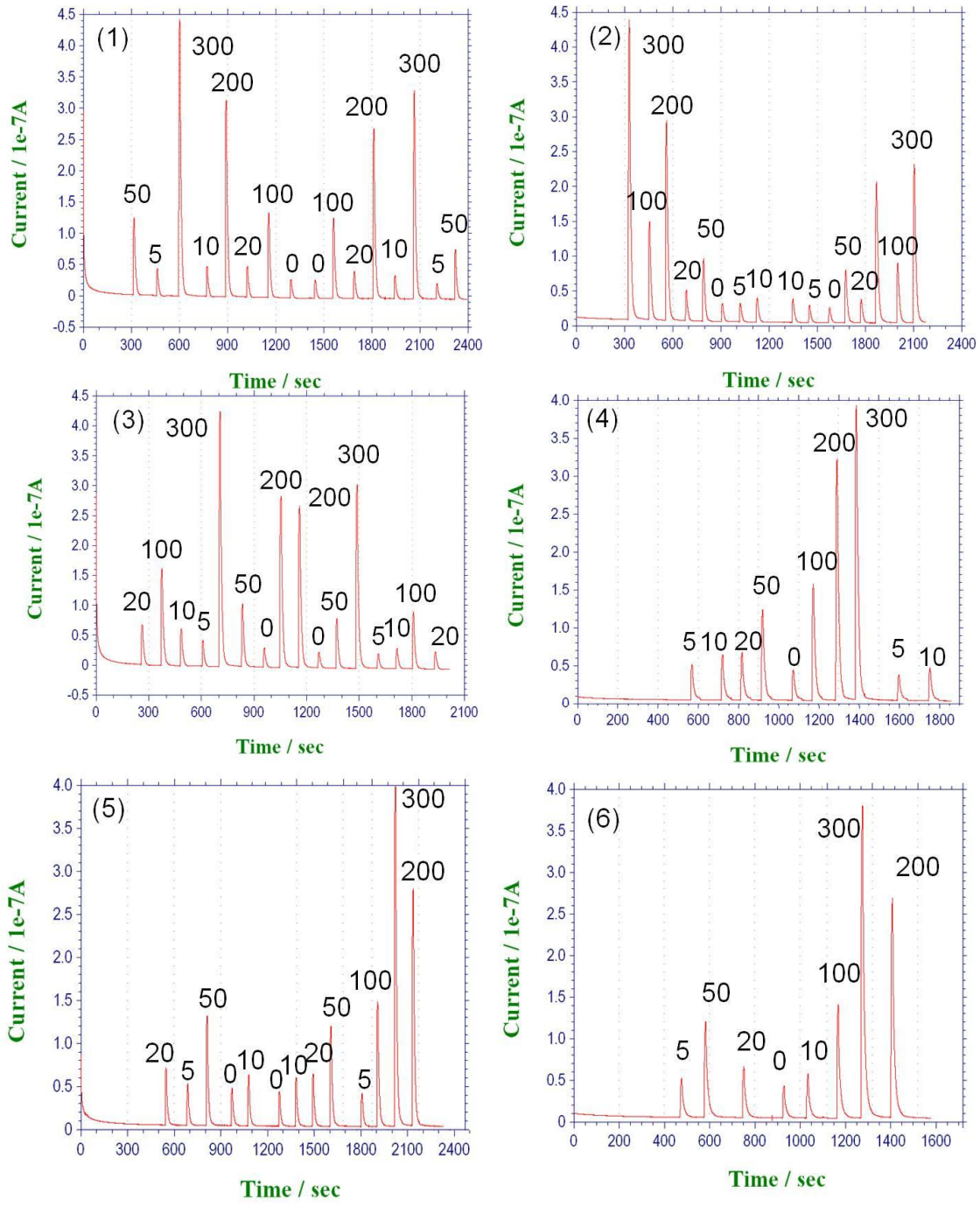

Fig. 3-7 Amperometric results from injections of TCP hydrolyzate samples. TCP samples were injected in random order. In some sets, some samples were measured again after all samples have been measured once. We consider the first 8 peaks as "1st cycle". Only data in 1st cycle were used for calibration, since fouling effect makes the response in the 2nd cycle weaker than the 1st one.

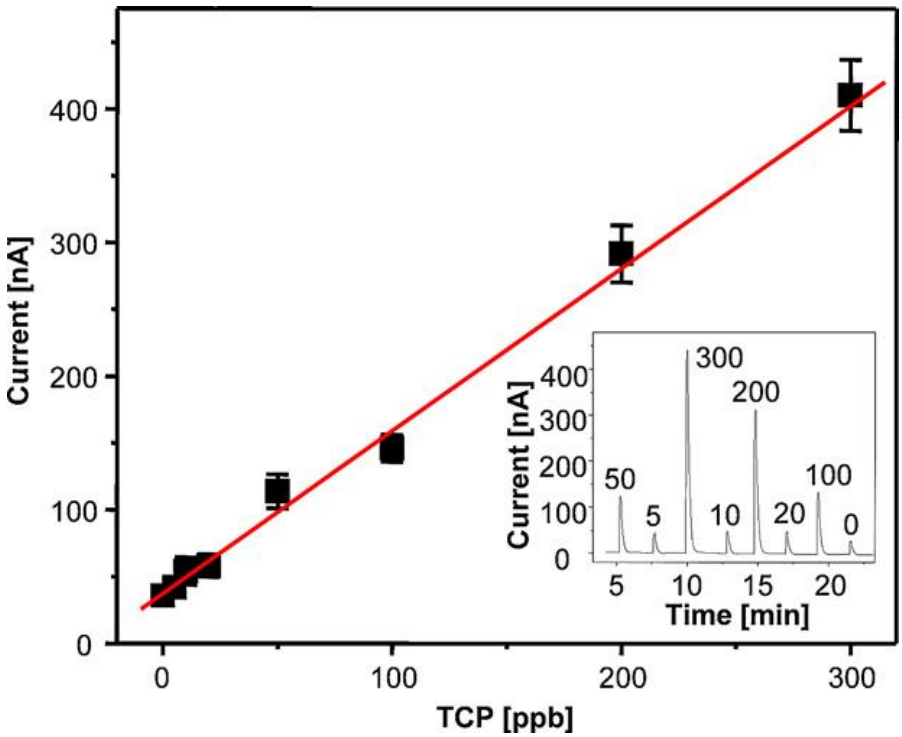

Fig. 3-8 Calibration curve of TCP hydrolysate samples. Linear concentration ranges from 5 ppb to 300 ppb in gas. The inset figure shows one set of raw amperometric results out of six times measurements. The linear fit for the inset figure is y = 1.22x + 36.5, and the R^2 is 0.99. The results show the ability of this sensing device to detect TCP in a wide concentration range. The conversion of concentration units between ppb in gas and M is as below. As mentioned in section 3.2.4, TCP was dissolved in 0.5 mL of methanol, which would be vaporized and dispersed in 11 L of N_2. Approximately, 11 L of gas is 0.5 mol. Therefore, 1 M of TCP in methanol solution corresponds to 1 ppb in gas.

3.3.4. Detection of hydrolysates from engine oils

To test the ability of this system to determine TCP from real samples, such as from jet engine oils, 2 μL of commercially available BP Turbo Oil 274, BP Turbo Oil 2380, and Mobile Jet Oil II were mixed in 0.5 mL of methanol and were used to prepare the hydrolysate samples with the same processes as TCP hydrolysates described above. The oil BP274 was selected because it does not contain TCP. Also, a

set of samples were prepared by spiking into BP274 oil with TCP in 0, 50, 100, and 200 ppb concentrations.

Fig. 3.9 and Fig. 3.10 (calibration curve) show results of measurements of TCP spiked BP274 oil samples. The slope of linear fit was around 1 nA/ppb which was close to Fig.3.8.

The data of oil hydrolysates are shown in Fig. 3.11 and Fig. 3.12 (calibration curve). For each set of amperometric measurement, several oil samples were injected in random order, one example of which is also shown in the inset of Fig. 3.12. This procedure was repeated three times, as shown in Fig. 3.11.

Concentrations of TCP in these oils are summarized in Table 3.1. Using the linear fit in Fig.3.8 (Detection of TCP hydrolysate samples), we calculated the concentration of TCP from peak current. And the conversion from ppb unit to % unit was done similarly as previously described in section 3.2.4. The electrochemical responses from the oil hydrolysates had a similar trend compared to the TCP concentrations in the oils as expected from the manufacturers' data. Thus, the system appears to be capable of detecting TCP in oils and may have application in aircraft and other transportation vehicles.

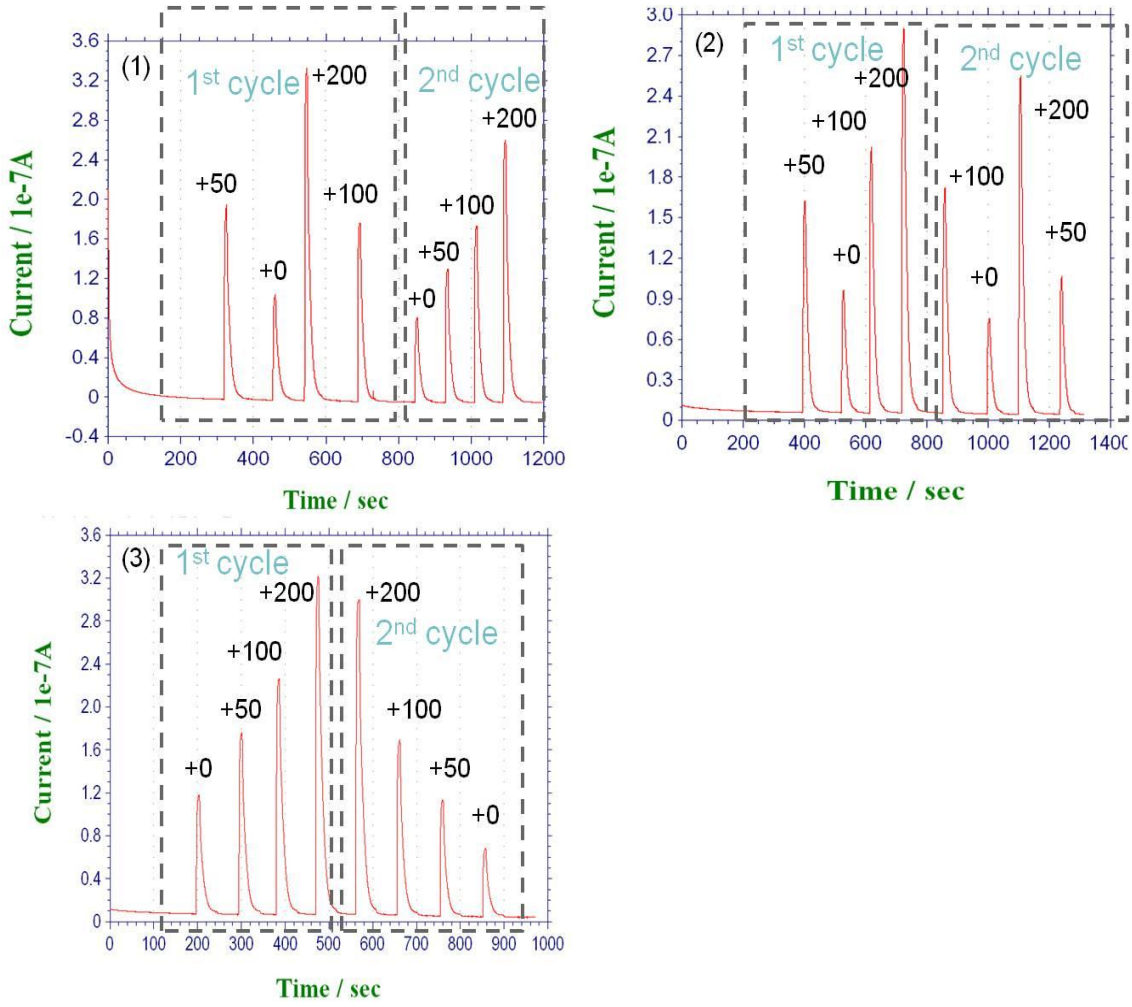

Fig. 3-9 Amperometric results from injections of TCP spiked BP274 hydrolyzate samples. For example, +50 means BP274 spiking with 50 ppb TCP. Injections were in random order. Only data in 1st cycle are used for calibration. The data +0, which represent BP274 sample, were also used in calibration of different oil samples.

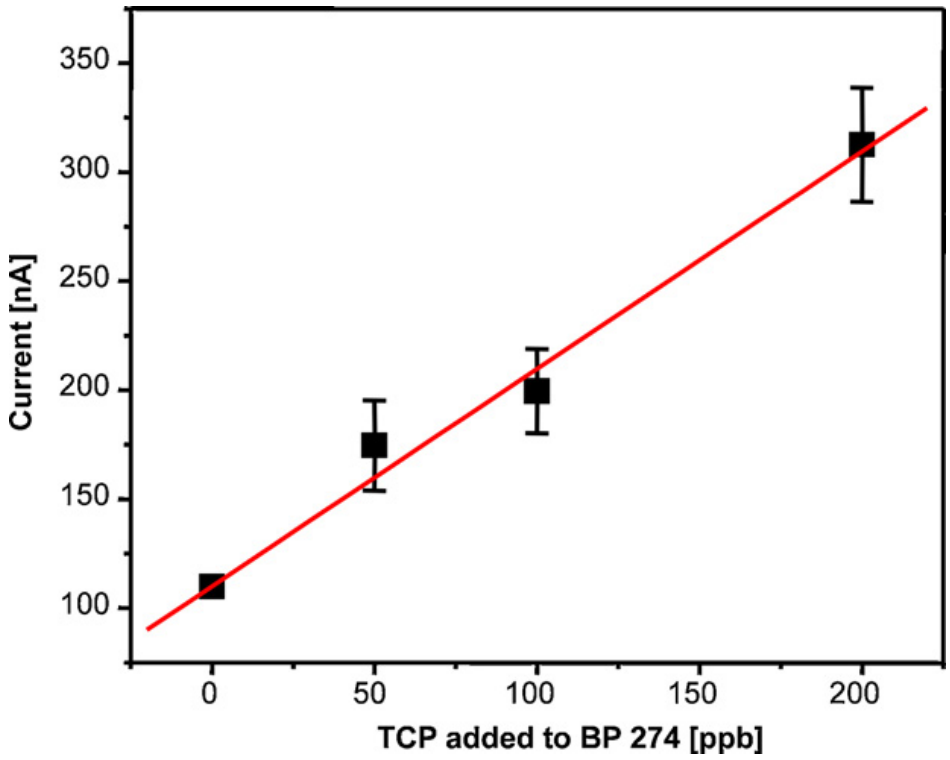

Fig. 3-10 Amperometric results of injections of oil spiking TCP hydrolysate samples. The slope of linear fit is around 1 nA/ppb, which is close to Fig. 3.8. R^2 of 0.99 represents the goodness of linear fit. All samples were measured randomly for three times.

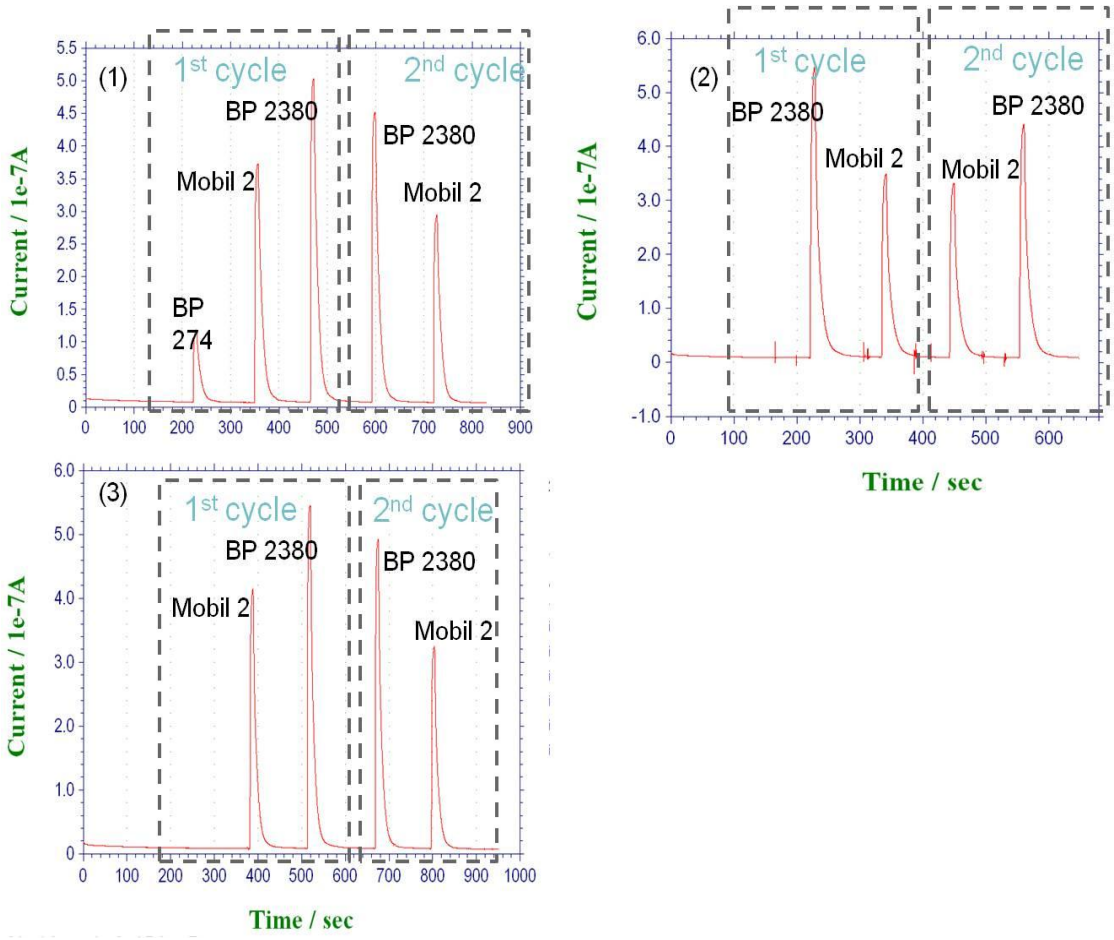

Fig. 3-11 Amperometric results from injection of oil hydrolyzate samples. The injections were in random order. Only data in 1st cycle are used for calibration.

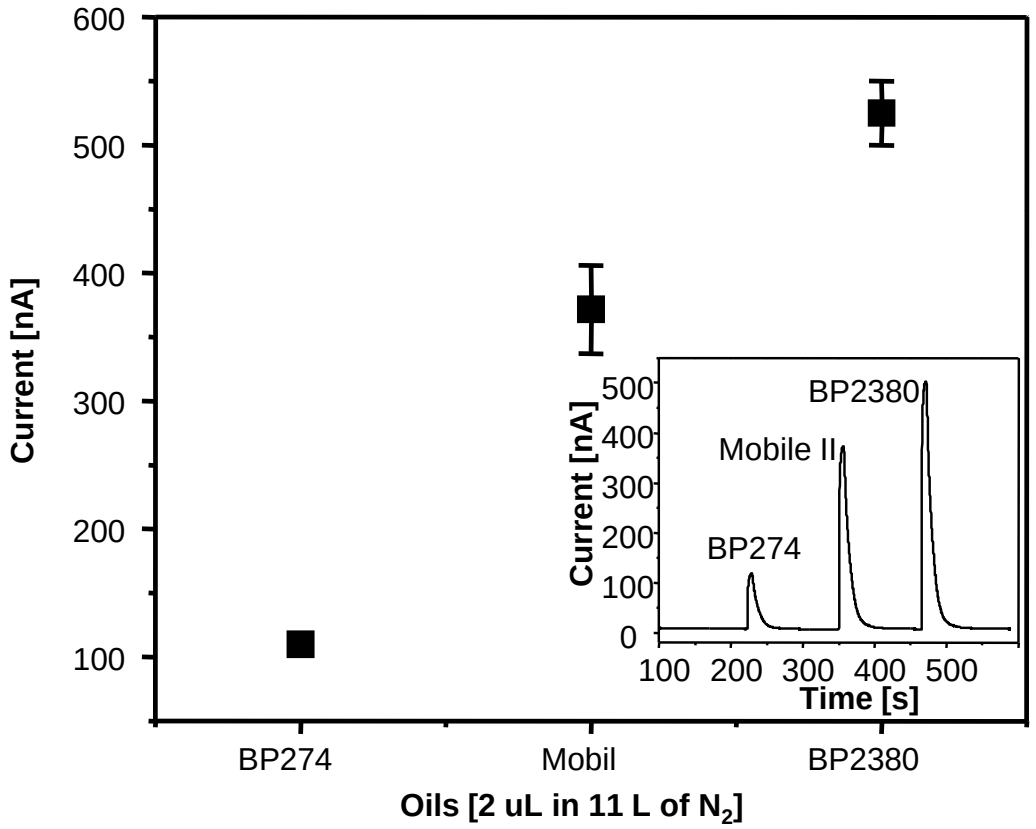

Fig. 3-12 Amperometric results of injections of different oil hydrolysate samples inset with one example of raw data. They were prepared, gasified, and hydrolysed in the automatic sampling system before detection. Note that fouling contributes to the existence of error bar and the concentrations of TCP in these oil samples are much higher than what would be expected. The data in Fig. 3.9 were included for calibrating the BP274 injection current.

Table 3-1 Amperometric results of oil hydrolysate samples. The conversion from concentration in ppb to concentration in % is mentioned in text.

Oils	TCP Claimed (Manufactures)	Experimental data			
		Current [nA]	Stdev. [nA]	Conc. [ppb]	Conc. [%]
BP Turbo Oil 274	N/A	110	2	60	0.6%
Mobile Jet Oil II	1-3%	372	34	275	2.8%
BP Turbo Oil 2380	1-5%	525	25	400	4%

3.4. Conclusions

In summary, a portable and remote electrochemical sensing system has been developed for the fast determination of tricresyl phosphate (TCP) in gas phase. The TCP gas sample was produced from both TCP methanol samples and commercial jet engine oils. TCP was hydrolyzed by alkaline catalyst to cresol which makes electrochemical detection possible. An automatic TCP sampling system built in our lab was successfully used to convert TCP to hydrolysate buffer solution, which was detected in a portable sensing system. We have demonstrated that a detection limit for TCP down to 5 ppb in gas was realised. The response to commercial jet engine oils was similar to that of TCP methanol samples. The advantages of this system, such as easy operation, remote analysis, quick response, and low cost, make on site monitoring of aircraft cabin air, as well as other air environments, potentially practical.

However, electrode fouling brought variation of signals and limited the performance of sensor. Therefore, in Chapter 4, PEDOT:PSS functional interfaces are introduced to electrode and enhance the performance of sensor.

4. Anti-fouling PEDOT:PSS modification for continuous monitoring of TCP

4.1. Introduction

Chapter 3 shows a portable real-time electrochemical sensor with linear response for ppb level of gaseous TCP [32, 160]. Since TCP itself is electrochemically inactive, it was converted to electro-active cresol for detection. However, the sensor system suffered from electrode fouling which limited its repetitive usage in long term applications. A long lasting electrode is needed for on-site continuous monitoring, so electrode surfaces must be modified to minimize or eliminate fouling.

Electrode fouling is a common problem during electrochemical analysis of phenolic compounds, such as cresol, and causes decay in signal response during repetitive measurements [65-72, 94]. The fouling is caused by the formation of a passive polymeric film on the electrode surface [65, 66, 75, 76]. Upon anodic oxidation of cresol, phenoxy radicals form, which then couple to form dimers or oligomers, and finally, a polymeric film deposits on electrode surface [165]. This polymeric film is tough, thermally stable, and so chemically inert that little oxidation or hydrolysis will occur in either acidic or basic media [69]. The films are characterized by low permeability [96] and strong adhesion to the electrode, which blocks the surface, and yields electrode fouling [68, 70-72, 94]. Various surface treatments and modifications have been used to reduce or even avoid electrode fouling by preventing polymeric substrates from absorbing onto the surface of electrode [28, 112].

Having advantages of high electronic conductivity and porosity [45], conducting polymers have attracted considerable interests in recent years. Modification of conductive polymer for preventing electrode fouling has been reported by many researchers [106-109]. Poly(3,4-ethylenedioxythiophene) (PEDOT) is one of the widely used conductive polymers. Patra et al. [45], Heras et al. [33], and Lupu et al [38] applied PEDOT on electrodes through electropolymerization for detection of phenolic compounds. The surfactant poly(sodium-4-styrenesulfonate) (NaPSS) was

additionally used during PEDOT electropolymerization to avoid the problems of [162]: 1) the low solubility of thiophene structures in water, 2) the oxidation potentials higher than that of water, 3) and the water-catalyzed formation of thienyl cation radicals which can activate concomitant reactions and prevent the formation of the main polymer [166]. Moreover, the hydrophobic hydrocarbon residues of PSS exhibit strong affinity for PEDOT, while the hydrophilic sulphonic groups are oriented towards or even protrude into the solution and may hence induce poor adhesion of the fouling polymeric film [33, 49]. NaPSS also induces the formation of a permeable and less compact polymer network, and yields high (ionic) conductivity and permeability to the fouling polymeric film. This makes the permeation of phenolic compounds through the film and oxidation inside possible, ensuring electroneutrality [33, 49]. To the best of our knowledge, this work is the first to study the TCP detection on PEDOT:PSS modified electrode. In this chapter, a sensing system with a PEDOT:PSS modified glassy carbon electrode for potentially continuous monitoring of TCP in gas is investigated.

4.2. Experimental setup

4.2.1. Reagents and solutions

All aqueous solutions were prepared using de-ionized Milli-Q water (18 mΩ cm). 3,4-ethylenedioxythiophene (EDOT) (Sigma-Aldrich, MO), poly(sodium-4-styrenesulfonate) (NaPSS) (Sigma-Aldrich, MO, MW≈70,000), and lithium perchlorate ($LiClO_4$) (Sigma-Aldrich, MO) were used for electro-synthesis of PEDOT:PSS [33]. The stock 20 mM tri-*p*-cresyl phosphate (*p*-TCP) (Sigma-Aldrich, MO) solution was prepared in methanol (BDH-VWR) and diluted to obtain TCP samples with concentrations of interest. All TCP samples were converted to cresol with the aid of alkaline catalyst. Alkaline catalyst was made from NaOH (Fisher, NJ) and neutral aluminum oxide (Al_2O_3) (Sigma-Aldrich, MO) and packed in Pipet filter tips (USA Scientific, Inc. 20 µL beveled filter tips). *p*-cresol (Acros Organics, NJ, 99+%) was dissolved in 0.2 M Na_2HPO_4/0.2 M KH_2PO_4/10 mM NaCl buffer (0.4 M

phosphate buffer, pH = 6.67). Na_2HPO_4, KH_2PO_4, and NaCl were obtained from Sigma-Aldrich, MO.

4.2.2. Electropolymerization of PEDOT:PSS on glassy carbon electrode

Electrodes and preparation of TCP samples are the same as Chapter 3. The electropolymerization of monomer of EDOT was performed under amperometric conditions in aqueous solution. The solution contained 5 mM EDOT (0.71 g/L), 0.1 M NaPSS (20.6 g/L), and 0.1 M $LiClO_4$ (10.6 g/L). The unicell glassy carbon electrode was polished with alumina as mentioned in section 2.2, rinsed and sonicated with de-ionized water in an ultrasonic bath for 5 min, flushed with ethanol and water, and dried with N_2 gas. 0.5 mC of charge was applied on the glassy carbon electrode with 2 mm diameter in order to obtain the thickness of interest of electropolymerization layer, unless otherwise stated. The potential was maintained at 0.95 V vs. Ag/AgCl/3 M KCl. The color of electrode surface turned yellow after modification. For comparison, different amount of charges have been applied including 0.3, 1, 1.3, 2, 4, 20 mC on the same electrode.

4.3. Results and Discussions

4.3.1. Microscopy images of electrode fouling

The formation of fouling layer was studied by SEM, EDS, and AFM. For SEM imaging, the electrodes were Au sputter coated prior to analysis. One electrode was left polished, while the other one was fouled by 10 injections of 10 μM cresol in 0.4 M PB buffer in amperometry mode. The polished electrode and fouled electrode were compared in SEM images (Fig.4.1.a,b). Only sputter coated Au was seen on polished electrode, but additional structures were observed from the surface of fouled electrode. EDS shows the existence of oxygen on the fouled electrode, which could come from the fouling products of cresol (Fig.4.1.c).

AFM images also confirm the existence of fouling layer on electrode surface (Fig.4.1.d,e,f). Electrodes with 3mm diameter were used. One electrode was polished for imaging and the other two were applied with 5 and 20 μC, respectively, in 10 μM cresol in 0.4 M PB buffer in amperometry. The bare electrode was so flat that the surface profile varied below 15 nm (Fig.4.1.d). In contrast, the surface profile of fouled electrodes varied in the range of 0-30 nm (Fig.4.1.e) and 0-32 nm (Fig.4.1.f). Comparing to the electrode fouled with 5 μC of charge, the image of the one with 20 μC was brighter which indicates more substrate had been formed on surface and implicates the growth of fouling layer.

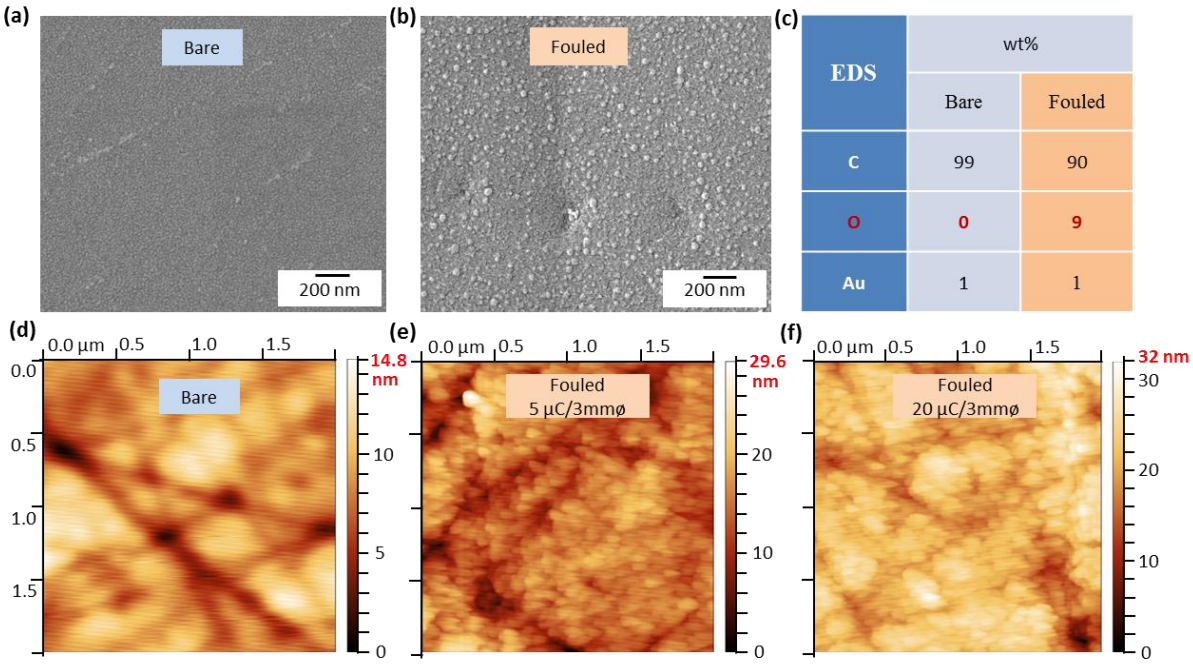

Fig. 4-1 Observations of fouling on glassy carbon electrode from SEM, EDS, and AFM. (a) SEM image of Au sputtering coated bare electrode, (b) SEM image of fouled electrode, (c) EDS results of the bare and fouled electrodes, (d) AFM image of bare electrode, (e) AFM image of 3 mm ø electrode fouled by 5 μC of charge in amperometry, and (f) AFM image of 3 mm ø electrode fouled by 20 μC of charge in amperometry.

4.3.2. Controlled PEDOT:PSS modification on glassy carbon electrode

To reduce the fouling from oxidation of cresol, PEDOT:PSS modification was applied on glassy carbon electrode via electropolymerization. One important parameter for modification is the reproducibility. To show the ability to control modification, 4 unicell glassy carbon electrodes (2 mm ø) were immersed in EDOT/NaPSS solution and applied 0.5 mC of charge (potential= 0.95 V in single-potential amperometry mode). Fig 4.2a-e shows the results of these modifications. The amperometry profiles were almost the same for these 4 electrodes as shown in Fig.4.2a, and all of these 4 electrodes had the same color after modification which indicates the uniform and controllable configuration. Additionally, 4 more electrodes were coated with 1, 1.3, 2, and 4 mC of charge. The color of modified electrode surface changed with different amounts of charge (Fig.4.2f-i).

SEM was also carried out to compare the electrode surfaces modified with 0.3, 0.5, and 2 mC of charge. Images from left to right correspond to increasingly more charge (Fig.4.2j-l). During SEM imaging, the configuration was seen to be uniform over the whole electrode surface and so representative SEM images in small areas can be produced. Fig.4.2j-l illustrate the change in morphology and particle size of the PEDOT layer. Cracks formed on the PEDOT:PSS layer prepared by applying 2 mC of charge.

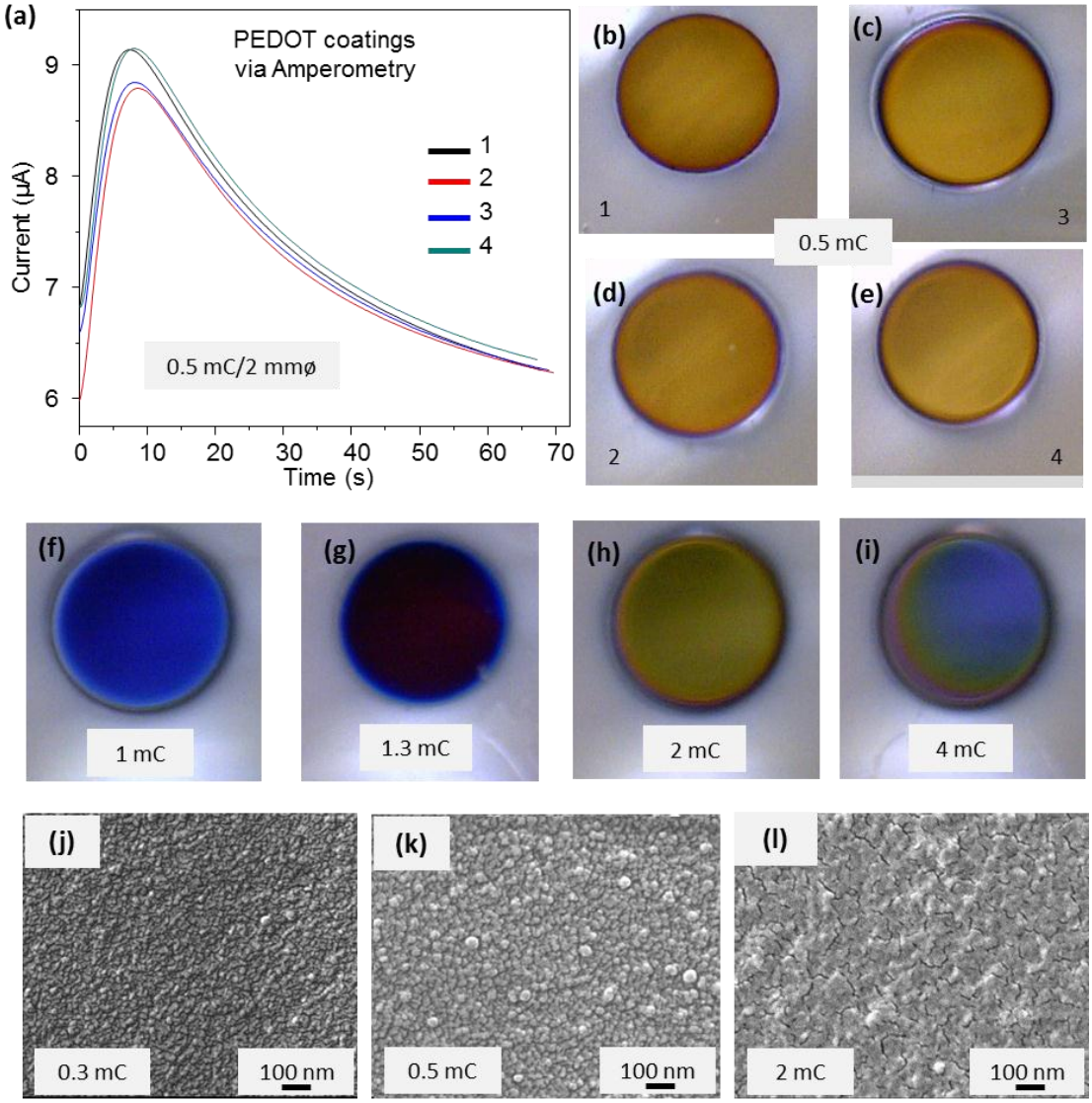

Fig. 4-2 PEDOT:PSS modification of glassy carbon electrodes. (a) Amperometric results of 4 electrodes applied with 0.5 mC of charge in EDOT:PSS solution, (b-e) Optical images of these 4 electrodes after modification with 0.5 mC of charge, (f-i) Optical images of 4 electrodes after modification with 1, 1.3, 2, 4 mC of charge, (j-l) SEM images of electrode surface applied with 0.3, 0.5, and 2 mC of charge in EDOT/PSS solution.

4.3.3. Detection of cresol with modified electrodes

The controlled PEDOT:PSS modification described above was used to reduce fouling effect in the amperometric detection of cresol. 10 μM cresol in 0.4 M

phosphate buffer was injected successively on both modified (left side of Fig.4.3a) and un-modified electrodes (right side of Fig.4.3a). The peak currents decayed in both cases after repeated exposure to cresol, but magnitude of the decrease was much lower in the modified electrode. For comparison, the peak height was normalized to the first peak in each case being normalized to 100%. The successive peaks were seriously decayed on bare electrode but much less fouling occurred on modified electrode (Fig.4.3b). The comparison indicates that for continuous on-site monitoring of TCP, the bare electrode is not a good candidate. Although thoroughly polishing the electrode could remove the fouling layer, this would require trained personnel and adds complexity to sensor operation. Modified electrodes, however, overcome this limitation.

.

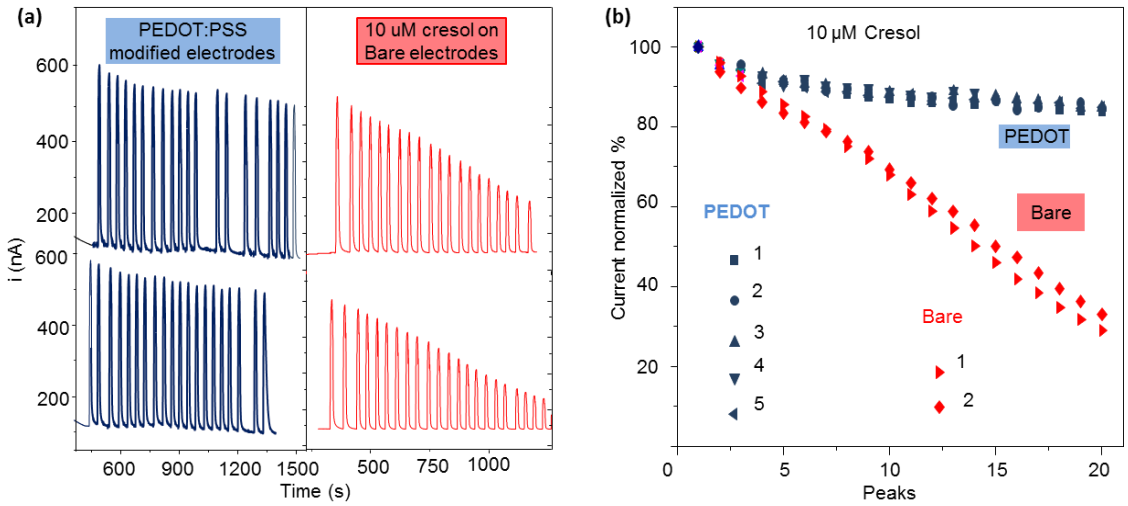

Fig. 4-3 Amperometric results of 10 µM cresol on bare and modified electrodes. (a) Initial amperometric peaks obtained from successive injections of 10 µM cresol in 0.4 M phosphate buffer. Two experiments have been carried out on bare electrode and 5 on modified electrodes, two examples of which are shown here. (b) Calibration of peak current *vs* peaks. Note that the first peak in each case has been normalized to 100%. Unicell glassy carbon electrodes with 2 mm diameter were used.

With modified electrodes, a series of cresol samples with concentrations of 0.2, 0.5, 1, 2, 5, 7.5, 10 µM were detected in amperometry mode 3 times at each

concentration). Two representative examples of initial amperometric results are shown in Fig.4.4a. All samples were injected in random order to avoid system error and to show fouling clearer since signal from a sample would decay more if a higher concentration was previously injected. The calibration curve is shown in Fig.4.4b. A linear relationship between the peak current and the concentration of cresol was obtained, confirmed by the R^2 being very close to unity. The error bars which were contributed mainly from electrode fouling were too small to be distinguished from the data symbols. Therefore, the detection of 0.2 to 10 μM cresol was reliable with the modified electrode.

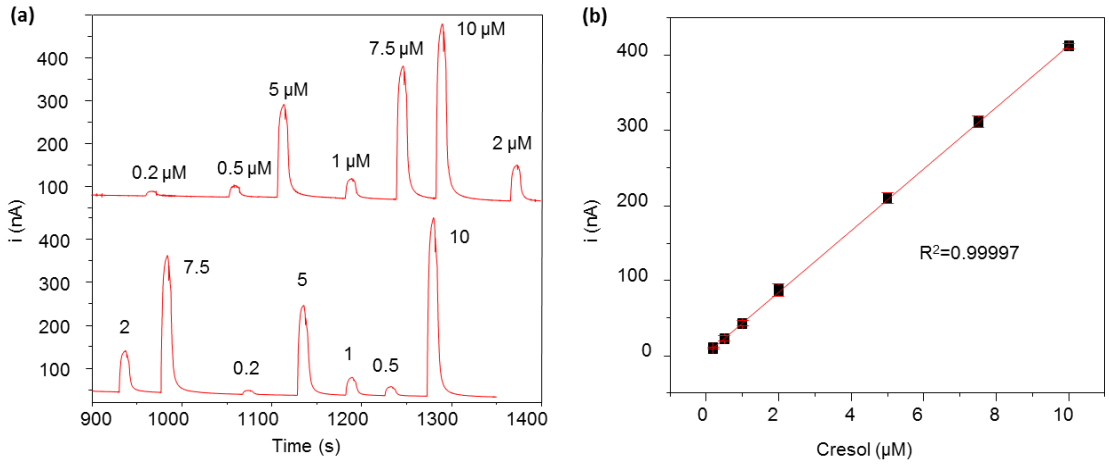

Fig. 4-4 Amperometric results of injections of 0.2-10 μM cresol in 0.4 M phosphate buffer. (a) Two representative sets of continuously amperometric results. Different concentrations of cresol samples were injected in random order to avoid potential system error and by this way electrode fouling could be seen more clearly. (b) Calibration curve of detection of cresol with different concentrations on modified electrode. The coefficient of determination R^2 indicates the variation of linear fit. Error bars are marked as bars above and below current symbols. Unicell glassy carbon electrodes with 2 mm diameter were used.

4.3.4. Detection of TCP with modified electrodes

Finally, to show the ability of detecting TCP samples, several TCP samples with 10, 20, 30, 50, 100, 200, 300 ppb were gasified, hydrolyzed, and detected with PEDOT:PSS modified electrode. Experiments have been carried out three times. The calibration of all three experiments is shown in the left frame of Fig.4.5a. Error bars indicate the variation between all three experiments. A linear relationship was observed between current signal and concentration of sample in the range of 50-300 ppb. For comparison, the corresponding results from bare electrodes are shown in the right side of Fig.4.5a, excluding 10 and 20 ppb TCP. Although a linear relation was also observed, the error bars were much bigger due to electrode fouling. Note that the bare electrode was polished after measurement of each set of 4 samples. The fouling effect would be much more serious if the electrode were left unpolished through the whole measurement, which was done for modified electrode. To observe the comparison clearly, the responses from modified electrodes were normalized to 100% and the signals from bare electrode and error bars were relatively calibrated (Fig.4.5b). Comparing the error bars from modified electrode with those from bare electrode, modified electrode was seen to get much less fouling. Indicated by these results, the sensing system with PEDOT:PSS modified electrode is able to continuously monitor TCP in gas phase in the concentration range of 50 to 300 ppb.

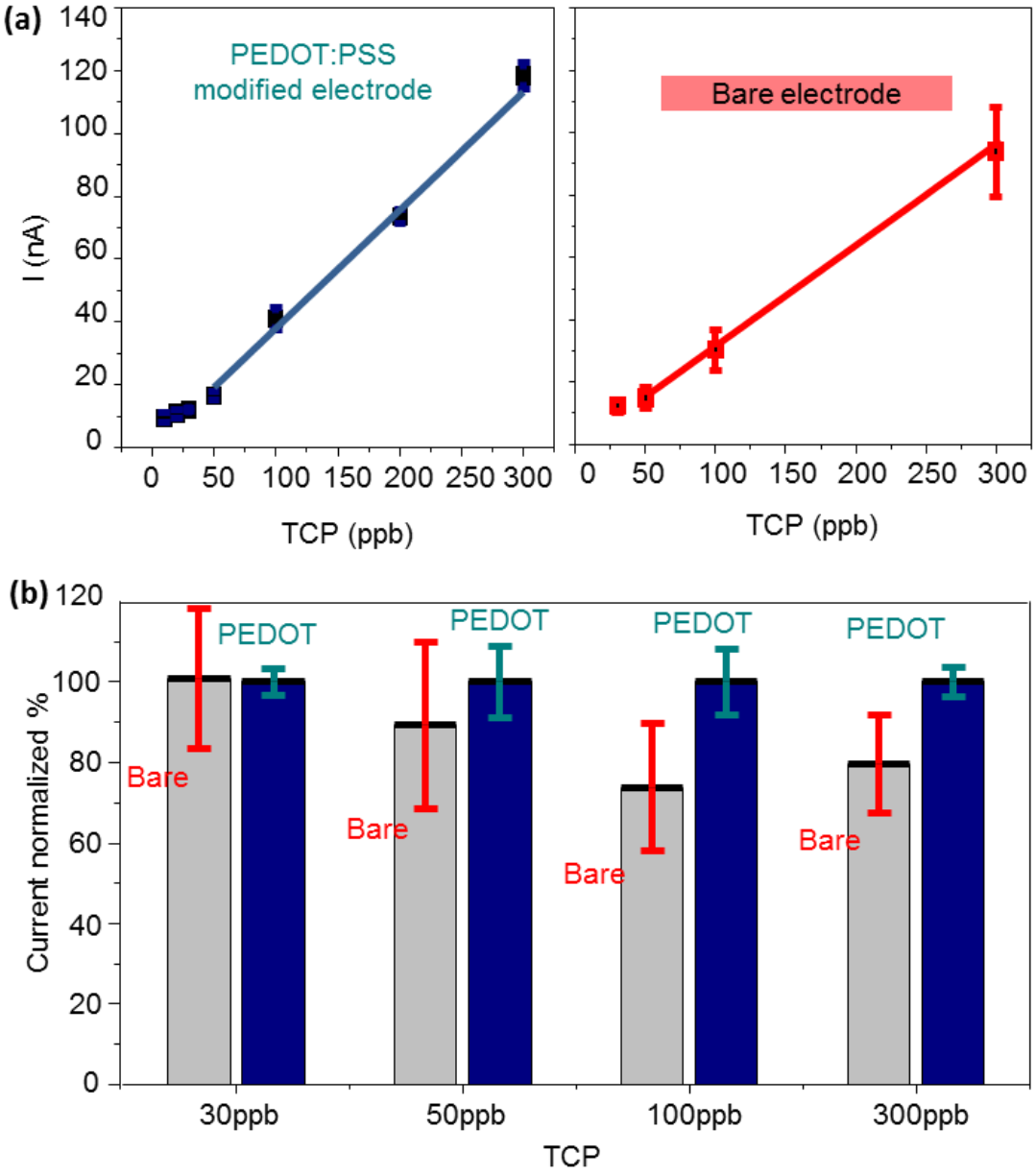

Fig. 4-5 Detection of TCP on bare/modified electrode. (a,left) Calibration of detection of TCP samples with concentrations of 10, 20, 30, 50, 100, 200, and 300 ppb on PEDOT:PSS modified electrode, (a,right) Calibration of detection of 30, 50, 100, and 300 ppb TCP on bare electrode. 10 and 20 ppb were not detected and compared with modified electrode, (b) Responses from modified electrode were normalized to 100% and the error bars and signals from bare electrode were relatively calibrated. Unicell glassy carbon electrodes with 2 mm diameter were used. Note that the bare electrode was polished after measurement of each set of 4 samples, while modified electrode was not polished through three sets of measurements.

4.4. Conclusions

An electrochemical sensing system for continuous monitoring of TCP in gas phase has been developed. The electrode fouling occurring upon oxidation of cresol brought a critical problem for continuous monitoring in long term applications. PEDOT:PSS modification was controllable and was able to greatly reduce the electrode fouling. By applying PEDOT:PSS modification, this sensing system obtained reliable results from detecting TCP in the concentration range of 50-300 ppb. This modification could be used in a wider range of applications. In Chapter 5 and 6, we would focus on the detailed mechanisms of electrode fouling.

5. Study of Current-Potential Curves

As a basic point, the current-potential relationship is used directly or indirectly in almost all of electrochemical methods. For example, the current-potential (*i*-*V*) curve is obtained from Cyclic Voltammetry (CV) and Linear Sweep Voltammetry (LSV), and in chronoamperometry, the current-time (*i*-*t*) curve is obtained by monitoring the current response to a constant potential or potential steps that changes with time. Therefore, the current-potential relationship is important and should be understood before grasping any information from electrochemical data. the current-potential relationship will be deduced specifically.

Based on the theoretical study of literature, such as the book of "Electrochemical Methods" written by A.J. Bard and L.R. Faulkner, this chapter will deal with this relationship for reversible/ireversible reactions in a simplified and a rigorous approach, and for irreversible reactions [4], which can be used for the flow analysis system of cresol. For reversible reactions, the interfacial electron-transfer kinetics is rapid, and thus only mass transfer limits the reactions. The simplified approach is a semi-empirical treatment of steady state mass transfer. It uses the Nernstian behavior, and assumes a linear concentration gradient and that the current is proportional to this gradient. The rigorous approach utilizes the Nerstian behavior, diffusion equations, and boundary conditions. Interestingly, both of the two approaches yield identical *i*-*E* curves [4]. For irreversible reactions, the kinetics is not as rapid. Therefore, kinetic parameters such as the transfer coefficient (α) should be involved.

5.1 A simplified approach to steady-state mass transfer limited reversible reactions

In this section, the oxidation of a species at an anode will be considered. The reaction is reversible as shown below,

$$Re \underset{\longleftarrow}{\overset{+V}{\longrightarrow}} Ox + ne \tag{5.1}$$

where *Re* is the reduced state, *Ox* the oxidized state, n the number of electrons transferred in reaction, *e* the electron.

Assume that the kinetics of electron transfer at the interface of electrode-electrolyte is rapid, i.e., the energy barrier for this reaction is negligible. The concentrations of *Re* and *Ox* are always at equilibrium with the electrode potential. The relationship follows the *Nernst equation*,

$$E = E^{0'} + \frac{RT}{nF} \ln \frac{C_{Ox}(x=0)}{C_{\mathrm{Re}}(x=0)} \tag{5.2}$$

where E is the potential, $E^{0'}$ the *formal potential* which is an adjusted form of the *standard potential* [4], R (the *universal gas constant*)$\approx$ 8.314 J $K^{-1}mol^{-1}$, T (temperature)= 298 K, F (the *Faradaic constant*)$\approx$ 96485 C mol^{-1}, *Ox* the oxidized state of species, *Re* the reduced product, *C(x=0)* the concentration of the Ox/Re species at the electrode surface.

The surface concentrations of *Re* and *Ox* at equilibrium may differ from the bulk ones, which creates a concentration gradient. Most of time, the electrochemical device is designed in the way that only diffusion contributes to mass transfer. The migration is eliminated by addition of a high concentration of inert electrolyte, such as 0.4 M HPO_4^{2-}/H_2PO^{4-} used in previous chapters, and convection is avoided by preventing perturbation and vibration. Therefore, diffusion of species from bulk solution to the electrode surface determines the signal current. A common method utilizing this design is the rotating disk electrode (RDE), where the working electrode is rotated in the electrolyte at a constant rate. The flow-mode with a constant flow rate has similar behavior as this device, where the electrolyte passes across the electrode surface with laminar flow.

It is reasonable to assume that a stagnant diffusion layer of thickness δ exists at the electrode surface [167]. The concentration of species beyond x= δ is equal to the bulk concentration, C*. Thus, the rate of mass transfer is proportional to the concentration gradient at the electrode surface,

$$v_{mt} = D(dC / dx)_{x=0} \tag{5.3}$$

where D is the diffusion coefficient (cm^2/s). Assuming further that a linear concentration gradient exists within the diffusion layer,

$$v_{mt} = D(dC / dx)_{x=0} = D[C^* - C(x=0)] / \delta \tag{5.4}$$

Since the reaction is mass transfer limited, the net rate of the anodic oxidation is determined by the rate at which the species *Re* is brought to the electrode surface. Thus,

$$v_{mt} = nFAi \tag{5.5}$$

where *A* is the surface area of electrode, *i* is the current. Then, combining equations 5.4 and 5.5, we obtain

$$nFAi = D[C^* - C(x=0)] / \delta \tag{5.6}$$

$$i = nFA^*(D / \delta)^*[C^* - C(x=0)] \tag{5.7}$$

Based on the above equation, some derivations will be made for eliminating $C_{Ox}(x=0)$ and $C_{Re}(x=0)$ in the Nernst Equation to obtain the *i-V* relationship.

In most sensing processes, the analyte is presented without the corresponding *Re/Ox* state. Take our project for example, when detecting cresol in solution, its

oxidized product is usually absent in the samples. Therefore, we consider the case where *Ox* is initially absent in bulk solution,

$$C_{Ox}^{*} = 0 \tag{5.8}$$

$$i = nFA*(D_{Ox}/\delta)*C_{Ox}(x=0) \tag{5.9}$$

$$C_{Ox}(x=0) = i/(nFA\delta/D_{Ox}) \tag{5.10}$$

In the reduced product part, we introduce a factor i_l, the *limiting current* (limited by diffusion). It occurs when $C_{Re}(x=0)=0$, and thus *Re* transfers to the electrode surface at the largest rate. At this condition, the anodic oxidation of cresol reaches a maximum because it is being oxidized as fast as it is brought to the surface,

$$i_l = nFA*(D_{\mathrm{Re}}/\delta)*C_{\mathrm{Re}}^{*} \tag{5.11}$$

According to Equation 5.7,

$$i = nFA*(D_{\mathrm{Re}}/\delta)*[C_{\mathrm{Re}}^{*} - C_{\mathrm{Re}}(x=0)] \tag{5.12}$$

Combining Equation 5.11 and 5.12, we obtain

$$C_{\mathrm{Re}}(x=0) = \frac{i_l - i}{nFAD_{\mathrm{Re}}/\delta} \tag{5.13}$$

Substitution of Equations 5.10 and 5.13 into 5.2 gives,

$$E = E^{0'} + \frac{RT}{nF}\ln\frac{\frac{i}{D_{Ox}/\delta}}{\frac{i_l - i}{D_{\mathrm{Re}}/\delta}} = E^{0'} + \frac{RT}{nF}\ln\frac{i}{i_l - i} + \frac{RT}{nF}\ln\frac{D_{\mathrm{Re}}}{D_{Ox}} \tag{5.14}$$

We define a variable of the *additional potential* (E_A), which often varies following the applied potential, as,

$$E_A = E - E^{0'} + \frac{RT}{nF} \ln \frac{D_{Ox}}{D_{\mathrm{Re}}} \tag{5.15}$$

Thus, we obtain the *current-potential relationship* for steady-state, mass transfer limited, reversible reactions,

$$E_A = \frac{RT}{nF} \ln \frac{i}{i_l - i} \tag{5.16}$$

It can be converted to be,

$$i = i_l (1 - \frac{1}{1 + e^{mE_A}}) \tag{5.17}$$

or,

$$i = lC_{Re}^{*} (1 - \frac{1}{1 + e^{mE_A}} \tag{5.18}$$

where l and m are constants defined as below,

$$l = nFAD_{Re} / \delta \tag{5.19}$$

$$m = nF / RT \tag{5.20}$$

The *i-E* relation from Equation 5.16 and 5.17 is depicted as Fig 5.1, where the *limiting current* is normalized to 100%. The *limiting current* is proportional to the concentration of species.

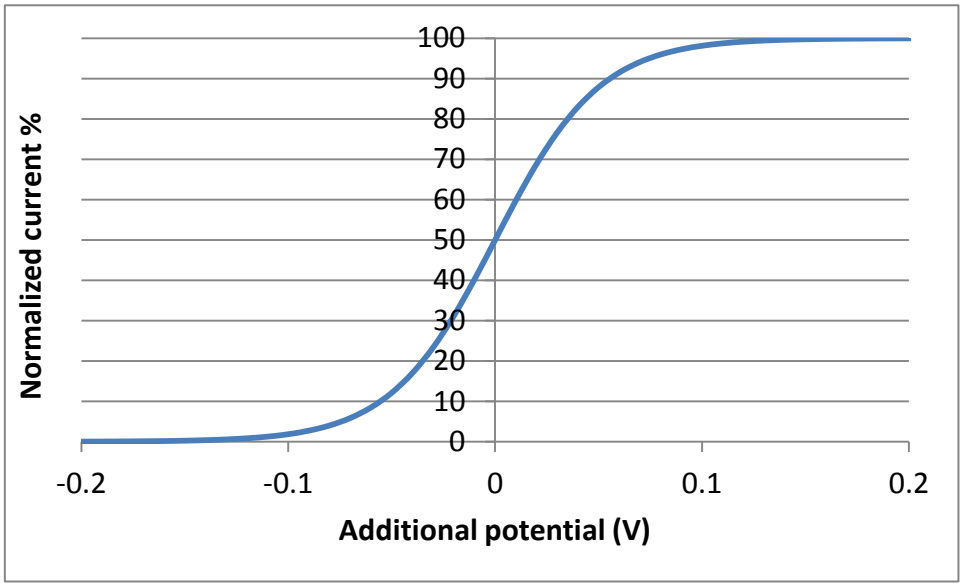

Fig. 5-1 The *i-E* curve based on the naive approach. Additional potential equals to 0 when $E = E^{0'} + \frac{RT}{nF} \ln \frac{D_{Ox}}{D_{\mathrm{Re}}}$.

For comparison, an experimental *i-E* curve was obtained from a CV scan of 10 μM $Fe(CN)_6^{4-}$ solution with constant flow rates of 20 or 100 ml/h, as shown in Fig. 5.2. The flow mode was realized by an experimental set-up which includes a syringe pump to provide the constant flow rate and an injector to operate the smooth switch from buffer to analyte solution (will be shown in Chapter 6).

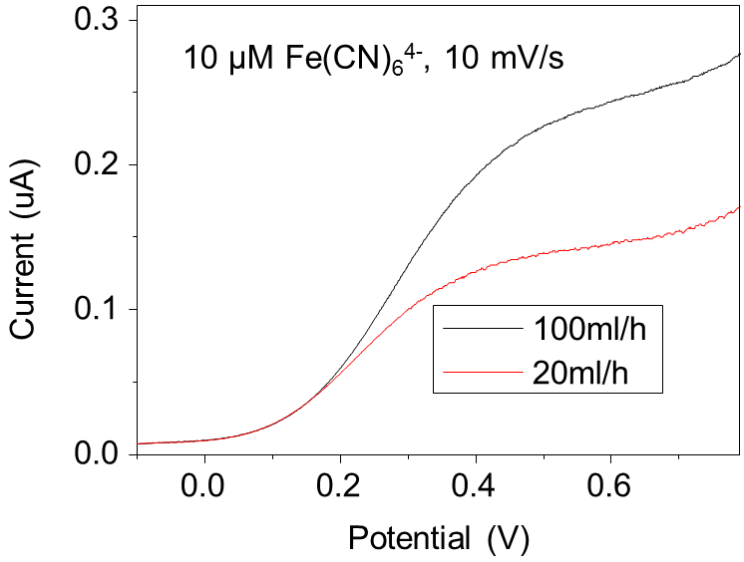

Fig. 5-2 The *i-E* curve of 10 μM $Fe(CN)_6^{4-}$ solution obtained in flow mode. The flow rates were 20 ml/h and 100 ml/h.

5.2 A rigorous approach to electrode reactions

The last section introduced a simple way to describe the *i-E* relationship for steady-state, diffusion controlled, reversible reactions. It was based on the assumptions that the concentration gradient from the electrode surface to the bulk solution was linear and the current was proportional to this gradient. Although these simplifications are reasonable in some degree and the above equation explains some experimental results, a more rigorous solution is necessary. The rigorous approach utilizes Laplace transformation to solve the diffusion equation, the boundary conditions, and Nernstian behavior for reversible reactions. For irreversible reactions, an estimation will be provided, but the derivations in detail is beyond the scope of this dissertation.

Same as last section, only diffusion is considered to contribute to mass transfer, and *Ox* is initially absent. Assuming that the linear diffusion equation holds for both *Ox* and *Re* states,

$$\frac{\partial C(x,t)}{\partial t} = D\frac{\partial^2 C(x,t)}{\partial x^2} \tag{5.21}$$

The boundary conditions are,

$$C_{Re}(x,0) = C_{Re}^{*}, \tag{5.22}$$

$$\lim_{x\to\infty} C_{Re}(x,t) = C_{Re}^{*}, \tag{5.23}$$

$$C_{Ox}(x,0) = 0, \tag{5.24}$$

$$\lim_{x\to\infty} C_{Ox}(x,t) = 0 \tag{5.25}$$

By applying the Laplace transform (readers who are interested can refer to the Appendix A in Bard's book [4]), we obtain the concentration profile of both *Re* and *Ox* states,

$$\overline{C_{Re}}(x,s) = \frac{C_{Re}^{*}}{s} + f_A(s)e^{-(s/D_{Re})^{1/2}x} \tag{5.26}$$

$$\overline{C_{Ox}}(x,s) = f_B(s)e^{-(s/D_{Re})^{1/2}x} \tag{5.27}$$

where *s* is a Laplace variable that is complementary to *t*, and $f_A(s)$ and $f_B(s)$ are functions of *s*.

In order to evaluate both functions of $f_A(s)$ and $f_B(s)$, the flux balance on the electrode surface is used,

$$D_{Re}\left(\frac{\partial C_{Re}(x,t)}{\partial x}\right)_{x=0} + D_{Ox}\left(\frac{\partial C_{Ox}(x,t)}{\partial x}\right)_{x=0} = 0 \tag{5.28}$$

Its Laplace transformation yields

$$D_{Re}\left(\frac{\partial \overline{C_{Re}}(x,s)}{\partial x}\right)_{x=0} + D_{Ox}\left(\frac{\partial \overline{C_{Ox}}(x,s)}{\partial x}\right)_{x=0} = 0 \tag{5.29}$$

Substitution of Eq. 5.26 and 5.27 into 5.29 gives,

$$D_{Re}\left(\frac{\partial\left(\frac{C_{Re}^{*}}{s}+f_A(s)e^{-(s/D_{Re})^{1/2}x}\right)}{\partial x}\right)_{x=0}+D_{Ox}\left(\frac{\partial\left(f_B(s)e^{-(s/D_{Re})^{1/2}x}\right)}{\partial x}\right)_{x=0}=0 \quad (5.30)$$

Thus,

$$D_{Re}\left(0+[-(s/D_{Re})^{1/2}]f_A(s)e^{-(s/D_{Re})^{1/2}x}\right)\Big|_{x=0}+D_{Ox}\left([-(s/D_{Ox})^{1/2}]f_B(s)e^{-(s/D_{Ox})^{1/2}x}\right)\Big|_{x=0}=0 \quad (5.31)$$

or,

$$-(sD_{Re})^{1/2}\,f_A(s)e^{0}-(sD_{Ox})^{1/2}\,f_B(s)e^{0}=0 \quad (5.32)$$

Thus, $f_B(s)$ can be eliminated,

$$f_B(s)=-(D_{Re}/D_{Ox})^{1/2}\,f_A(s) \quad (5.33)$$

Substituted to Eq. 5.27,

$$\overline{C_{Ox}}(x,s)=-(D_{Re}/D_{Ox})^{1/2}\,f_A(s)e^{-(s/D_{Re})^{1/2}x} \quad (5.34)$$

For simplicity, we introduce a variable r as the ratio of surface concentrations of Re/Ox,

$$r=C_{Re}(0,t)/C_{Ox}(0,t)=C_{Re}(0,s)/C_{Ox}(0,s) \quad (5.35)$$

Combination of Eq. 5.34 and 5.35 gives,

$$C_{Re}(0,s) = -r(D_{Re}/D_{Ox})^{1/2}\, f_A(s) e^{-(s/D_{Re})^{1/2} x} \tag{5.36}$$

Combination of Eq. 5.36 and 5.26 gives,

$$\frac{C_{Re}^{*}}{s} + f_A(s) e^{-(s/D_{Re})^{1/2} x}\Big|_{x=0} = -r(D_{Re}/D_{Ox})^{1/2}\, f_A(s) e^{-(s/D_{Re})^{1/2} x}\Big|_{x=0} \tag{5.37}$$

or,

$$\frac{C_{Re}^{*}}{s} + f_A(s) = -r(D_{Re}/D_{Ox})^{1/2}\, f_A(s) \tag{5.38}$$

Thus, $f_A(s)$ can be eliminated,

$$f_A(s) = \frac{C_{Re}^{*}}{s}\left(\frac{-1}{1+r(D_{Re}/D_{Ox})^{1/2}}\right) \tag{5.39}$$

Substituted to Eq. 5.26 and 5.36, the concentration profile becomes,

$$\overline{C_{Re}}(x,s) = \frac{C_{Re}^{*}}{s} + \frac{C_{Re}^{*}}{s}\left(\frac{-1}{1+r(D_{Re}/D_{Ox})^{1/2}}\right) e^{-(s/D_{Re})^{1/2} x} \tag{5.40}$$

$$\overline{C_{Ox}}(x,s) = -(D_{Re}/D_{Ox})^{1/2}\, \frac{C_{Re}^{*}}{s}\left(\frac{-1}{1+r(D_{Re}/D_{Ox})^{1/2}}\right) e^{-(s/D_{Re})^{1/2} x} \tag{5.41}$$

Since the flux of species, J, at the electrode surface is proportional to the current,

$$-J_{Re}(0,t) = \frac{i(t)}{nFA} = D_{Re}\left(\frac{\partial C_{Re}(x,t)}{\partial x}\right)_{x=0} \tag{5.42}$$

Applying the derivative on Eq. 5.40 and substituted to Eq. 5.42 yields,

$$i(t) = nFAD_{Re}\frac{C_{Re}^{*}}{\pi t}\left(\frac{-1}{1+r(D_{Re}/D_{Ox})^{1/2}}\right)\left(-(\pi t/D_{Re})^{1/2}\right) \tag{5.43}$$

or,

$$i(t) = \frac{nFAD_{Re}^{1/2}C_{Re}^{*}}{\pi^{1/2}t^{1/2}(1+r(D_{Re}/D_{Ox})^{1/2})} \tag{5.44}$$

Same as previous section, we introduce the limiting current i_l, which occurs when $C_{Re}(x=0)=0$. It occurs when the potential is high enough and all *Re* is oxidized once it comes to the surface. Then (the ratio of *Re*/*Ox) r*= 0, and thus the i_l is,

$$i_l(t) = \frac{nFAD_{Re}^{1/2}C_{Re}^{*}}{\pi^{1/2}t^{1/2}} \tag{5.45}$$

This equation is known as the *Cottrell equation.* Comparison of Eq. 5.45 and 5.44 gives,

$$i = \frac{i_l}{1+r(D_{Re}/D_{Ox})^{1/2}} \tag{5.46}$$

or,

$$\frac{C_{Re}(x=0)}{C_{Ox}(x=0)} = r = (D_{Ox}/D_{Re})^{1/2}\frac{i_l - i}{i} \tag{5.47}$$

Now, we consider the reversible reactions. The Nernst Equation (Eq. 5.2) holds in this case. Combination of Eq. 5.2 and 5.47 gives,

$$E = E^{0'} + \frac{RT}{2nF}\ln\frac{D_{\mathrm{Re}}}{D_{Ox}} + \frac{RT}{nF}\ln\frac{i}{i_l - i} \tag{5.48}$$

By this point, we see that the i-E relationship is almost identical to Eq. 5.14 developed in previous section, except by a factor of 2. Similarly, we define E_A as an additional potential,

$$E_A = E - E^{0'} + \frac{RT}{2nF} \ln \frac{D_{Ox}}{D_{\mathrm{Re}}} \tag{5.49}$$

Thus, we obtain the identical *current-potential relationship* for mass transfer limited reversible reactions,

$$E_A = \frac{RT}{nF} \ln \frac{i}{i_l - i} \tag{5.50}$$

and,

$$i = i_l (1 - \frac{1}{1 + e^{mE_A}}) \tag{5.51}$$

where *m* is the same constant defined as Eq. 5.20, $m = nF / RT$.

Then, for the irreversible reactions, some kinetic parameters such as the transfer coefficient (α) should be considered. The *current-potential relationship* changes very little (readers who are interested can refer to Bard's book [4]),

$$E_A = \frac{RT}{\alpha F} \ln \frac{i}{i_l - i} \tag{5.52}$$

and,

$$i = i_l (1 - \frac{1}{1 + e^{mE_A}}) \tag{5.53}$$

$$m = \alpha F / RT \tag{5.54}$$

the transfer coefficient $\alpha \sim 0.5$ in most of cases.

This current-potential relationship will be used in Chapter 6 dealing with the irreversible oxidation of cresol during electrochemical analysis. In this case, the *Re* is cresol, and the *Ox* is the oxidation product of cresol.

6. A study of electrode fouling during electrochemical analysis of phenolic compounds

6.1. Introduction

As mentioned in Chapter 1, electrode fouling is a common problem during electrochemical analysis of phenolic compounds. In the project involved with this dissertation, we were developing an electrochemical device for long-term monitoring of TCP in the aircraft cabin environment. The formation of a polymeric fouling layer on the electrode created a current decay and therefore some error in results, and shortened the time during which the device was reliable. That is why anti-fouling modifications were conducted on the electrode surface as mentioned in Chapter 4. A deeper understanding about electrode fouling is necessary for scientific investigation and development of appropriate countermeasures for its effect. The chemical reactions that occur during anodic oxidation of phenolic compounds have been discussed in Chapter 1. The efforts people have made to study the chemical and physical properties of the fouling layer have also been described. In addition, the mechanism of how the polymeric layer causes the electrode fouling is always of interest.

One model that is based on “area blocking”/”active site poisoning” predicted a linear relationship between the rate of passivation and the remaining unblocked electrode area, and thus the logarithm of current decreased linearly with time [77]. This model might be useful only at the beginning stage of electrode fouling, since this poly-phenolic film was readily available to create a complete coverage on electrodes [168]. In long term fouling, a model concerning the whole fouling layer on the electrode is needed. With the ellipsometric method, Babai and Gottesfeld studied the growth of the polymeric layer during the oxidation of phenolic compounds in acidic medium on platinum electrodes, and considered that film diffusion was mainly responsible for the electrode fouling [98]. They observed that the rate of film growth

changed inversely with the square root of time and varied with applied potential, and concluded that the charge diffusion through the layer controlled the current decay. However, this simple film diffusion based model suggested a slope of -1/2 on the plot of log *i vs.* log *t*, which deviates from our recorded current decay curve. The deviation of explanation may have been caused by the ellipsometric technique only gave 10-20 readings per curve and hid the real curve tendency [77]. Gattrell and Kirk studied the influences of the species concentration and applied potential on electrode fouling with GPC, XPS, CV, and amperometric methods, and created a semi-empirical model based on electron tunneling [77]. The tunneling current decreased nearly exponentially with the film thickness and was proportional to passed charge. Since the whole fouling layer was too thick for electron tunneling (10-100 nm), the authors considered that the fouling layer was not uniform and consisted of successive blocking films. The upper region of the polymeric film was made of lower MW substrates and therefore allowed electrons to tunnel through the thinner layers. Thus, electron tunneling through the lower region, instead of the whole polymeric film, was the rate determining step. To fit the experimental data, they used the multiplication of the Tafel equation by the electron tunneling possibility [4, 169, 170]. They expected that the current decay curve consisted of a short initiation region with relative constant current and a fouling region where the current dropped inversely proportionally with time. However, the model contradicted with the experimental data that we obtained. Some inappropriate experimental designs may be responsible to the contradiction. The chronoamperometry with a potential step was used, which brought the superimposition of double-layer charging current and transient Cottrell current (Equation 5.45) on the fouling current. An insufficient amount of data points may also be responsible for deviation from the obtained experimental data.

It was reported that potential drop was created by the thiol layer [171] and electrodeposited polypyrrole on electrodes [172]. The fouling layer had similar dielectric properties. In this chapter, a potential drop based model was proposed to explain and quantitatively predict the fouling current during electroanalysis of cresol in terms of time and applied potential. To realize a steady state, the devices were set

up in flow mode with constant flow rates and constant applied potential. Copper deposition was utilized to demonstrate and quantitatively measure the potential drop.

6.2. Materials and Methods

6.2.1. Reagents and solutions

All aqueous solutions were prepared with de-ionized Milli-Q water (18 MΩ cm). The stock 20 mM *p*-cresol (Acros Organics, NJ, 99+%) solution was prepared and diluted in 0.2 M Na_2HPO_4/0.2 M KH_2PO_4/10 mM NaCl buffer (0.4 M phosphate buffer, pH = 6.67) to obtain cresol samples with concentrations of interest. Na_2HPO_4, KH_2PO_4, and NaCl were obtained from Sigma-Aldrich, MO. For copper deposition, 10 mM cupric sulfate ($CuSO_4$ $5H_2O$, 99.3%, Fisher Scientific) plus 10 mM sulfuric acid (H_2SO_4, GR ACS, 95-98%) aqueous solution was prepared. For impedance measurements, aqueous solutions of 1 mM potassium ferricyanide ($K_3Fe(CN)_6$, Reagent ACS, Acros Organics) and 1mM potassium ferrocyanide ($K_4Fe(CN)_6$, GR ACS, EMD) were used.

6.2.2. Flow system and electrochemical devices

The flow mode analysis was realized by the setup shown in Fig.6-1. A dual syringe pump (infuse only, KD Scientific, MA) along with two 20 mL plastic syringe (BD) provided the constant flow rate (20 mL/h, unless otherwise stated). The solution that flowed through the electrode set was swapped between 0.4 M phosphate buffer and cresol by the manual sample injector (Rheodyne LLC, CA). The unicell electrode set (BASi, IN) consists of one glassy carbon working electrode block (2 mm ø), one auxiliary electrode (stainless steel) and reference electrode (Ag/AgCl) block, and one circular gasket. A yellow coating solution was applied for the reference electrode before use to create a reliable AgCl layer as per instruction from the company. The working electrode was polished with alumina slurries (1, 0.3, and 0.05 μm sequentially). 10 mM NaCl was included in every solution that was measured to maintain the potential of reference electrode. All amperometric experiments were

performed with CH1910B Bi-Potentiopstat (CH Instruments, Inc., TX) and a desktop computer.

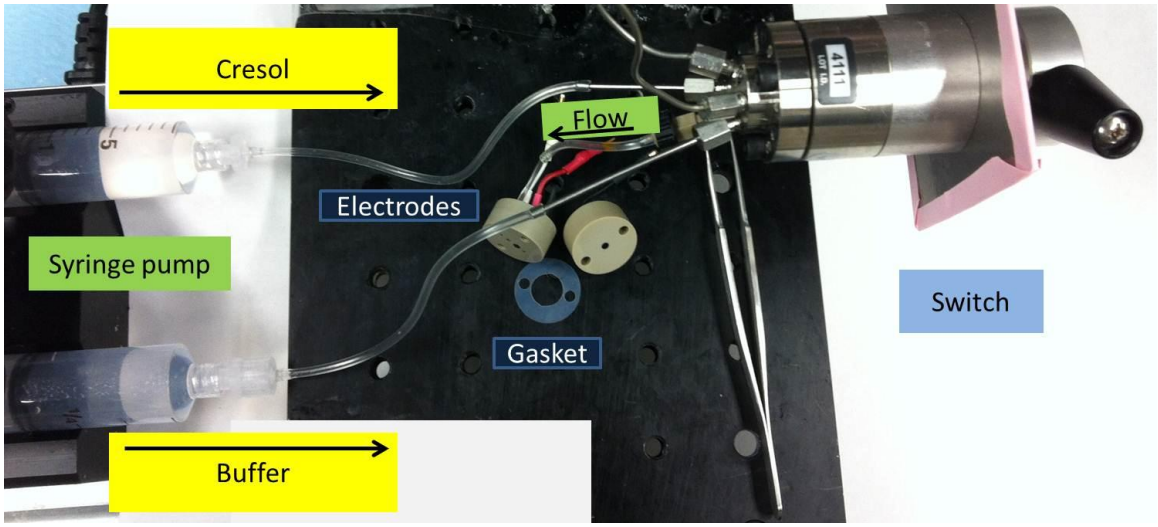

Fig. 6-1 Experimental setup for the flow mode analysis. A dual channel syringe pump (left side) was used to provide constant flow rate. A sample injector (right side) was used to swap the flow solution that ran through the unicell electrode set (center).

Impedance technology was performed with μAutolab potentiostat (Metrohm Autolab B.V., The Netherlands). The unicell working electrode was immersed in the aqueous solution of 1mM/1mM $Fe(CN)_6^{3-/4-}$ and 100 mM KCl, along with a Pt counter electrode, and an Ag/AgCl/Sat. KCl reference electrode (BASi, IN). The applied DC potential was 0.21 V, corresponding to the midpoint of oxidation and reduction peaks in CV curve. The AC amplitude was 5 mV, and the frequency range was 10 kHz to 0.1 Hz, divided logarithmically to 50 points.

6.2.3. Air bubbled fouled electrodes

In some experiments to create a fouling layer on electrode surface, an air bubble was introduced and stuck onto the electrode. The air bubble covered certain area of the electrode surface and prevented that area from fouling. Thus, the electrode had

one part of surface fouled and another part un-fouled, simultaneously. The color difference between fouled and unfouled area was significant and could be seen in optical microscope images. The area ratio between the air bubbled and the whole electrode surface was measured with the ImageJ software.

It was found that the air bubble was easy to stick to the electrode when the unicell electrodes were placed in such a way that the inlet and outlet tips were horizontal and at equal heights. To avoid air bubble during electrode fouling in other cases, keeping the inlet and outlet tips upright was favored.

6.2.4. Cu deposition on electrodes

Cu depositions on polished and fouled glassy carbon working electrodes were conducted in batch mode along with the Pt counter electrode and the Ag/AgCl/Sat. KCl reference electrode. The deposition was accomplished by applying linear sweep voltammetry (LSV) from 0.5 V to -0.8 V or one cycle of cyclic voltammetry (CV) in the same range (negatively scan first), unless otherwise stated.

6.2.5. Characterizations of fouling layer and Cu deposition

The air bubbled fouled electrodes were checked with Ellipsometry (the thickness of fouling layer) and Profilometry (the thickness and surface roughness of the fouling layer). AFM was used to characterize the fouling layer. AFM data were processed with the software of Gwyddion. A digital microscope (Dino-Lite, Taiwan, ROC) and an optical microscope (BX41, Olympus, Japan) were used to obtain the images of fouling layer, polished electrode surface, and copper deposition on the electrode surface. SEM (JSM-7000F field emission scanning electron microscope, JEOL Ltd, Japan) incorporated with EDS detector (X-Max, Oxford Instruments, UK) were used to characterize the Cu deposition.

6.3. Results and Discussions

6.3.1. Characterizations of potential drop

Although the glassy carbon is considered as electrochemically inert and a good type of working electrode material, the sp^2 carbon readily chemisorbs oxygen and is oxidized when exposed to air at room temperature, which will change its activity and influences the charge transfer at the interface of carbon-electrolyte [173, 174]. In order to reduce the variation due to the surface oxide, the electrode was polished freshly with Al_2O_3 slurries (mentioned in section 6.2.2) before use.

The amperometric process, with a constant applied potential of 0.75 V vs. Ag/Ag/10 μM NaCl, was used to demonstrate the electrode fouling (Fig.6.2.a). In the time range of 0-400 s, phosphate buffer was flowing through the electrode set, during which the double layer charging current was diminished [4]. At 400 s, the charging current became negligible and the background was close to 0. The sample injector was manually switched, and 10 μM *p*-cresol was allowed to flow over the working electrode. This operation was kept smooth and rapid to avoid disturbing the flow rate. Once cresol reached the electrode surface, it was oxidized to the phenolic radicals and formed polymeric substrates which covered the electrode surface and brought about electrode fouling. The electrode fouling continued until the flow over the electrode was swapped back to phosphate buffer. Thus, the duration of cresol flow was the time of electrode fouling (the mass transfer effect from sample injector to electrode was ignored). A series of fouling time froms 0 to 600 s was used and electrodes with different degrees of fouling were obtained. 0 means polished electrode without fouling. The current decay during electrode was similar for each case (Fig.6-2a).

When immersed into Cu^{2+} acid solution, the above 0-600 s fouled electrodes were applied with a potential sweep from 0.5 to -0.8 and then reversely swept to 0.5 V vs. Ag/AgCl/Sat. KCl for Cu deposition. The obtained CV curves were shown in Fig.6.2.c, and part of the forward potential sweep was zoomed in Fig.6.2.b. At polished electrode (0 fouled), Cu started to deposit around 0 V. But the deposition was delayed further at more fouled electrode. In the reverse potential scan, the stripping of deposited Cu happened and started at similar potential. Cu deposition was

also conducted on polished electrodes with different scan rates, the potential of Cu deposition did not vary significantly (data not shown). The delay of Cu deposition on fouled electrode was proposed to be due to the potential drop across the fouling layer.

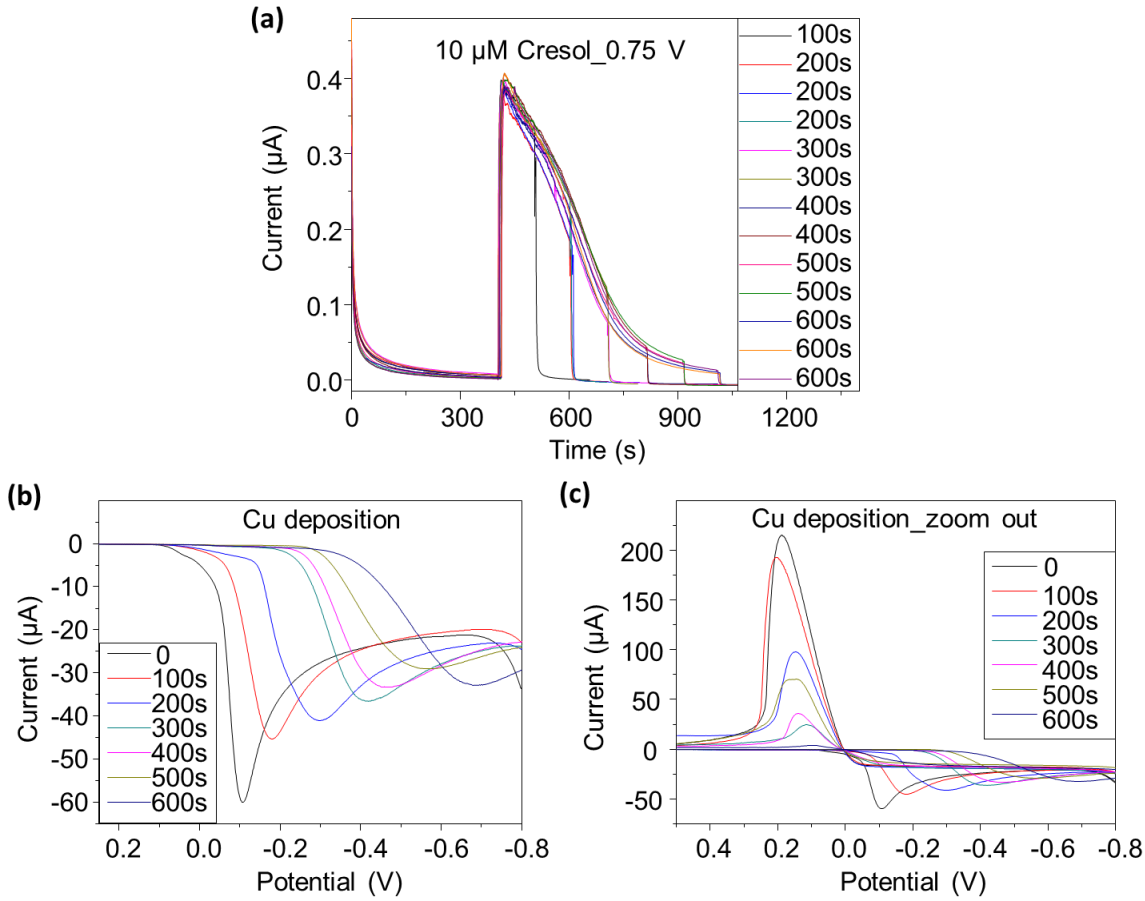

Fig. 6-2 Amperometric results and voltammograms of electrode fouling and Cu deposition. (a) Electrodes were fouled at 0.75 V vs. Ag/AgCl/10 µM NaCl with 10 µM cresol for 0, 100, 200, 300, 400, 500, and 600 s. (b,c) Electrodes were conducted with Cu deposition. One representative example set of potential sweep curves were shown. The scan rate was 10 mV/s. The forward potential sweep was negative, from 0.5 to -0.8 V, in which Cu deposition peaks presented. The peaks of Cu stripping were presented in the following positive sweep. All glassy carbon working electrodes had a diameter of 2 mm.

The Cu deposition on the electrode surface was characterized with optical microscope, SEM, and EDS (Fig.6-3). By applying a potential sweep from 0.5 to -0.1 V, the polished electrode was already deposited with Cu crystals (Fig.6-3a), however, the Cu deposition did not occur on 300 s fouled electrode (Fig.6-3b). Cu deposition occurred on the fouled electrode if the potential swept was sufficiently negative as mentioned above. The deposited Cu on fouled electrode was harder to strip than the polished one [171]. After a CV cycle of 0.5- -0.8 V, almost all of the deposited Cu on polished electrode was stripped (Fig.6-3c, right side of image), while most of the deposited Cu remained on fouled electrode (Fig.6-3d). The SEM and EDS results confirmed the deposition of Cu.

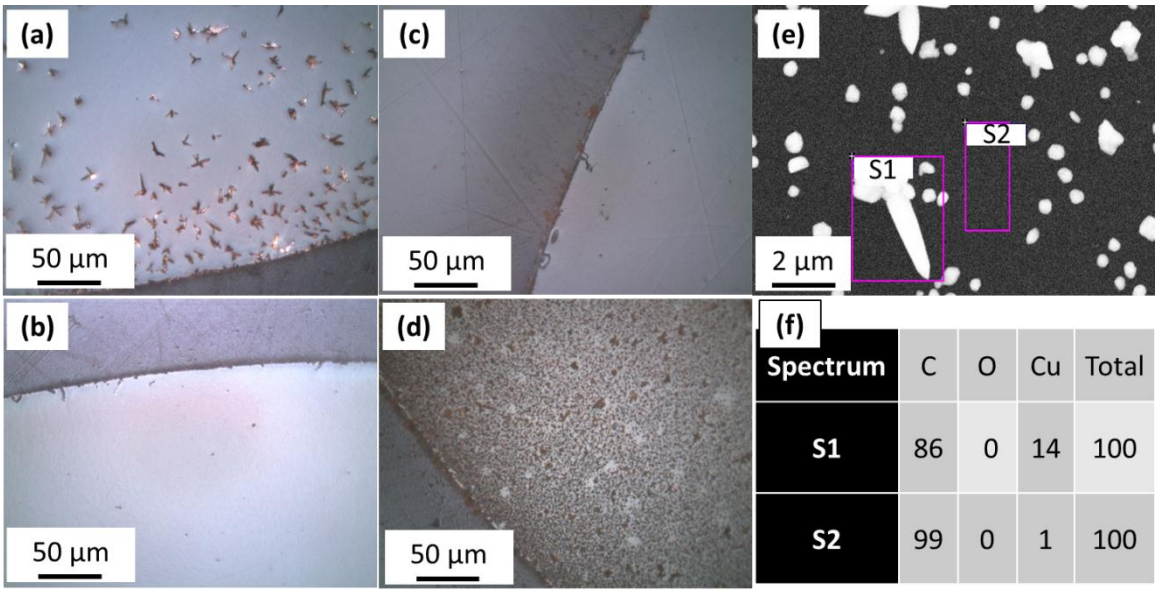

Spectrum	C	O	Cu	Total
S1	86	0	14	100
S2	99	0	1	100

Fig. 6-3 Observation of Cu deposition on electrodes with optical microscope (a-d), SEM (e), and EDS (f). Cu deposition with potential sweep from 0.5 to -0.1 V on polished electrode (a) and 300 s fouled electrode (b); Cu deposition with potential sweep from 0.5 to -0.8 V and to 0.5 V on polished electrode (c) and 300 s fouled electrode (d); SEM images of Cu deposition on polished electrode (e); and corresponding EDS results (f).

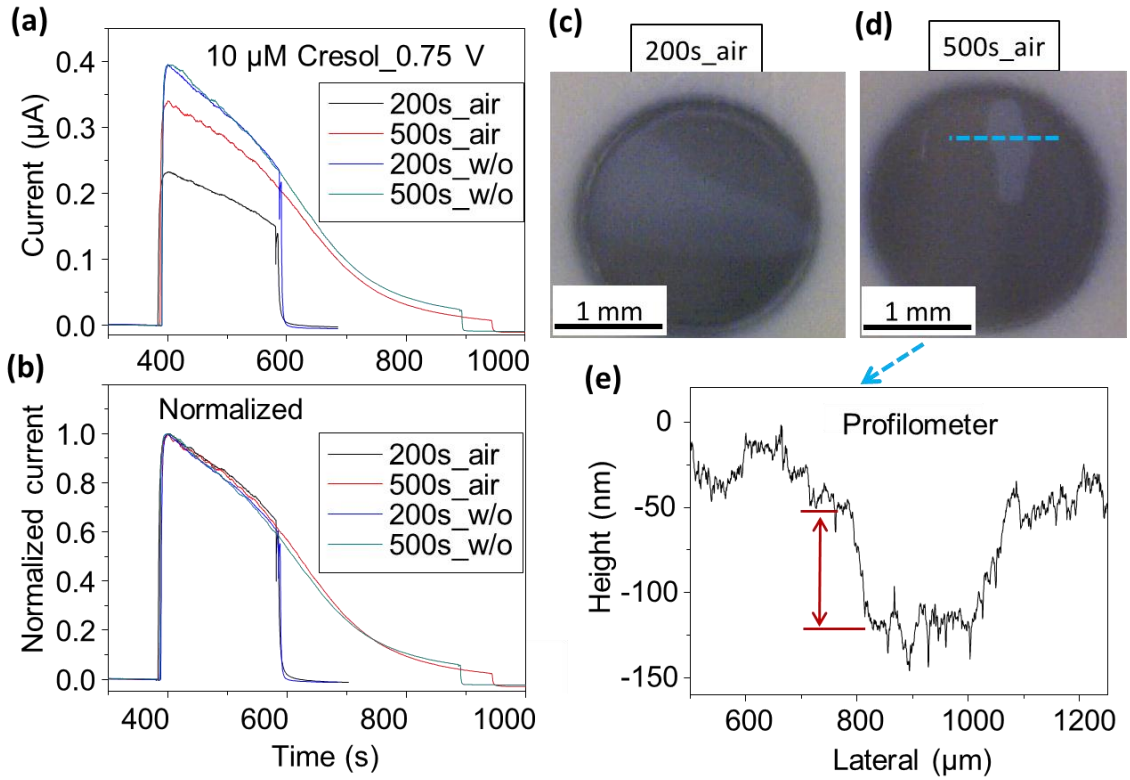

Fig. 6-4 Characterization of with or without air bubbled fouled electrodes. (a) Current intensity curves of 10 μM cresol analysis in the amperometry mode. The applied potential was 0.75 V. (b) Normalized current intensities. The highest current was normalized to unity. (c,d) Optical images of air bubbled 200 s and 500 s fouled electrodes. (e) Profilometry results of the line scan across the air bubbled area on 500 s fouled electrode.

With the air bubbled 200s and 500s fouled electrodes, the comparison of Cu deposition on unfouled and fouled surface was realized on the same electrode. Such kind of electrodes were characterized with amperometry (Fig.6-4a,b), optical microscopy (c,d), profilometry (e), and ellipsometry (data not shown). Compared to electrodes without air bubbling, the air bubbled ones had decreased current intensities during cresol analysis (a), but had equal normalized response (b). The difference of the current intensity was considered to result from the variation of the exposed area to electrolyte, since the current decay tendency was the same for all four electrodes.

Since the fouled and unfouled area had different colors in optical microscopy images, the position of the air bubble could be traced (c,d). With the profilometer, the morphology of air bubbled 500 s fouled electrode was checked. A line scan was conducted across the air bubble and a height jump of ~75 nm at the edge of fouling layer was obtained. Correspondingly, the ellipsometry results showed that the thickness of the fouling layer on air bubbled 200 s fouled electrode was ~30 nm (data not shown).

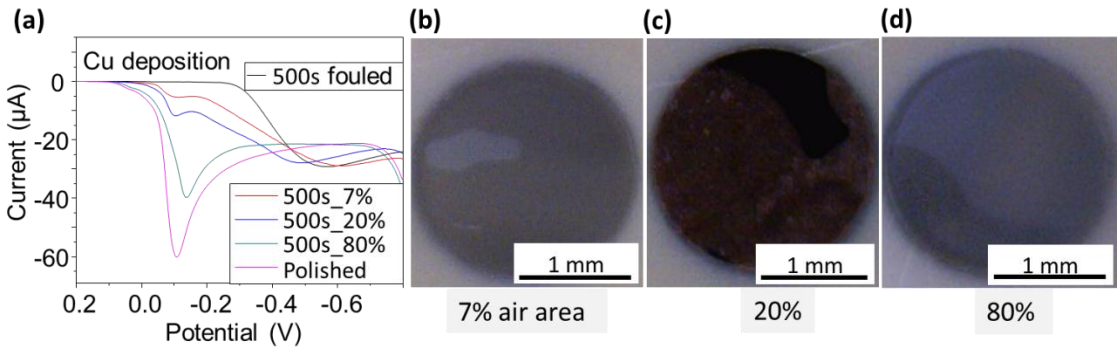

Fig. 6-5 Cu deposition and optical images of air bubbled 500 s fouled electrodes. (a) Cu deposition on polished, fouled w/o air bubbled, air bubbled fouled electrodes. Only part of the forward potential sweep was shown. The order of the labels corresponded to the **positions** of the current intensity at ~-0.1 V. (b,c,d) Optical images of electrodes that were covered by an air bubble with different sizes. Values in percentage indicated the ratio of air bubble covered to the whole electrode surface.

The size of the air bubble that covered the electrode surface during cresol fouling could also be varied. Three air bubbled 500 s fouled electrodes were prepared carefully and the ratios of the air bubbled to the whole electrode surface were varied and measured to be 7%, 20%, and 80% (Fig.6-5b,c,d). Along with one 500 s fouled electrode without air bubbled and one freshly polished electrode, these electrodes were conducted with Cu deposition (a). The deposition started on polished electrode around 0 V, while was delayed by ~0.4 V on 500 s fouled electrode. On the air bubbled fouled electrodes, the reduction peak that was similar as on the polished one also presented, and the peak current value increased with higher ratio of the air

bubbled area. This phenomenon confirmed that the potential drop across the fouling layer delayed the Cu deposition.

6.3.2. Quantitative determination of potential drop

In order to create a scientific electrode fouling model, the potential drop across the fouling layer was measured quantitatively with Cu deposition. In this case, the air bubble was avoided during electrode fouling. All of the current-potential curves of Cu deposition were conducted with 1st and 2nd differentiations with respect to the time. One example for polished electrode was shown in Fig. 6-6. The minimum of the 1st derivative corresponded to the highest reduction rate prior to the reduction peak, while the minimum of the 2nd derivative corresponded to the highest reduction acceleration.

Both of minimum of 1st and 2nd derivative were measured and subtracted from the averaged value for polished electrodes, by which the potential drop was calibrated in terms of the 1st and 2nd differentiations. The average values of potential drop were calculated and fitted linearly for electrodes fouled with different times (Fig. 6-7). The potential drop amount increased linearly with fouling time, at the rate of ~0.6 mV/s. The value of $6*10^{-4}$ V/s would be used to relate the potential drop with time in quantitative discussion that follows (Eq. 6.1).

$$\Delta E_f = 6*10^{-4} t \tag{6.1}$$

Note that at the beginning of electrode fouling (e.g. 1st 5 s of cresol flow), the fouling substrates were not enough to cover the surface completely, as in the model mentioned in the introduction part. However, this stage would not last for long [168] (e.g., 5 s for 10 μM cresol flow, ideally) and was ignored in this chapter where hundreds of seconds of fouling time were considered. More accurate model may be obtained if the incomplete fouled stage was involved, but it was beyond the scope of discussion in this chapter.

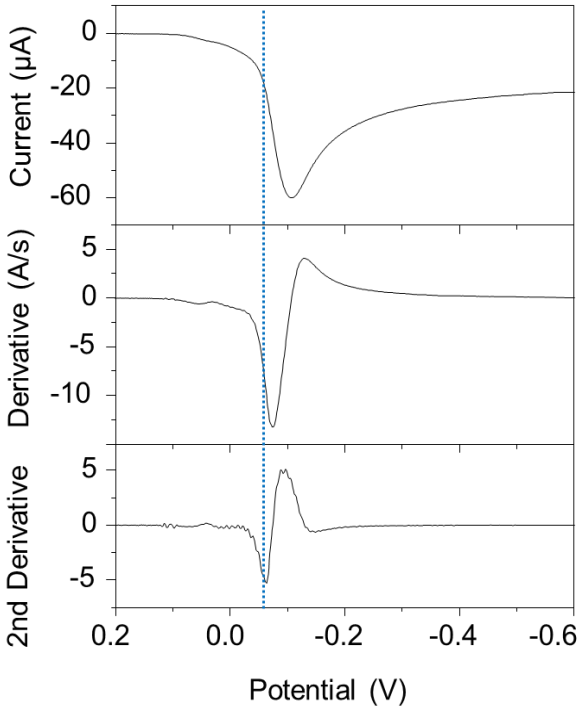

Fig. 6-6 Example of the 1st and 2nd differentiations of the current-potential curve of Cu deposition on polished electrode.

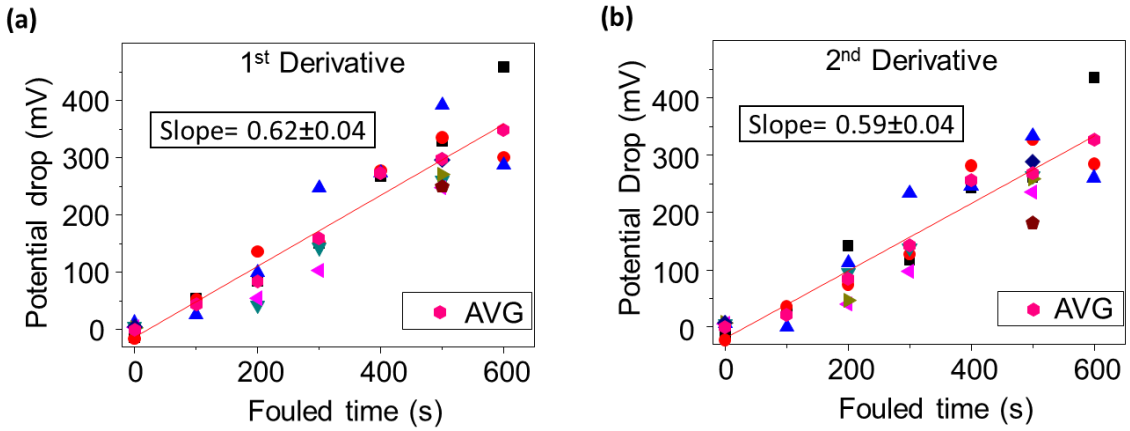

Fig. 6-7 Calibration of the potential drop measured with Cu deposition. The values of potential drop were obtained by subtracting the derivative minimum from the averaged value for polished electrodes. (a) Summary of all values of potential drop obtained with the 1st differentiation. (b) Summary from the 2nd differentiation.

6.3.3. The potential drop based model to electrode fouling

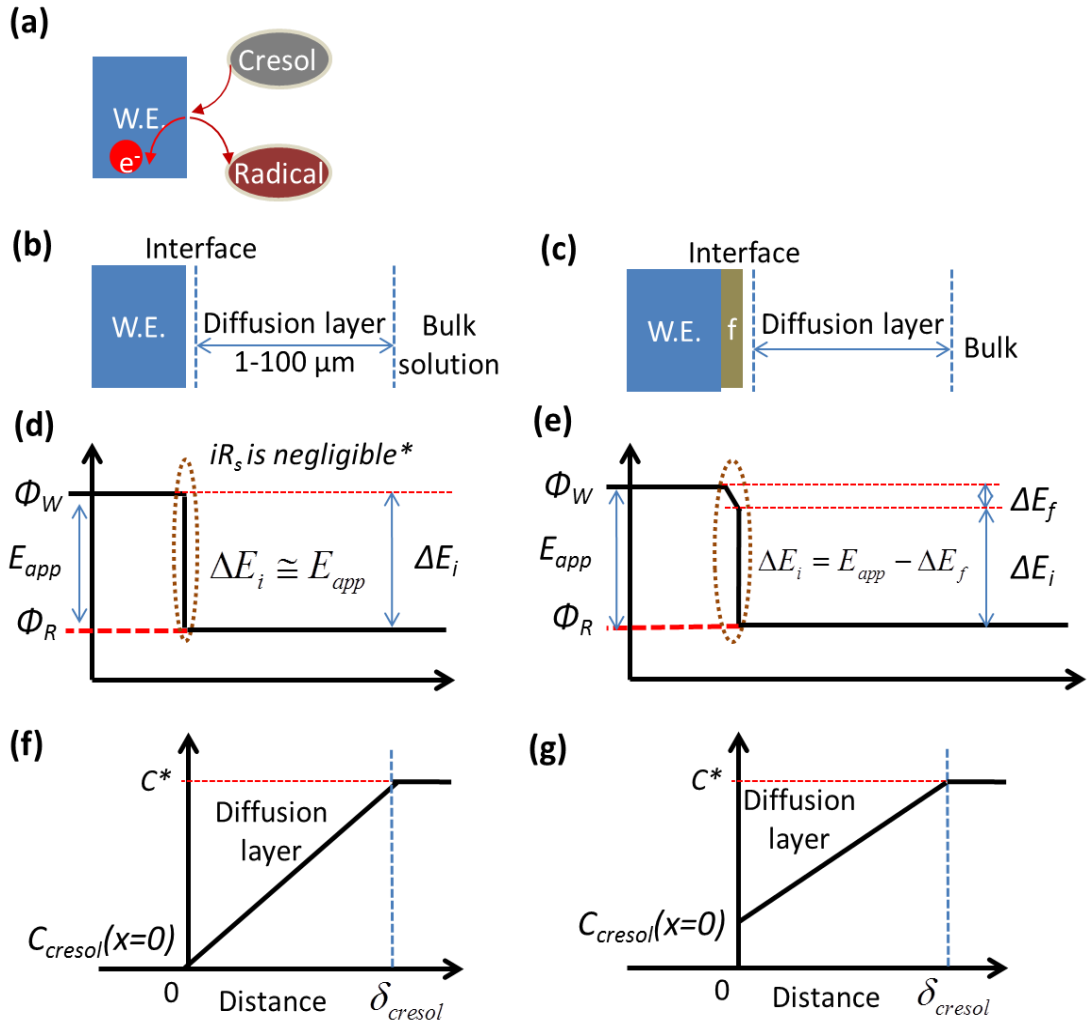

Fig. 6-8 Schematic representative of the effect of the fouling layer on the potential profile and concentration profile close to electrode surface [4, 175]. (a) Cresol was oxidized at the interface of electrode-electrolyte. (b,c) The configurations of the working electrode, fouling layer, interface, diffusion layer, and bulk solution. (d,e) The potential profile close to the electrode surface w/ or w/o the fouling layer. The potential drop from the solution is ignored. (f,g) The simplified concentration profile of cresol close to the electrode surface. The concentration gradient was assumed to be linear.

W.E. means the working electrode, f the fouling layer, ϕ_W the work functions of working electrode, ϕ_R of reference electrode, E_{app} the applied potential, R_s the solution resistance, iR_s the potential drop across the electrolyte solution, ΔE_i the interface potential, ΔE_f the fouling layer potential drop, C^* the bulk concentration, C(x=0) the surface concentration, δ the thickness of "simplified" diffusion layer.

The idea of potential drop across the fouling layer is shown schematically in Fig.6-8. The interface of electrode-electrolyte is of interest (Fig.6-8a), because the interface potential, ΔE_i, determines the oxidation of cresol [4, 175]. A cresol diffusion layer presented between the interface and the bulk solution (Fig.6-8b), and the fouling layer placed between the electrode and electrolyte (Fig.6-8c). Since current flows through the solution, a potential drop of iR_s exists. However, the solution potential drop is always small and negligible (e.g. 1 μA*10 Ω= 0.01 mV). Thus, ΔE_i is similar as the applied potential ΔE_{app} on polished electrodes (Fig.6-8d). If fouling layer exists, a potential drop ΔE_f is created across it, and thus the ΔE_i is less than ΔE_{app} by the amount of ΔE_f on polished electrodes (Fig.6-8e). The change in potential influences the surface concentration of cresol and decreases the concentration gradient (Fig.6.8f,g), which causes the current decay.

As discussed in Chapter 5, the current intensity is related to the interface potential. For the irreversible oxidation of cresol,

$$i = i_l(1 - \frac{1}{1+e^{mE_A}}) \tag{6.2}$$

where i_l is the diffusion *limiting current*, E_A the *additional potential* that comes from the applied potential, $m = \alpha F/RT$, the transfer coefficient α~ 0.5, F (the *Faradaic constant*)≈ 96485 C mol^{-1}, R (the *universal gas constant*)≈ 8.314 J $K^{-1}mol^{-1}$, T (temperature)= 298 K, thus m~20 V^{-1}.

Introducing the relationship between the potential drop and time (Eq. 6.1), we obtain,

$$i = i_l(1 - \frac{1}{1+e^{m(E_{A0} - 6*10^{-4}t)}}) \tag{6.3}$$

Thus, the current is determined by the *limiting current* i_l, the *initial additional potential* E_{A0}, and the fouling time (starting from the point when cresol was oxidized).

In the case of amperometry analysis of 10 μM cresol at 0.75 V, the first two variables are constant, and thus the current varies only with time.

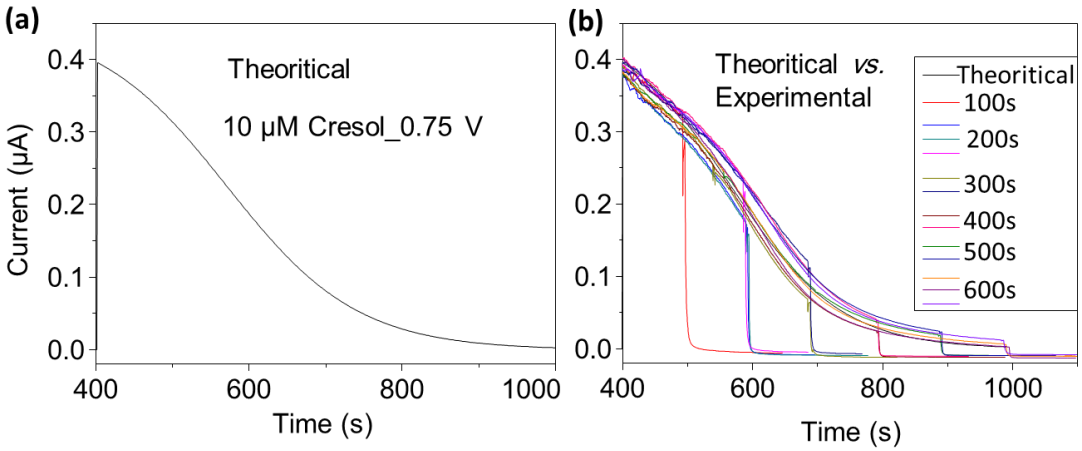

Fig. 6-9 Model curve and experimental curves of cresol fouling. (a) One example of the theoretical current decay during amperometry analysis of cresol. (b) The comparison of theoretical and experimental current curves for analysis of 10 μM cresol at 0.75 V. The theoretical curve overlapped other curves.

The model curve in Fig. 6-9 was obtained using values of: i_l = 450 nA, E_{A0}= 0.1 V, α= 0.5, m= 20 V^{-1}. The model curves compares well with the experimental data, in spite of the missing consideration of the beginning fouling stage when the fouling layer does not completely cover the electrode surface and may influence the interface potential differently.

6.3.4. Characterizations of the fouling layer

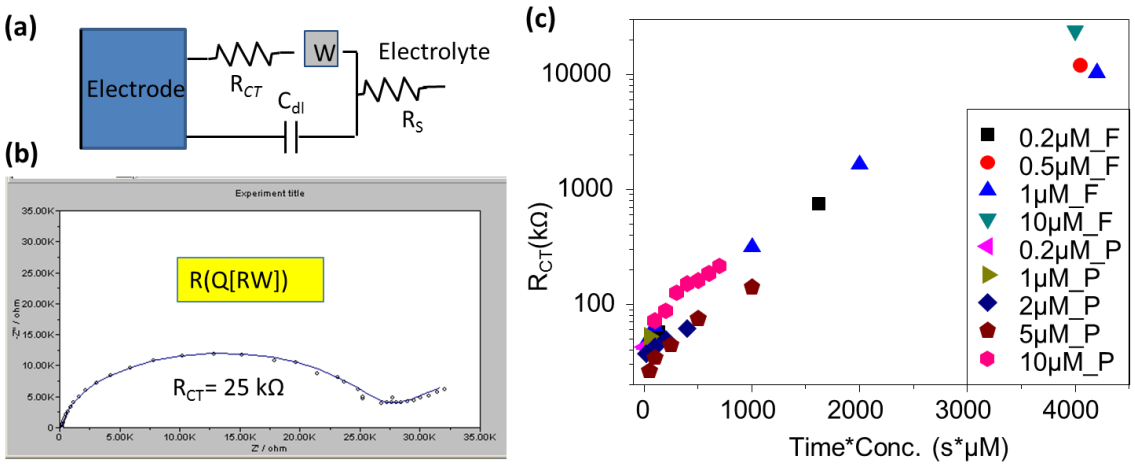

Fig. 6-10 Impedance results with respect to the fouling time and cresol concentration. (a) The equivalent electric circuit used for the fouled electrode immersed in $Fe(CN)_6^{3-/4-}$ solution. (b) One example of impedance spectra of fouled electrodes. The curve overlap data points was the fit analysis based on the model of R(Q[RW]), which represented above electric circuit. (c) Calibration of all measured R_{CT} values with respect to the product of fouling time and the concentration of cresol used for electrode fouling.

The fouling layer was characterized with impedance and AFM. In impedance experiments, an equivalent electric circuit diagram was developed for model fitting of the spectrum (Fig.6-10a). R_{CT} representes the charge transfer resistance at the electrode-electrolyte interface, W is the Warburg diffusion element and placed in series with R_{CT}. C_{dl} is the double layer capacitance, but usually is replaced with a constant phase element (CPE) Q because of the imperfect electrode surface [175]. Q is placed in parallel with above two elements. Rs representes the resistance of the $Fe(CN)_6^{3-/4-}$ solution, which is placed in series with other elements. One example of impedance spectrum is shown in Fig.6-10b. The model of R(Q[RW]) is utilized for the analysis and measurement of the value of R_{CT}. ( ) means parallel elements inside, and [ ] means in series elements inside. The fitting curve compares well with the data

points and shows a circle profile at high frequency range, corresponding to the kinetics of charge transfer at the electrode surface. Ideally, the difference between the two interceptions of fitting curve and x axis is the value of R_{CT}. All of measured R_{CT} are plotted with respect to the fouling time and the concentration of cresol used for electrode fouling (Fig.6-10c). Since the current intensity is proportional to the cresol concentration [30-32], the multiplication of the flow time and concentration is proportional to the charge flow, the amount of oxidized cresol, and thus is relatable to the thickness of fouling layer. The linear relationship between the logarithm of R_{CT} and the product of t*C indicates an electron tunneling mechanism for the oxidation of $Fe(CN)_6^{4-}$ on the fouling layer, and that the thickness of the fouling layer increases linearly with time. This result might be a reason why the potential drop across the fouling layer increases linearly with time.

Since $Fe(CN)_6^{3-/4-}$ is an inner-sphere redox couple, it contacts electrode surface directly and its current response is sensitive to the surface environment, such as the dielectric fouling layer [168]. Oppositely, the outer-sphere redox couple ferrocene is not comparatively sensitive to the surface.

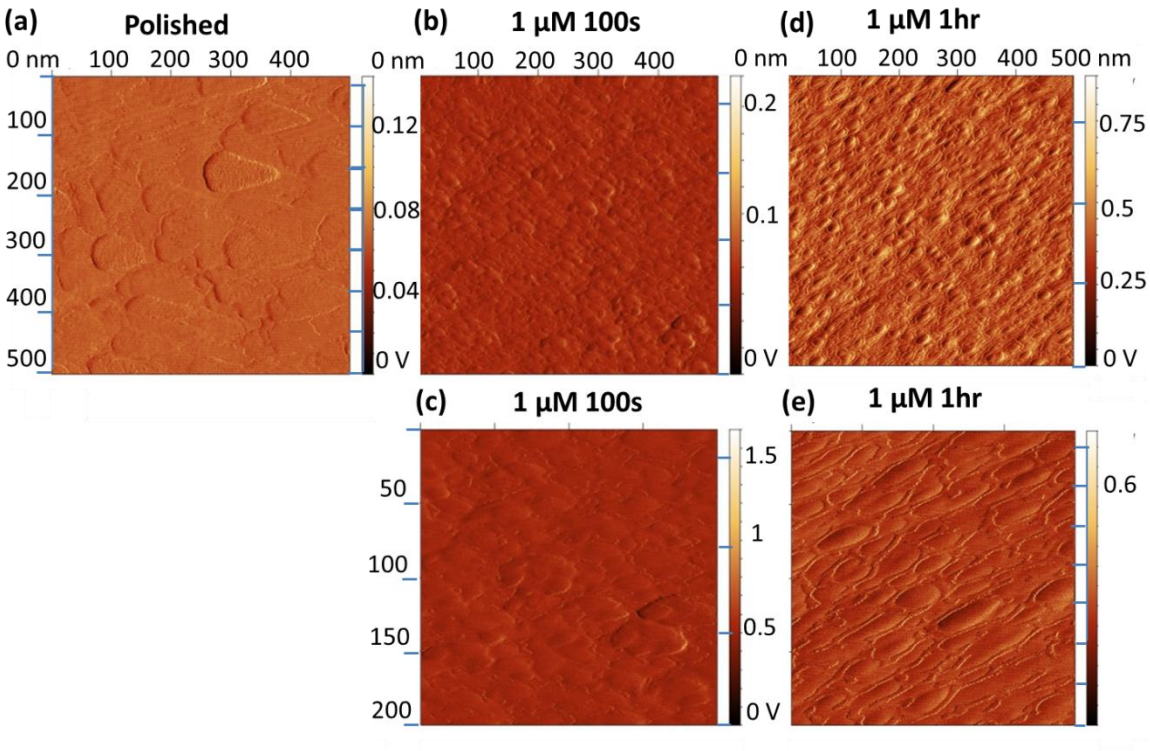

Fig. 6-11 AFM images of polished and fouled electrodes. (a) The image of a polished electrode. The scan size is 500 nm. (b) The image of a 1 µM cresol 100 s fouled electrode with the scan size of 500 nm, (c) with the scan size of 200 nm. (d) The image of a 1 µM cresol 1hr fouled electrode with the scan size of 500 nm, (e) with the scan size of 200 nm.

The morphology of fouled electrodes observed with AFM is significantly different from the polished electrode (Fig.6-11). The bumps with the size of ~50 nm on polished electrode surface indicate the structure of glassy carbon (Fig.6-11a). After fouling, the electrode surface shows bumps with smaller size. With heavy fouling, a ring structure is shown around the bumps (Fig.6-11d,e).

6.3.5. Electrode fouling during repetitive injections of cresol

Injections of cresol samples, instead of continuous flow, were also conducted in the same device setup, and the electrode fouling at different applied potentials was

characterized (Fig.6-12). The current decay of the 0.55 V scan was the latter part of the 0.65 V scan which was a part of the 0.75 V scan. To verify this intuition, data were processed in the same manner as follows: 1) all first peaks were normalized to unity (Fig.6-13a), 2) 0.55 V and 0.65 V scans were shifted for 20 and 10 peaks, respectively, and multiplied by a factor equal to the value of the corresponding peak in 0.75 V scan (Fig.6-13b), 3) All results of 0.55, 0.65, and 0.75 V scans were combined together (Fig.6-14). In the analysis of all scans, the same current decay tendency was seen, which could be evidence of the above potential drop based model for electrode fouling. It indicates that the potential drop based model could also be applied for cresol injections, not only for continuous flow of cresol sample.

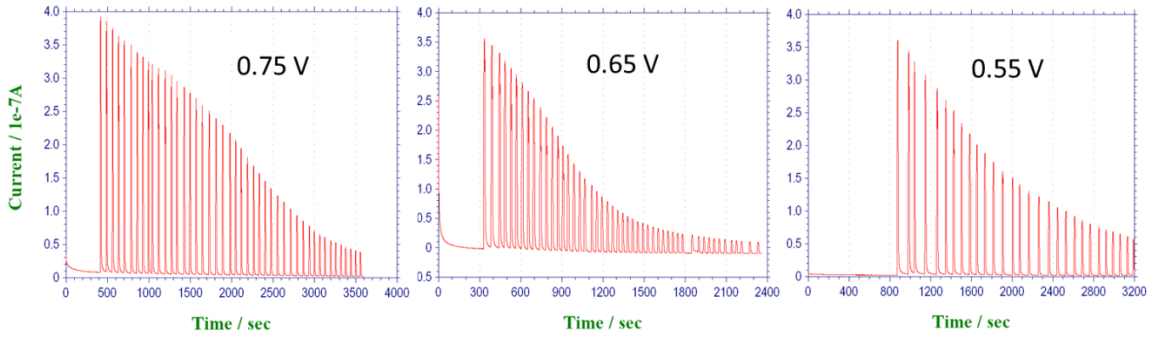

Fig. 6-12 Amperometric results of repetitive injections of 10 μM cresol at different potentials. Potentials were kept at 0.75 V (left), 0.65 V (middle), and 0.55 V (right). Only one example for each case was shown representatively .

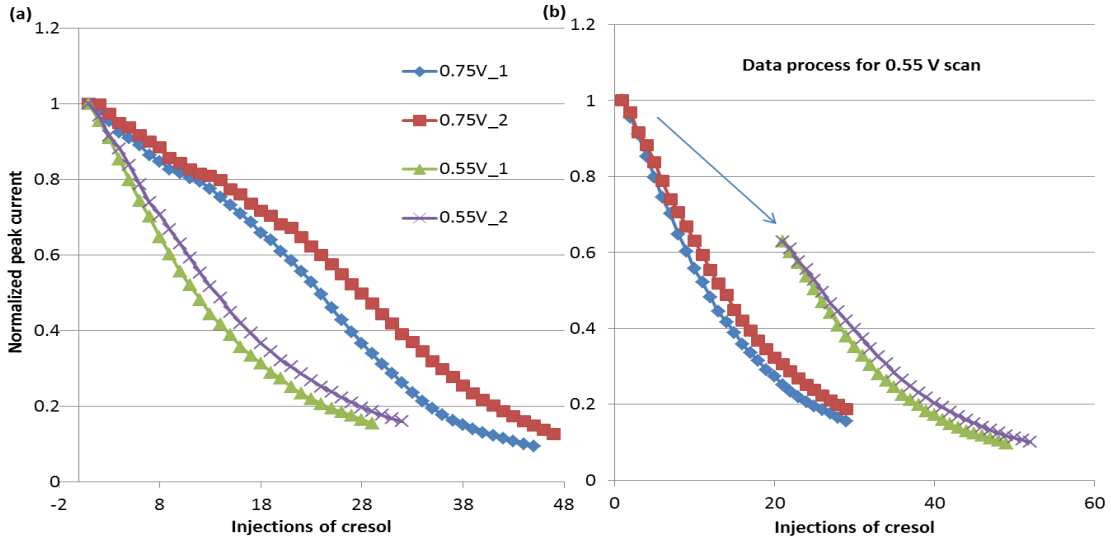

Fig. 6-13 Data process for all amperometric results: (a) Every first peak was normalized to 1, (b) All scans were normalized corresponding to 0.75 V scan. Only examples of 0.55 V and 0.75 V scans were shown.

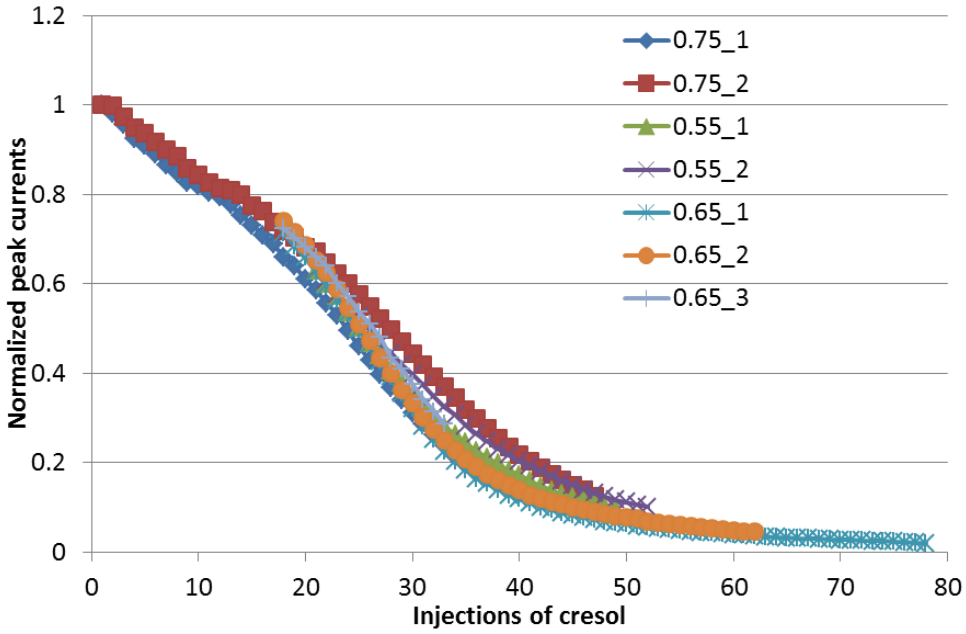

Fig. 6-14 Calibration curve for all amperometric results of electrode fouling.

6.4. Conclusions

The data were consistent with a potential drop based model of the electrode fouling. With respect to the time of continuous flow of cresol, the thickness of the fouling layer increased linearly, as did the potential drop across the fouling layer. This scientific model is able to predict the electrode fouling with respect to the time. Further research could optimize the model and enable the prediction with respect to cresol concentration and applied potential. This model possibly could similarly be applied to other phenolic compounds.

Methods to reduce or avoid electrode fouling should be preventing the accumulation of the fouling layer on surface, and thus avoiding the potential drop. This could be realized by: 1) applying modifications on electrode surface which repel the oxidation products; 2) disrupting the reaction of radical coupling and further oxidizing radicals soluble products; 3) introducing specific molecules that act as the electron receptors and combine with radicals to form soluble products.

7. Overall conclusions

The studies presented in this dissertation demonstrated the successful development of an electrochemical device for continuous monitoring gaseous TCP (tricresyl phosphate) in long term, which has the potential to be used on-site in aircraft cabin. Besides the completion in the practical project, a scientific model has been created for deep understanding of the electrode fouling during electrochemical analysis of phenolic compounds.

TCP is a type of organophosphate and has been known as a neurotoxin. However, it has been widely added into the commercial jet engine oil products acting as the flame retardant and plasticizer. During the oil leakage, TCP can enter the aircraft cabin and harm the health of the crews and passengers. Although some kinds of newly produced airplanes has started to use different air recirculation system which can reduce the danger of TCP contamination, most of aircrafts currently in service may still be affected by it. Current detecting methods for the analysis of TCP include HPLC and GC; however, they suffered from the cumbersomeness, time-consuming, and need of skilled operators. Electrochemical devices have the advantages of ease of operation, high sensitivity, rapid response, and the possibility of miniaturization.

An electrochemical device for the analysis of TCP has been described. Several problems have been solved. 1) TCP is not electro-active, thus it was hydrolyzed to cresol for analysis. High reproducibility in the hydrolysis process was realized by using rigorous experiments conditions in terms of the temperature, the flow rate of TCP, the collecting time, the amount of catalyst, and the flushing of buffer. 2) Since TCP has low saturated vapor pressure at room temperature, the gaseous sample was not readily available. The gasification was done by N_2 bubbling the TCP methanol solution that was placed in a close container, and an oil bath was used to heat the solution at a controllable temperature. Immediately, the gasified TCP sample entered the catalyst and was converted. Rigorous experimental setup enabled the complete gasfication of TCP, e.g., proper tubes and connectors were chosen to avoid any gas

leakage at such high temperature and pressure. An automatic system for TCP sampling has been built in our lab and was controlled by the software of Labview. 3) The flushing of the catalyst made the hydrolyzate samples alkaline and brought error to electrochemical signals. This affect has been reduced much by using phosphate buffer at the concentration of 0.4 M. Finally, with this electrochemical device, a linear range of response for 30-300 ppb TCP has been realized, and the response to real TCP-contained engine oil was similar as TCP methanol samples.

The electrode fouling was another critical problem we faced to develop this device. Electrode fouling is a common problem during the electrochemical analysis of phenolic compounds, such as cresol. Although the fouled electrode can be regenerated by polishing, this operation is not practical for continuous monitoring TCP in aircraft cabin. After trying several strategies to enhance the performance of the electrode, PEDOT:PSS composites have been chosen as the anti-fouling modifier on the electrode surface. With the electrode that was modified with PEDOT:PSS at proper conditions, the updated electrochemical device was able to give a similar linear range of response to gaseous TCP. Moreover, the response to cresol and TCP hydrolyzate samples was reliable for much longer time.

Besides the completion in the practical project, much research has been done in science area. A scientific model has been created for deep understanding of the electrode fouling. Based on this model, the current decay due to the electrode fouling was determined by the potential drop across the fouling layer. The potential drop effect was confirmed with Cu deposition and the luckily created air bubbled fouled electrode. The value of potential drop was quantitatively measured with Cu deposition. By combining the current-potential relationship and the potential drop values, the potential-drop-based model has been successfully created for the flow analysis system of cresol. This model was comparable with experimental results well and was able to predict the current decay due to the electrode fouling in terms of the fouling time, applied potential, and concentration of cresol. This model was considered to hold correct for the electrode fouling during the electrochemical analysis of most phenolic compounds. And it is helpful for designing the anti-fouling strategies.

References

1. Oxford Enlish Dictionary, *Sensor*. 2012, Oxford University Press.
2. Eggins, B.R., *Chemical sensors and biosensors*. Analytical techniques in the sciences. 2002, Chichester ; Hoboken, NJ: J. Wiley. xxi, 273 p.
3. Ramanathan, M., *Development Of Functional Material Scaffolds for Sensing Applications*. 2010, Auburn University.
4. Bard, A.J. and L.R. Faulkner, *Electrochemical methods : fundamentals and applications*. 2nd ed. 2001, New York: Wiley. xxi, 833 p.
5. Stetter, J.R., W.R. Penrose, and S. Yao, *Sensors, chemical sensors, electrochemical sensors, and ECS.* Journal of The Electrochemical Society, 2003. **150**: p. S11.
6. Balasubramanian, S.G.S., *Development of smart functional surfaces for biosensor applications*. 2008: ProQuest.
7. Brecht, A. and G. Gauglitz, *Recent developments in optical transducers for chemical or biochemical applications1.* Sensors and Actuators B: Chemical, 1997. **38**(1-3): p. 1-7.
8. Homola, J., S.S. Yee, and G. Gauglitz, *Surface plasmon resonance sensors: review.* Sensors and Actuators B: Chemical, 1999. **54**(1-2): p. 3-15.
9. Sharma, A.K., R. Jha, and B. Gupta, *Fiber-optic sensors based on surface plasmon resonance: a comprehensive review.* Sensors Journal, IEEE, 2007. **7**(8): p. 1118-1129.
10. Stenberg, E., et al., *Quantitative determination of surface concentration of protein with surface plasmon resonance using radiolabeled proteins.* Journal of colloid and interface science, 1991. **143**(2): p. 513-526.
11. Kim, D.C. and D.J. Kang, *Molecular recognition and specific interactions for biosensing applications.* Sensors, 2008. **8**(10): p. 6605-6641.
12. Jung, Y., J.Y. Jeong, and B.H. Chung, *Recent advances in immobilization methods of antibodies on solid supports.* Analyst, 2008. **133**(6): p. 697-701.

13. Rosenstock, L., et al., *Chronic central nervous system effects of acute organophosphate pesticide intoxication. The Pesticide Health Effects Study Group.* Lancet, 1991. **338**(8761): p. 223.
14. Craig, P.H. and M.L. Barth, *Evaluation of the hazards of industrial exposure to tricresyl phosphate: a review and interpretation of the literature.* Journal of Toxicology and Environmental Health Part B: Critical Reviews, 1999. **2**(4): p. 281-300.
15. Casida, J.E., et al., *Mechanisms of selective action of pyrethroid insecticides.* Annual review of pharmacology and toxicology, 1983. **23**(1): p. 413-438.
16. Abou-Donia, M.B. and D.M. Lapadula, *Mechanisms of organophosphorus ester-induced delayed neurotoxicity: type I and type II.* Annual review of pharmacology and toxicology, 1990. **30**(1): p. 405-440.
17. Kinugasa, H., et al., *Evaluation of toxicity in the aquatic environment based on the inhibition of acetylcholinesterase.* Nippon Suisan Gakkaishi, 2001. **67**(4): p. 696-702.
18. David, M.D. and J.N. Seiber, *Accelerated hydrolysis of industrial organophosphates in water and soil using sodium perborate.* Environmental Pollution, 1999. **105**(1): p. 121-128.
19. David, M.D. and J.N. Seiber, *Analysis of Organophosphate Hydraulic Fluids in U.S. Air Force Base Soils.* Archives of Environmental Contamination and Toxicology, 1999. **36**: p. 235-241.
20. Winder, C. and J.-C. Balouet, *The Toxicity of Commercial Jet Oils.* Environmental Research, 2002. **89**: p. 146-164.
21. Boethling, R.S. and J.C. Cooper, *Environmental fate and effects of triaryl and tri-alkyl/aryl phosphate esters.* Residue Rev, 1985. **94**: p. 49-99.
22. Federal-Register, *Aryl Phosphates*, in *Response to the Interagency Testing Committee*. 1983. p. 57452-57460.
23. AFL-CIO, *Aircraft air quality: What's wrong with it and what needs to be done*. 2003, The Aviation Subcommittee of The Transportation & Infrastructure Committee U.S. House of Representatives: Washington D. C. p.

1-40.

24. Habboush, A.E., S.M. Farroha, and H.I. Khalaf, *Extraction-gas chromatographic method for the determination of organophosphorus compounds as lubricating oil additives.* Journal of Chromatography A, 1995. **696**: p. 257-263.
25. Ofstad, E.B. and T. Sletten, *Composition and water solubility determination of a commercial tricresylphosphate.* Sci. total. Environ., 1985. **43**: p. 233-241.
26. Mutsuga, M., et al., *Determination Method of Tricresyl Phosphate in Polyvinyl Chloride.* Food Hygiene and Safety Science (Shokuhin Eiseigaku Zasshi), 2003. **44**(1): p. 26-31.
27. Bhattacharyya, J., et al., *Detection and estimation of tricresyl phosphate in mustard oil.* Forensic Science, 1974. **3**: p. 263-270.
28. Pedrosa, V.A., et al., *Copper nanoparticles and carbon nanotubes-based electrochemical sensing system for fast identification of tricresyl-phosphate in aqueous samples and air.* Sensors and Actuators B: Chemical, 2009. **140**(1): p. 92-97.
29. Simonian, A., G. Vertelov, and W. Gale, *Electrochemical Detection of Tricresyl Phosphate.* ECS Trans, 2006. **3**: p. 21-34.
30. Yang, X., et al., *Portable and remote electrochemical sensing system for detection of tricresyl-phosphate in gas phase.* Sensors and Actuators B: Chemical, 2012. **161**(1): p. 564-569.
31. Yang, X., et al. *Prevention of Electrode Fouling Can Significantly Improve an Accuracy of Tricresyl Phosphate Detection*. 2012: ECS.
32. Yang, X., et al., *Portable Electrochemical Sensor for Detection of Tricresyl-Phosphate.* ECS Transactions, 2011. **35**(35): p. 35-43.
33. Heras, M.A., et al., *A poly(3,4-ethylenedioxythiophene)-poly(styrene sulphonate) composite electrode coating in the electrooxidation of phenol.* Electrochimica Acta, 2005. **50**(7-8): p. 1685-1691.
34. Lu, W., G.G. Wallace, and M.D. Imisides, *Development of Conducting Polymer Modified Electrodes for the Detection of Phenol.* Electroanalysis,

2002. **14**(5): p. 325-332.

35. Chauke, V., F. Matemadombo, and T. Nyokong, *Remarkable sensitivity for detection of bisphenol A on a gold electrode modified with nickel tetraamino phthalocyanine containing Ni-O-Ni bridges.* Journal of Hazardous Materials, 2010. **178**(1-3): p. 180-186.
36. Rajeshwar, K. and J.G. Ibanez, *Environmental electrochemistry: fundamentals and applications in pollution abatement*. 1997: Academic Pr.
37. Rose, T.L. *Proceedings of the Symposium on Water Purification by Photocatalytic, Photoelectrochemical, and Electrochemical Processes*. 1994: The Electrochemical Society.
38. Lupu, S., et al., *Electrochemical sensors based on platinum electrodes modified with hybrid inorganic-organic coatings for determination of 4-nitrophenol and dopamine.* Electrochimica Acta, 2009. **54**(7): p. 1932-1938.
39. Ortega, F., et al., *Phenol oxidase-based biosensors as selective detection units in column liquid chromatography for the determination of phenolic compounds.* Journal of Chromatography A, 1994. **675**(1-2): p. 65-78.
40. Rogers, K.R., et al., *Viscosity and binder composition effects on tyrosinase-based carbon paste electrode for detection of phenol and catechol.* Talanta, 2001. **54**(6): p. 1059-1065.
41. Lete, C., et al., *New composite materials used in the phenol electroanalysis. Part I. Poly (Azulene)/Prussian Blue and Prussian Blue/Poly (Azulene) films* Rev. Roum. Chim, 2010. **55**(6): p. 335-340.
42. Manahan, S.E., *Environmental chemistry*. 1991, Chelsea, USA: CRC; Lewis publishers.
43. Canofeni, S., et al., *Comparison of immobilisation procedures for development of an electrochemical PPO-based biosensor for on line monitoring of a depuration process.* Analytical letters, 1994. **27**(9): p. 1659-1669.
44. Nistor, C., et al., *Improved stability and altered selectivity of tyrosinase based graphite electrodes for detection of phenolic compounds.* Analytica Chimica Acta, 1999. **387**(3): p. 309-326.

45. Patra, S. and N. Munichandraiah, *Electro-oxidation of Phenol on Polyethylenedioxythiophene Conductive-Polymer-Deposited Stainless Steel Substrate.* Journal of The Electrochemical Society, 2008. **155**(3): p. F23-F30.
46. Yavuz, Y. and A.S. Koparal, *Electrochemical oxidation of phenol in a parallel plate reactor using ruthenium mixed metal oxide electrode.* Journal of Hazardous Materials, 2006. **136**(2): p. 296-302.
47. Gundersen, J.L., W.G. MacIntyre, and R.C. Hale, *pH-dependent sorption of chlorinated guaiacols on estuarine sediments: The effects of humic acids and TOC.* Environmental science & technology, 1996. **31**(1): p. 188-193.
48. Ndlovu, T., et al., *Electrochemical Detection of o-Nitrophenol on a Poly (propyleneimine)-gold Nanocomposite Modified Glassy Carbon Electrode.* Int. J. Electrochem. Sci, 2010. **5**: p. 1179-1186.
49. Pigani, L., et al., *Electro-oxidation of chlorophenols on poly(3,4-ethylenedioxythiophene)-poly(styrene sulphonate) composite electrode.* Electrochimica Acta, 2007. **52**(5): p. 1910-1918.
50. Krishnan, A.V., et al., *Bisphenol-A: an estrogenic substance is released from polycarbonate flasks during autoclaving.* ENDOCRINOLOGY-PHILADELPHIA-, 1993. **132**: p. 2279-2279.
51. Brotons, J.A., et al., *Xenoestrogens released from lacquer coatings in food cans.* Environmental Health Perspectives, 1995. **103**(6): p. 608.
52. Su, W.-Y., S.-M. Wang, and S.-H. Cheng, *Electrochemically pretreated screen-printed carbon electrodes for the simultaneous determination of aminophenol isomers.* Journal of Electroanalytical Chemistry, 2011. **651**(2): p. 166-172.
53. Environmental Protection Agency, *Toxic substance control act*, E.P. Agency, Editor. 1979: Washington, DC.
54. Janda, V. and K. Krijt, *Recovery of phenols from water by continuous steam distillation--extraction.* Journal of Chromatography A, 1984. **283**: p. 309-314.
55. PRAKASH, J.M.R. and J. BEHARI, *Electrochemical detection and catalytic oxidation of phenolic compounds over nickel complex modified graphite*

electrode. Applied Ecology and Environmental Research, 2004. **2**(2): p. 25-33.

56. Domenech, A., et al., *2, 4, 6-Triphenylpyrylium ion encapsulated into zeolite Y as a selective electrode for the electrochemical determination of dopamine in the presence of ascorbic acid.* Analytical Chemistry, 2002. **74**(3): p. 562-569.
57. Chen, S.M. and W.Y. Chzo, *Simultaneous voltammetric detection of dopamine and ascorbic acid using didodecyldimethylammonium bromide (DDAB) film-modified electrodes.* Journal of Electroanalytical Chemistry, 2006. **587**(2): p. 226-234.
58. Mahanthesha, K., et al., *Cyclic Voltammetric Investigations of Dopamine at Alizarin Modified Carbon Paste Electrode.* Int. J. Electrochem. Sci, 2010. **5**: p. 1962-1971.
59. Mussmann, P., K. Levsen, and W. Radeck, *Gas-chromatographic determination of phenols in aqueous samples after solid phase extraction.* Fresenius' journal of analytical chemistry, 1994. **348**(10): p. 654-659.
60. Louter, A.J.H., et al., *Automated derivatization for on-line solid-phase extraction-gas chromatography; phenolic compounds.* Journal of High Resolution Chromatography, 1997. **20**(7): p. 363-368.
61. Jauregui, O. and M. Galceran, *Determination of phenols in water by on-line solid-phase disk extraction and liquid chromatography with electrochemical detection.* Analytica Chimica Acta, 1997. **340**(1-3): p. 191-199.
62. Buchholz, K.D. and J. Pawliszyn, *Optimization of solid-phase microextraction conditions for determination of phenols.* Analytical Chemistry, 1994. **66**(1): p. 160-167.
63. Alimpiev, S.S., et al., *Selective detection of phenol impurities in water.* Analytical Chemistry, 1995. **67**(1): p. 181-186.
64. Townshend, A., P.J. Worsfold, and C.F. Poole, *Encyclopedia of analytical science*. Vol. 8. 1995: Academic press London.
65. Ferreira, M., et al., *Electrode passivation caused by polymerization of different phenolic compounds.* Electrochimica Acta, 2006. **52**(2): p. 434-442.
66. Gattrell, M. and D.W. Kirk, *A Study of the Oxidation of Phenol at Platinum*

and Preoxidized Platinum Surfaces. Journal of The Electrochemical Society, 1993. **140**(6): p. 1534-1540.

67. Rodgers, J.D., W. Jedral, and N.J. Bunce, *Electrochemical oxidation of chlorinated phenols.* Environmental science & technology, 1999. **33**(9): p. 1453-1457.
68. Fleischmann, M., et al., *A Raman spectroscopic investigation of the electropolymerization of phenol on silver electrodes.* Electrochimica Acta, 1983. **28**(11): p. 1545-1553.
69. Giuliano, M. and M.M. Marco, *An Overview of Phenol Electropolymerization for Metal Protection.* Journal of The Electrochemical Society, 1987. **134**(12): p. 643C-652C.
70. Ežerskis, Z. and Z. Jusys, *Electropolymerization of chlorinated phenols on a Pt electrode in alkaline solution Part I: A cyclic voltammetry study.* Journal of applied electrochemistry, 2001. **31**(10): p. 1117-1124.
71. Ežerskis, Z. and Z. Jusys, *Electropolymerization of chlorinated phenols on a Pt electrode in alkaline solution Part III: A Fourier transformed infrared spectroscopy study.* Journal of applied electrochemistry, 2002. **32**(7): p. 755-762.
72. Ežerskis, Z., G. Stalnionis, and Z. Jusys, *Electropolymerization of chlorinated phenols on a Pt electrode in alkaline solution. Part II: An electrochemical quartz crystal microbalance study.* Journal of applied electrochemistry, 2002. **32**(1): p. 49-55.
73. Wang, J., M. Jiang, and F. Lu, *Electrochemical Quartz Microbalance Investigation of Surface Fouling due to Phenol Oxidation.* Electroanal. Chem. 444: 127, 1998. **33**.
74. Tahar, N.B. and A. Savall, *Mechanistic Aspects of Phenol Electrochemical Degradation by Oxidation on a Ta/ PbO Anode.* Journal of The Electrochemical Society, 1998. **145**: p. 3427.
75. Fichter, F., *Die elektrolytische Oxydation des Toluols.* Zeitschrift für Elektrochemie und angewandte physikalische Chemie, 1913. **19**(20): p.

781-784.

76. Nishiyama, A., et al., *Anodic oxidation of 4-hydroxycinnamic acids and related phenols.* Chemical and pharmaceutical bulletin, 1983. **31**(8): p. 2845-2852.

77. Gattrell, M. and D.W. Kirk, *A Study of Electrode Passivation during Aqueous Phenol Electrolysis.* Journal of The Electrochemical Society, 1993. **140**(4): p. 903-911.

78. Mengoli, G. and M.M. Musiani, *Phenol electropolymerization: a straight route from monomers to polymer coatings.* Progress in organic coatings, 1994. **24**(1-4): p. 237-251.

79. Beck, F., *Electrodeposition of polymer coatings.* Electrochimica Acta, 1988. **33**(7): p. 839-850.

80. Mourcel, P., et al., *Depositing organic polymers on steel by electropolymerization: Their growth mechanism and passivating nature.* Journal of Electroanalytical Chemistry and Interfacial Electrochemistry, 1983. **145**(2): p. 467-472.

81. Arribas, A.S., et al., *Application of Carbon Nanotube-Modified Electrodes as Electrochemical Sensors for the Continuous Monitoring of 2,4-Dichlorophenol.* Electroanalysis, 2011. **23**(1): p. 237-244.

82. Comninellis, C. and C. Pulgarin, *Anodic oxidation of phenol for waste water treatment.* Journal of applied electrochemistry, 1991. **21**(8): p. 703-708.

83. Gattrell, M. and D.W. Kirk, *The electrochemical oxidation of aqueous phenol at a glassy carbon electrode.* The Canadian Journal of Chemical Engineering, 1990. **68**(6): p. 997-1003.

84. Oloman, C., *Reactor design in electro-organic synthesis*. Vol. 79. 1983, New York, NY, ETATS-UNIS: American institute of chemical engineers.

85. Gattrell, M. and D.W. Kirk, *A Fourier Transform Infrared Spectroscopy Study of the Passive Film Produced during Aqueous Acidic Phenol Electro-oxidation.* Journal of The Electrochemical Society, 1992. **139**(10): p. 2736-2744.

86. Mengoli, G., *Feasibility of polymer film coatings through electroinitiated*

polymerization in aqueous medium. Electric Phenomena in Polymer Science, 1979: p. 1-31.

87. Mengoli, G., S. Daolio, and M. Musiani, *The influence of amines on the anodic coupling of phenols to polyoxyphenylene films.* Journal of applied electrochemistry, 1980. **10**(4): p. 459-471.

88. Mengoli, G. and M. M Musiani. *Phenol electropolymerization in acid medium*. 1987: Wiley Online Library.

89. Mengoli, G. and M. Musiani, *Protective coatings on iron by anodic oxidation of phenols in oxalic acid medium.* Electrochimica Acta, 1986. **31**(2): p. 201-210.

90. Sharifian, H. and D.W. Kirk, *Electrochemical Oxidation of Phenol.* Journal of The Electrochemical Society, 1986. **133**(5): p. 921-924.

91. Joglekar, H.S., S.D. Samant, and J.B. Joshi, *Kinetics of wet air oxidation of phenol and substituted phenols.* Water Research, 1991. **25**(2): p. 135-145.

92. Devlin, H.R. and I.J. Harris, *Mechanism of the oxidation of aqueous phenol with dissolved oxygen.* Industrial & Engineering Chemistry Fundamentals, 1984. **23**(4): p. 387-392.

93. Taylor, W.I. and A.R. Battersby, *Oxidative coupling of phenols*. Vol. 1. 1967: M. Dekker.

94. Ežerskis, Z. and Z. Jusys, *Electropolymerization of chlorinated phenols on a Pt electrode in alkaline solution. Part IV: A gas chromatography mass spectrometry study.* Journal of applied electrochemistry, 2002. **32**(5): p. 543-550.

95. Max Fremery, Hermann Hover, and G. Schwarzlose, *Elektrochemische Benzol-Oxidation, ein nebenproduktfreier Weg zum Hydrochinon.* Chemie Ingenieur Technik, 1974. **46**(15): p. 635-639.

96. Glarum, S.H. and J.H. Marshall, *Polarization Relaxation in Electrodeposited Polyphenylene-Oxide Films.* Journal of The Electrochemical Society, 1985. **132**(12): p. 2939-2944.

97. Wang, J., et al., *Scanning tunneling microscopic investigation of surface*

fouling of glassy carbon surfaces due to phenol oxidation. Journal of Electroanalytical Chemistry and Interfacial Electrochemistry, 1991. **313**(1-2): p. 129-140.

98. Babai, M. and S. Gottesfeld, *Ellipsometric study of the polymeric surface films formed on platinum electrodes by the electrooxidation of phenolic compounds.* Surface Science, 1980. **96**(1-3): p. 461-475.
99. Glarum, S.H. and J.H. Marshall, *The Impedance of Poly(aniline) Electrode Films.* Journal of The Electrochemical Society, 1987. **134**(1): p. 142-147.
100. Glarum, S.H., et al., *Characterization of Polyphenylene Oxide Anodic Films.* Journal of The Electrochemical Society, 1987. **134**(1): p. 81-84.
101. Chidsey, C.E.D., *Free energy and temperature dependence of electron transfer at the metal-electrolyte interface.* Science, 1991. **251**(4996): p. 919.
102. Buttry, D. and A. Bard, *Electroanalytical Chemistry, vol. 17 Marcel Dekker.* New York, 1991: p. 1.
103. Nakajima, T. and T. Kawagoe, *Polyaniline: Structural analysis and application for battery.* Synthetic Metals, 1989. **28**(1-2): p. 629-638.
104. Albertas, M., *Electrocatalysis at conducting polymers.* Synthetic Metals, 1999. **107**(2): p. 75-83.
105. Bartlett, P.N. and R.G. Whitaker, *Strategies for the development of amperometric enzyme electrodes.* Biosensors, 1987. **3**(6): p. 359-379.
106. Lupu, S., et al., *Polythiophene derivative conducting polymer modified electrodes and microelectrodes for determination of ascorbic acid. effect of possible interferents.* Electroanalysis, 2002. **14**(7-8): p. 519-525.
107. Malinauskas, A., *Electrocatalysis at conducting polymers.* Synthetic Metals, 1999. **107**(2): p. 75-83.
108. Mark, H.B., et al., *The electrochemistry of neurotransmitters at conducting organic polymer electrodes: electrocatalysis and analytical applications.* Bioelectrochemistry and bioenergetics, 1995. **38**(2): p. 229-245.
109. Rosatto, S.S., L.T. Kubota, and G. de Oliveira Neto, *Biosensor for phenol based on the direct electron transfer blocking of peroxidase immobilising on*

silica-titanium. Analytica Chimica Acta, 1999. **390**(1-3): p. 65-72.

110. Coury, L.A., E.M. Birch, and W.R. Heineman, *Gamma-irradiated polymer-modified graphite electrodes with enhanced response to catechol.* Analytical Chemistry, 1988. **60**(6): p. 553-560.

111. Molyneux, P. and S. Vekavakayanondha, *The interaction of aromatic compounds with poly(vinylpyrrolidone) in aqueous solution. Part 5.-Binding isotherms for phenols and O-substituted phenols.* Journal of the Chemical Society, Faraday Transactions 1: Physical Chemistry in Condensed Phases, 1986. **82**(2): p. 291-317.

112. Wheeler, S.K., L.A. Coury Jr, and W.R. Heineman, *Fouling-resistant, polymer-modified graphite electrodes.* Analytica Chimica Acta, 1990. **237**: p. 141-148.

113. Lete, C., et al., *New composite materials used in the phenol electroanalysis. Part II. Poly (2-[(E)-2-Azulene-1-Yl)vinyl] thiophene-Prussian Blue.* Rev. Roum. Chim, 2010. **55**(11-12): p. 995-1000.

114. Obirai, J., F. Bedioui, and T. Nyokong, *Electro-oxidation of phenol and its derivatives on poly-Ni(OH)TPhPyPc modified vitreous carbon electrodes.* Journal of Electroanalytical Chemistry, 2005. **576**(2): p. 323-332.

115. Oni, J., et al., *Metallophthalocyanine-modified glassy carbon electrodes: effects of film formation conditions on electrocatalytic activity towards the oxidation of nitric oxide.* Sensors and Actuators B: Chemical, 2005. **105**(2): p. 208-213.

116. Halbert, M.K. and R.P. Baldwin, *Electrocatalytic and analytical response of cobalt phthalocyanine containing carbon paste electrodes toward sulfhydryl compounds.* Analytical Chemistry, 1985. **57**(3): p. 591-595.

117. Todd, W.J., et al., *Electrochemically Induced Metalation of Polymeric Phthalocyanines.* Journal of the American Chemical Society, 1998. **120**(19): p. 4887-4888.

118. Zagal, J.H., *Metallophthalocyanines as catalysts in electrochemical reactions.* Coordination Chemistry Reviews, 1992. **119**: p. 89-136.

119. Zecevic, S., et al., *Spectroscopic and electrochemical studies of transition metal tetrasulfonated phthalocyanines:: Part V. Voltammetric studies of adsorbed tetrasulfonated phthalocyanines (MTsPc) in aqueous solutions.* Journal of Electroanalytical Chemistry, 1985. **196**(2): p. 339-358.

120. Bedioui, F., G. Gutierrez, and C. Charreton, *Metalloporphyrin, metallophtalocyanine and related macrocycle complex-base film modified electrodes: Review of selected significant designs and applications to the electrochemical detection of pollutants.* Recent Res Devel. Electrochemical, Reviews Parts, 1999. **2**: p. 91-108.

121. Cataldi, T.R.I., D. Centonze, and G. Ricciardi, *Electrode modification with a poly (NiII-tetramethyldibenzotetraaza[14]annulene) film. Electrochemical behavior and redox catalysis in alkaline solutions. I.* Electroanalysis, 1995. **7**(4): p. 312-318.

122. Cataldi, T.R.I., et al., *Study of the nickel-based chemically modified electrode obtained by electrochemical deposition of an NiII-tetramethyl-dibenzo-tetraaza [14] annulene complex. Redox catalysis of carbohydrates in alkaline solutions. II.* Electroanalysis, 1995. **7**(5): p. 435-441.

123. Goux, A., et al., *Nickel tetraaminophthalocyanine based films for the electrocatalytic activation of dopamine.* Electroanalysis, 2003. **15**(11): p. 969-974.

124. Roslonek, G. and J. Taraszewska, *Electrocatalytic oxidation of alcohols on glassy carbon electrodes electrochemically modified with nickel tetraazamacrocyclic complexes: mechanism of f.* Journal of Electroanalytical Chemistry, 1992. **325**(1-2): p. 285-300.

125. Trevin, S., et al., *Electropolymerized nickel macrocyclic complex-based films: designand electrocatalytic application.* J. Mater. Chem., 1997. **7**(6): p. 923-928.

126. Achar, B., et al., *Synthesis and structural studies of metal (II) 4, 9, 16, 23-phthalocyanine tetraamines.* Polyhedron, 1987. **6**(6): p. 1463-1467.

127. Obirai, J., et al., *Synthesis, spectral and electrochemical properties of a new family of pyrrole substituted cobalt, iron, manganese, nickel and zinc phthalocyanine complexes.* Journal of Porphyrins and Phthalocyanines, 2003. **7**(7): p. 508-520.

128. Ewing, A.G., B. Feldman, and R.W. Murray, *Permeation of neutral, cationic, and anionic electrode reactants through a polycationic polymer film as a function of electrolyte concentration.* The Journal of Physical Chemistry, 1985. **89**(7): p. 1263-1269.

129. Bartlett, P.N., P. Birkin, and E. Wallace, *Oxidation of β-nicotinamide adenine dinucleotide (NADH) at poly (aniline)-coated electrodes.* J. Chem. Soc., Faraday Trans., 1997. **93**(10): p. 1951-1960.

130. Gardner, J.W. and P.N. Bartlett, *Sensors and sensory systems for an electronic nose*. 1992: Springer.

131. Malitesta, C., et al., *Glucose fast-response amperometric sensor based on glucose oxidase immobilized in an electropolymerized poly (o-phenylenediamine) film.* Analytical Chemistry, 1990. **62**(24): p. 2735-2740.

132. Elliott, J.M., L.M. CabuchÃ©, and P.N. Bartlett, *Electrochemical Characterization of a Templated Insulating Polymer-Modified Electrode.* Analytical Chemistry, 2001. **73**(13): p. 2855-2861.

133. Arribas, A.S., et al., *Analytical applications of glassy carbon electrodes modified with multi-wall carbon nanotubes dispersed in polyethylenimine as detectors in flow systems.* Analytica Chimica Acta, 2007. **596**(2): p. 183-194.

134. Ajayan, P., *Nanotubes from carbon.* Chemical Reviews, 1999. **99**(7): p. 1787-1800.

135. Dai, H., *Carbon nanotubes: opportunities and challenges.* Surface Science, 2002. **500**(1-3): p. 218-241.

136. Ijima, S., *Helical nanotubules of peptidic carbon.* Nature, 1991. **345**: p. 56-58.

137. Banks, C.E., et al., *Investigation of modified basal plane pyrolytic graphite electrodes: definitive evidence for the electrocatalytic properties of the ends of carbon nanotubes.* Chem. Commun., 2004(16): p. 1804-1805.

138. Ambrosi, A., T. Sasaki, and M. Pumera, *Platelet graphite nanofibers for electrochemical sensing and biosensing: the influence of graphene sheet orientation.* Chemistry-An Asian Journal, 2010. **5**(2): p. 266-271.

139. Banks, C.E. and R.G. Compton, *Exploring the electrocatalytic sites of carbon nanotubes for NADH detection: an edge plane pyrolytic graphite electrode study.* Analyst, 2005. **130**(9): p. 1232-1239.

140. Wang, J., R.P. Deo, and M. Musameh, *Stable and sensitive electrochemical detection of phenolic compounds at carbon nanotube modified glassy carbon electrodes.* Electroanalysis, 2003. **15**(23 24): p. 1830-1834.

141. Yang, S., et al., *Modified glassy carbon electrode with Nafion/MWNTs as a sensitive voltammetric sensor for the determination of paeonol in pharmaceutical and biological samples.* Journal of applied electrochemistry, 2010. **40**(7): p. 1371-1378.

142. Prasad, B.B., et al., *Sol-gel derived multiwalled carbon nanotubes ceramic electrode modified with molecularly imprinted polymer for ultra trace sensing of dopamine in real samples.* Electrochimica Acta, 2011. **56**(20): p. 7202-7211.

143. Kumar, S. and S.-M. Chen, *Electroanalysis of NADH Using Conducting and Redox Active Polymer/Carbon Nanotubes Modified Electrodes-A Review.* Sensors, 2008. **8**(2): p. 739-766.

144. Salimi, A. and R. Hallaj, *Catalytic oxidation of thiols at preheated glassy carbon electrode modified with abrasive immobilization of multiwall carbon nanotubes: applications to amperometric detection of thiocytosine, l-cysteine and glutathione.* Talanta, 2005. **66**(4): p. 967-975.

145. Salimi, A., et al., *Modification of glassy carbon electrode with multi-walled carbon nanotubes and iron (III)-porphyrin film: Application to chlorate, bromate and iodate detection.* Electrochimica Acta, 2007. **52**(20): p. 6097-6105.

146. Salimi, A., A. Noorbakhsh, and M. Ghadermarzi, *Amperometric detection of nitrite, iodate and periodate at glassy carbon electrode modified with catalase*

and multi-wall carbon nanotubes. Sensors and Actuators B: Chemical, 2007. **123**(1): p. 530-537.

147. Huang, J., Y. Liu, and T. You, *Carbon nanofiber based electrochemical biosensors: A review.* Analytical Methods, 2010. **2**(3): p. 202-211.

148. Mahanthesha, K.R., et al., *Cyclic Voltammetric Investigations of Dopamine at Alizarin Modified Carbon Paste Electrode.* Int. J. Electrochem. Sci, 2010. **5**: p. 1962-1971.

149. Yi, H., et al., *Adsorption stripping voltammetry of phenol at Nafion-modified glassy carbon electrode in the presence of surfactants.* Talanta, 2001. **55**(6): p. 1205-1210.

150. Manriquez, J., et al., *Electrocatalysis of the oxidation of alcohol and phenol derivative pollutants at vitreous carbon electrode coated by nickel macrocyclic complex-based films.* Analytica Chimica Acta, 1999. **378**(1-3): p. 159-168.

151. Hilmi, A., J.H.T. Luong, and A.-L. Nguyen, *Capillary electrophoretic separation of chlorophenols using amperometric detection.* Journal of Chromatography A, 1997. **761**(1-2): p. 259-268.

152. Wang, J. and L.D. Hutchins, *Thin-layer electrochemical detector with a glassy carbon electrode coated with a base-hydrolyzed cellulosic film.* Analytical Chemistry, 1985. **57**(8): p. 1536-1541.

153. Mousty, C., *Biosensing applications of clay-modified electrodes: a review.* Analytical and Bioanalytical Chemistry, 2010. **396**(1): p. 315-325.

154. de Carvalho, R.M., L.T. Kubota, and S. Rath, *Influence of EDTA on the electrochemical behavior of phenols.* Journal of Electroanalytical Chemistry, 2003. **548**: p. 19-26.

155. Lapuente, R. and F. Cases, *P. Garce's, E. Morallo'n and JL Va'zquez.* J. Electroanal. Chem, 1998. **451**: p. 163.

156. WHO, W.H.O., et al., *Tricresyl phosphate*. 1990: World Health Organization.

157. Lide, D.R., *CRC handbook of chemistry and physics: a ready-reference book of chemical and physical data*. 2004: CRC Pr I Llc.

158. CAMEO-Chemicals, *Tricresyl Phosphate.* 1999.

159. van Netten, C. and V. Leung, *Comparison of the Constituents of Two Jet Engine Lubricating Oils and Their Volatile Pyrolytic Degradation Products.* Applied Occupational and Environmental Hygiene, 2000. **15**: p. 277 - 283.

160. Yang, X., et al., *Portable and RemoteElectrochemical Sensing System for Detection of Tricresyl-phosphate in Gas Phase.* Sensors and Actuators B: Chemical, 2011.

161. Bard, A.J. and L.R. Faulkner, *Electrochemical methods: fundamentals and applications*. 2006: A1bazaar.

162. Tamburri, E., et al., *Growth mechanisms, morphology, and electroactivity of PEDOT layers produced by electrochemical routes in aqueous medium.* Synthetic Metals, 2009. **159**(5-6): p. 406-414.

163. Du, X. and Z. Wang, *Effects of polymerization potential on the properties of electrosynthesized PEDOT films.* Electrochimica Acta, 2003. **48**(12): p. 1713-1717.

164. Koile, R.C. and D.C. Johnson, *Electrochemical removal of phenolic films from a platinum anode.* Analytical Chemistry, 1979. **51**(6): p. 741-744.

165. Epur, R., *Electrochemical Sensors for the Detection of Tricresyl Phosphate and Determination of Acid Content in Engine Oils*. 2009, Auburn University.

166. Sakmeche, N., et al., *Improvement of the electrosynthesis and physicochemical properties of poly (3, 4-ethylenedioxythiophene) using a sodium dodecyl sulfate micellar aqueous medium.* Langmuir, 1999. **15**(7): p. 2566-2574.

167. Bird, R.B., *Transport phenomena.* Applied Mechanics Reviews, 2002. **55**: p. R1.

168. Finklea, H., *Electrochemistry of organized monolayers of thiols and related molecules on electrodes.* Electroanalytical chemistry a series of advances, 1996. **19**: p. 109-335.

169. Tafel, J., *Über die Polarisation bei kathodischer Wasserstoffentwicklung.* Z. phys. Chem, 1905. **50**: p. 641.

170. Burstein, G.T., *A hundred years of Tafel's Equation: 1905-2005.* Corrosion Science, 2005. **47**(12): p. 2858-2870.

171. Sondag-Huethorst, J. and L. Fokkink, *Galvanic copper deposition on thiol-modified gold electrodes.* Langmuir, 1995. **11**(12): p. 4823-4831.

172. Schneider, O. and G. Schwitzgebel, *The mechanism of electrode passivation during the electrodeposition of polypyrrole from aqueous solutions containing fluoride anions.* Synthetic Metals, 1998. **93**(3): p. 219-225.

173. McCreery, R., *Electrochemical properties of carbon surfaces.* Interfacial electrochemistry. Theory, experiment, and applications. Marcel Dekker, New York, 1999: p. 631-47.

174. McCreery, R.L., *Carbon electrodes: structural effects on electron transfer kinetics.* Electroanalytical chemistry, 1991. **17**: p. 221-374.

175. Orazem, M.E. and B. Tribollet, *Electrochemical impedance spectroscopy*. Vol. 48. 2008: Wiley-Interscience.

8. Future work

8.1. Filters and absorbents to TCP

The repeatable sampling process and analysis of TCP indicates that the chosen alkaline catalyst is good at absorbing and hydrolyzing TCP. Therefore, it is a good candidate of absorbents and filter materials for TCP. Currently, no filter has been made specifically for TCP. Thus, we can aim at not only monitoring TCP in aircraft cabin, but also filtering it.

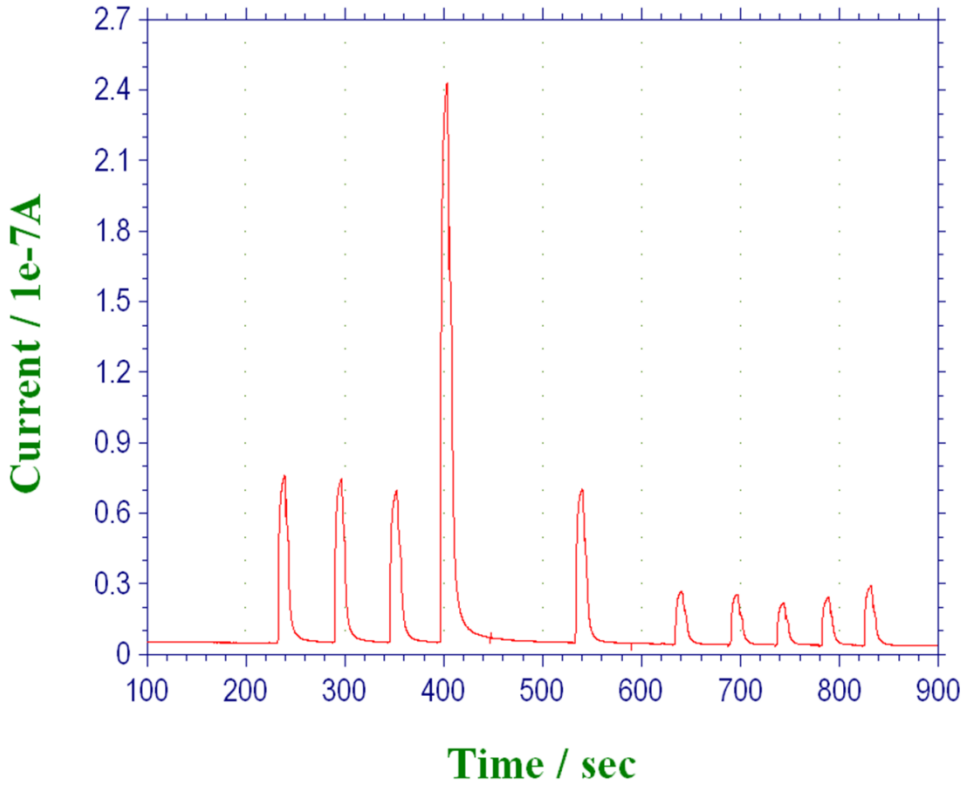

Fig. 8-1 Amperometric results of TCP hydrolysate samples. The ten peaks correspond to 100, 200, 50, 500, and 50 ppb TCP collected by the 1st column (first 5 peaks in order) and the 2nd column (latter 5 peaks). The applied potential was 0.65 V, the flow rate was 20 mL/h, and the injection time was 10 s for all samples.

The absorbing effect of the alkaline catalyst for gaseous TCP has been performed by using two successive catalyst columns (Fig. 8.1). The gasified TCP

flowed through the 1st column, where it was absorbed and converted to cresol. The tail gas flowed immediately through the 2nd column, and thus the remaining TCP or cresol in tail gas would be absorbed. Several sets of double columns have been tested with TCP samples at the concentrations of 20, 50, 100, 200, 500 ppb in N_2. The hydrolysate samples from both columns were detected (Fig. 8-1). The peaks of the samples from the 1st column (first 5 peaks) were much higher than the 2nd column (latter 5 peaks). For the peaks from the 1st column, although the linearity of response to 20-500 ppb TCP was not good, the response for 500 ppb was the highest and 20 ppb was the lowest. For the peaks from the 2nd column, the signals from different concentrations didn't vary much and were much smaller than the 1st column, which indicates that most part of TCP has been absorbed by the 1st column.

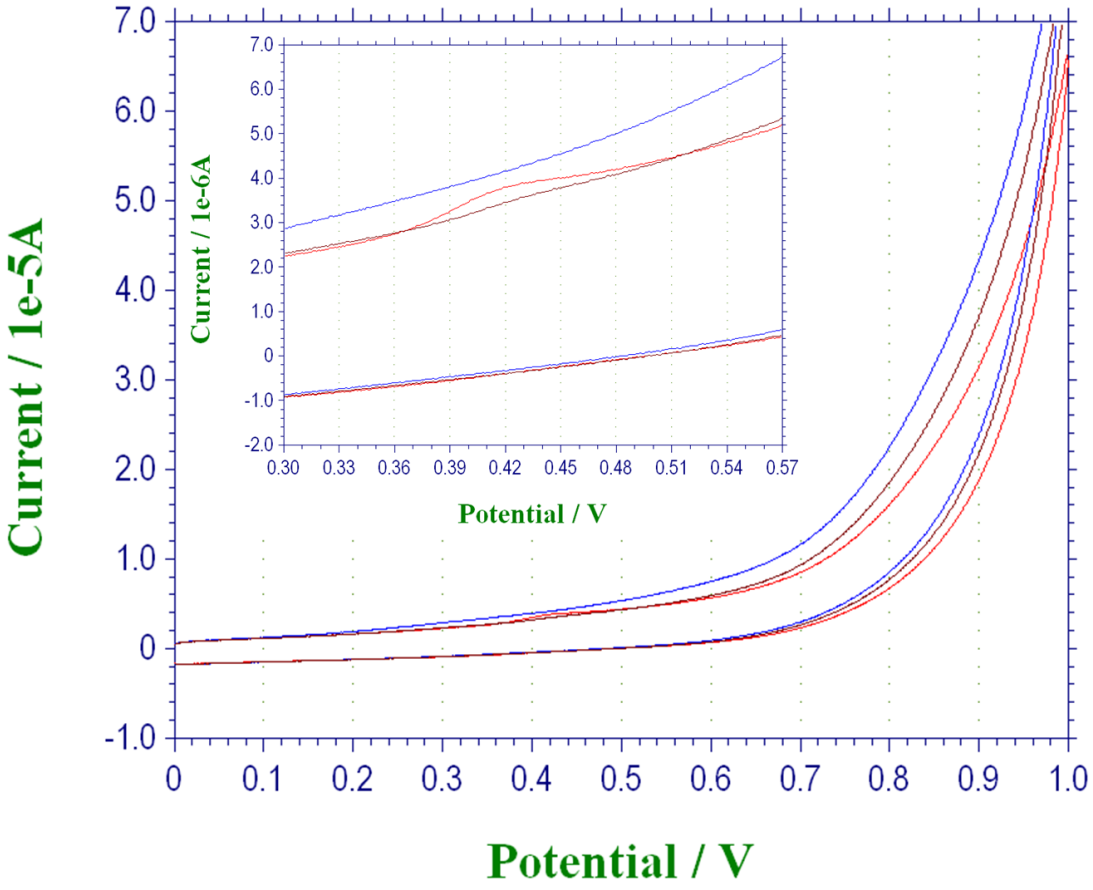

Fig. 8-2 CV results of the tail gas collection in 1M NaOH and cresol spiked medium. The mixture was spiked with cresol at the concentrations of 10 μM (blue), 20 μM (brown), and 50 μM (red). The potential range of 0.3-0.6 V was zoom in and shown

in the inset figure. The scan rate was 100 mV/s, and the volume of sample was 3 mL.

The tail gas of all of these 5 samples was collected by 3 mL of 1 M NaOH solution. The solution was checked with CV and showed no oxidation peak in the range of 0-1 V. Therefore, different amounts of cresol were injected to make the final concentrations as 10, 20, and 50 μM cresol. The series cresol spiked tail gas collection was detected with CV, and the oxidation peak was absent in 10 μM spiked collection, weak in 20 μM spiked, and more significant in 50 μM spiked (Fig. 8-2). These results indicates that the tail gas contained <20 μM cresol. The initial amount of TCP= 870 ppb * 0.5 mol (N_2) = 435 nmol = 145 μM (in 3 mL of NaOH) ~ 450 μM cresol. Thus, only <2% TCP remained in the tail gas, which confirmed that most part of TCP was absorbed by the 1st column.

Based on above discussion, the catalyst made from NaOH and Al_2O_3 is a good candidate of absorbent and filter materials for TCP. Some meaningful achievements could be realized in this area. Since most of aircrafts suffer to the potential TCP contamination (Chapter 1), the installation of TCP filtering system is needed.

The future work includes modifying the structure of the catalyst powder or replacing Al_2O_3 with other supporting materials; the candidates should have proper size for gas flow. The absorbing effect of the filter materials should also be checked with more accurate experiments.

8.2. Optimization of alkaline catalyst to TCP analysis

In current detecting method, the background signal (the signal from blank alkaline catalyst) was comparable with the signal from 20 ppb TCP. Therefore, although the detection limit of cresol was down to 200 nM, it was high for TCP. Decreasing the detection limit of TCP would be meaningful because TCP was harmful at extreme low concentration. The background signal could be reduced by replacing Al_2O_3 with other the supporting materials. The candidates are better to not

disturb the electrochemical signal, and have uniform particle size and not too small, otherwise they will penetrate the filter and enters the sample solution.

Amorphous graphite has been widely used as supporting materials since it is stable and chemically inert, however, it should be used carefully since it is conductive and will disturb the signal if the particles touch the electrode surface. Silica powder is not conductive and may be a good option. The molecular sieve may be a good alternative choice, especially the pore size could be chosen as small enough to capture the TCP molecules.

8.3. Strategies to anti-fouling

Based on the discussion in Chapter 6, several strategies could be tried for anti-fouling. They are: 1) applying modifications on electrode surface which repel the oxidation products; 2) disrupting the reaction of radical coupling and making radicals further oxidized to soluble products; 3) introducing specific molecules that act as the electron receptors and combine with radicals to form soluble products. The 1^{st} strategy includes the modifications with PEDOT:PSS, PNVP, PB, and other metallic compounds as mentioned in the chaper 1. The 2^{nd} one looks not easy. And the 3^{rd} one is meaningful to try. Many chemical receptors are available and may form soluble complexes with the phenoxide radicals.

Other than these strategies, enzyme immobilized electrodes could avoid fouling, because they used a totally different mechanism of analysis. For example, the tyrosinase based electrodes detected phenol with the mechanisms below,

$$\text{phenol} + O_2\ (\text{tyrosinase}) = \text{catechol}; \tag{8.1}$$

$$\text{catechol} + O_2\ (\text{tyrosinase}) = \textit{o}\text{-quinone} + H_2O; \tag{8.2}$$

$$\textit{o}\text{-quinone} + 2H^+ + 2e^- = \text{catechol (on electrode)}. \tag{8.3}$$

Rather than the direct oxidation of phenol, the enzyme immobilized electrode detected phenol inderectly, and only the reduction of quinone occured on the electrode.

All of phenol, catechol, and quinone are soluble in water, and thus no dielectric substrate will be stuck onto the electrode surface. Therefore, this method can totally avoid electrode fouling. The potential challenges include the stability of enzyme and the reproducibility.